EXPERIMENTAL AND THEORETICAL STUDY OF SOLUBILITY OF NEW ABSORBENTS IN NATURAL REFRIGERANTS.

Javier Mesones Mora

Dipòsit Legal: T 1549-2014

DOCTORAL THESIS

EXPERIMENTAL AND THEORETICAL STUDY OF SOLUBILITY OF NEW ABSORBENTS IN NATURAL REFRIGERANTS

Javier Mesones Mora

Supervised by:
Prof. Dr. Alberto Coronas
Dr. Daniel Salavera

Department of Mechanical Engineering
CREVER - Group of Applied Thermal Engineering

UNIVERSITAT ROVIRA I VIRGILI

Tarragona, June 2014

UNIVERSITAT
ROVIRA I VIRGILI
DEPARTAMENT D'ENGINYERIA MECÀNICA
Escola Tècnica Superior d'Enginyeria Química (ETSEQ).
Av. Països Catalans 26. 43007 Tarragona (Spain)

Los abajo firmantes Dr. Alberto Coronas, Catedrático de Universidad y Dr. Daniel Salavera, Profesor Lector, ambos del Departamento de Ingeniería Mecánica de la Universidad Rovira i Virgili de Tarragona.

HACEN CONSTAR:

Que el siguiente estudio titulado:

"Experimental and Theoretical Study of Solubility of New Absorbents in Natural Refrigerants"

presentado por el Sr. Javier Mesones Mora para optar al grado de Doctor, ha sido desarrollado bajo nuestra supervisión en el Grupo de investigación de Ingeniería Térmica Aplicada – CREVER del Departamento de Ingeniería Mecánica de la Universidad Rovira i Virgili.

Que todos los resultados han sido obtenidos de las experiencias y trabajos realizadas por dicho doctorando.

Que cumple los requisitos para poder optar al grado de Doctor en Ingeniería Termodinámica de Fluidos con Mención Internacional.

Y para que así conste a los efectos oportunos, firmamos este documento, en Tarragona, 11 de Junio de 2014.

Dedicated to my mother

"There is a driving force more powerful than steam,
electricity and atomic energy: the will"
Albert Einstein (1879-1955)

Acknowledgments

I would like to thank Dr. Alberto Coronas for letting me do this doctoral thesis as well as its support along all these years in CREVER group. I also would like to thank Dr. Daniel Salavera for all the unconditional help and valuable advices given in all the work carried out in this thesis, especially in laboratory tasks. Furthermore, I want to express my acknowledgment to Dr. María Soledad Larrechi for the help and advices provided in some tasks of this work.

Acknowledgments to Ministry of Science and Innovation (project ref. ENE2009- 14177) and Ministry of Economy and Competitiveness (project ref. DPI2012-38841-C02-01) for providing the financial support of this research, as well as to Universitat Rovira Virgili for funding my doctoral thesis and the stay in France through a scholarship.

Thanks to Dr. Jean-Yves Coxam for providing me the opportunity to do a stage in the Institute of Chemistry of Clermont-Ferrand (France) and also to Dr. Karine Ballerat-Busserolles for the help provided along the stay.

Finally I would like to thank to the rest of professors and colleagues from CREVER group as well as the secretary of Mechanical Engineering Department for their support and help received along all these years, creating a nice working environment and making the work easier and peaceful.

Abstract

In this doctoral thesis it has been carried out an experimental and theoretical study of solubility of new absorbents in natural refrigerants for absorption refrigeration cycles.

Commercial absorption refrigeration systems use H_2O/LiBr and NH_3/H_2O (refrigerant/absorbent) as working fluids with good performance in air conditioning and refrigeration applications. However these systems have some drawbacks that have driven research in improving their efficiency, enlarging the working ranges and extending to new applications. These limitations are caused by the physicochemical properties of such mixtures: crystallization, corrosion and operating vacuum pressure for H_2O/LiBr mixture or the need of rectification of the stream generated in the generator and the high level of the activation thermal energy required for NH_3/H_2O mixture.

The use of absorbents such as $LiNO_3$ or NaSCN in NH_3 allow the operation of the refrigeration system at lower temperatures than in the case of NH_3/H_2O mixture, facilitating the use of solar thermal energy at low temperature or waste heat as activation energy as well as avoiding the need of rectification in the cycle. On the other hand, the use of additives like NaOH to the conventional NH_3/H_2O mixture allows better separation of the ammonia in the generator.

In the case of absorption systems with H_2O/LiBr as working fluid, the addition of $LiNO_3$ and LiI involve a significant solubility improvement of the mixture, allowing the equipment to operate at higher temperatures in the absorber and the use of air-coolers for the heat dissipation to the environment.

The use of CO_2 as refrigerant and amines as absorbents have been currently proposed as alternatives to conventional ammonia/water systems, avoiding toxicity and flammability problems that ammonia presents.

Regarding the available information of physicochemical properties of the new working fluids, in the case of $NH_3/LiNO_3$ and NH_3/NaSCN the solubility data available in literature is scarce, old and incomplete. Also, for $NH_3/(H_2O$+NaOH) system, no solubility data were found in literature. Thus, in order to complete the solubility data of these mixtures it has been designed and built a new experimental device based on the visual-polythermal method with the capacity to work at moderate-high pressures to keep the ammonia in liquid state. Validation of the experimental device and methodology performed at atmospheric pressure with $H_2O/LiNO_3$ system and at a pressure conditions up to 20 bar with the system $NH_3/LiNO_3$. Additionally, to avoid the subjective criterion in the solubility temperature measurements, it has been developed a new image processing method based on the analysis of images taken and recorded during the experiment. From the experimental results obtained, the solubility temperature of $H_2O/LiNO_3$, $NH_3/LiNO_3$ and NH_3/NaSCN has been modelled by means of solid-liquid equilibrium and LIQUAC and symmetric electrolyte-NRTL models.

To improve the solubility of H_2O/LiBr mixture it has been performed an extension of the study of Koo et al. (1999) based on the addition of $LiNO_3$, LiI and LiCl (salt mole ratio 5:1:1:2) with the aim of improving solubility and reducing corrosiveness and vapour pressure of the mixture. Also it has been studied the effect of the addition of LiCl on the vapour pressure of the mixture by modelling the vapour pressure with asymmetric electrolyte-NRTL thermodynamic model. From the results obtained it has been proposed a new composition mixture with a salt mole ratio 7:1:0.5 (LiBr:$LiNO_3$:LiI). The addition of LiCl has been discarded because doesn't provides any improvement in solubility and vapour pressure of the mixture. Additionally, by using the visual-polythermal method it has been measured the solubility of this new mixture in a range of total salt mass fraction from 65 % to 69 %, obtaining a decrease of solubility temperature regarding the mixture proposed by Koo et al. (1999) from 8 K to 35 K.

Finally, it has been studied the flow-calorimetric methodology to measure the solubility limit for CO_2 in amines. This technique allows the simultaneous determination of enthalpies of solution and the solubility limit. This study has been performed with 2-methylpiperidine and 4-methylpiperidine aqueous solutions. These amines are used in CO_2 capture processes as they present liquid-liquid separation at a certain temperature and CO_2 composition, thus reducing the energy required for the desorption process. The comparison of experimental measurements made in previous experiments against specific experimental methodologies has shown deviations lower than 5 %, which confirms that this method is suitable for measuring the gas solubility limits in absorbents.

Resumen

En esta tesis doctoral se ha realizado un estudio teórico-experimental de la solubilidad de nuevos absorbentes en refrigerantes naturales para ciclos de refrigeración por absorción.

Los sistemas comerciales de refrigeración por absorción utilizan los fluidos de trabajo H_2O/LiBr y NH_3/H_2O con buenas prestaciones en aplicaciones de climatización y refrigeración. Sin embargo dichos sistemas presentan algunos inconvenientes y limitaciones que han impulsado la investigación en la mejora de su eficiencia, ampliación de intervalos de operación y nuevas aplicaciones. Esta problemática esta originada por las propiedades físico-químicas de dichas mezclas: problemas de cristalización, corrosión y presión de operación de vacío para la mezcla H_2O/LiBr o la necesidad de rectificación del flujo generado en el generador y la alta temperatura de activación requerida para la mezcla NH_3/H_2O.

El uso de absorbentes tales como $LiNO_3$ o NaSCN en NH_3 permite operar al sistema de refrigeración a temperaturas inferiores que en el caso de la mezcla NH_3/H_2O facilitando la utilización de energía solar térmica a baja temperatura o calor residual para su activación así como evitar la necesidad de rectificación en el ciclo. Por otra parte, el uso de aditivos como NaOH a la mezcla convencional NH_3/H_2O permite una mejor separación del amoniaco en el generador.

En el caso de sistemas de refrigeración de H_2O/LiBr, la adición de $LiNO_3$ y LiI supone una mejora significativa en la solubilidad de la mezcla, posibilitando que el equipo pueda operar a mayores temperaturas en el absorbedor y la utilización de aero-refrigeradores para la disipación del calor al ambiente.

Por otro lado, el uso de CO_2 como refrigerante y aminas como absorbentes han sido propuestos en recientemente como alternativas a los sistemas convencionales de NH_3/H_2O, evitando los problemas de toxicidad e inflamabilidad que el amoniaco presenta.

En lo referente a la información existente de las propiedades físico-químicas de las nuevas mezclas de trabajo, en el caso del $NH_3/LiNO_3$ y el NH_3/NaSCN los datos de solubilidad en la literatura son escasos, antiguos e incompletos. Así mismo, para la mezcla $NH_3/(H_2O$+NaOH) no se encontraron datos de solubilidad del NaOH en la mezcla amoniaco/agua. Por ello, para completar el estudio de la solubilidad de estas mezclas, se ha diseñado y construido un nuevo dispositivo experimental basado en el método politérmico-visual que puede trabajar a presiones moderadas-altas con objeto de mantener el amoníaco en estado líquido. La validación del dispositivo y metodología experimental se ha realizado a presión atmosférica con el sistema $H_2O/LiNO_3$ y en condiciones de presión de hasta 20 bar con el sistema $NH_3/LiNO_3$. Además, para conseguir una mayor objetividad en las mediciones de temperatura de solubilidad, se desarrolló un nuevo método de procesamiento de imágenes basado en el análisis de fotografías tomadas en el interior de la celda durante el experimento. A partir de los datos experimentales obtenidos, la temperatura de solubilidad de las mezclas $H_2O/LiNO_3$, $NH_3/LiNO_3$ y NH_3/NaSCN ha sido modelizada utilizando los modelos LIQUAC y Electrolyte-NRTL simétrico.

Para mejorar la solubilidad de la mezcla H_2O/LiBr se ha realizado una extensión del estudio efectuado por Koo et al. (1999) basado en la adición de $LiNO_3$, LiI y LiCl, en una relación molar 5:1:1:2, con el objeto de mejorar la solubilidad y reducir la corrosión y la presión de vapor de la mezcla. También se ha analizado el efecto de la adición del LiCl sobre la presión de vapor de las mezclas mediante la modelización con el modelo termodinámico Electrolyte-NRTL. A partir de los resultados obtenidos se propone una nueva mezcla con una relación molar 7:1:0.5 (LiBr:$LiNO_3$:LiI). El LiCl ha sido descartado ya que no supone una mejora ni en la solubilidad ni en la presión de vapor de la mezcla. Finalmente, mediante el método politérmico-visual se ha medido la solubilidad de esta nueva mezcla en un rango de fracción másica total de sales de 65 % a 69 %, obteniéndose un descenso respecto a la mezcla propuesta por Koo et al. (1999) de 8 K a 35 K para el intervalo de composición estudiado.

Finalmente, se ha utilizado la calorimetría de flujo para medir el límite de solubilidad de CO_2 en aminas. Esta técnica permite la simultánea determinación de entalpias de disolución y el límite de solubilidad. Dicho estudio se ha realizado con disoluciones acuosas de 2-Methylpiperydine y 4-Methylpiperydine. Estas aminas son utilizadas en procesos de captura de CO_2 ya que presentan un equilibrio líquido-líquido a partir de cierta temperatura y composición de CO_2, disminuyendo así la energía requerida en el proceso de desorción. La comparación de medidas experimentales realizadas previamente frente a metodologías experimentales específicas ha obtenido desviaciones menores al 5 %, lo que confirma que dicha metodología es adecuada para medir el límite de solubilidad de gases en absorbentes.

Publications in Journals

J. Mesones, T. Altamash, E. Pérez, D. Salavera, A. Coronas. *New device for measuring the solubility of inorganic salts in liquid ammonia*. Fluid Phase Equilibria 355 (2013) 46–51.

Y. Coulier, K. Ballerat-Busserolles, J. Mesones , A. Lowe, J-Y. Coxam. Excess molar enthalpies and heat capacities of {N-methylpiperidine – water} and {2-methylpiperidine – water} systems. (In preparation).

J. Mesones, D. Salavera, A. Coronas. Effect of the addition of $LiNO_3$, LiI and LiCl in the solubility of H_2O+LiBr mixtures. (In preparation)

J. Mesones, S. Steiu, D. Salavera, J.C. Bruno, A. Coronas. Solubility study of alkali hydroxides in ammonia+water mixtures. (In preparation)

Contributions to Congress

J. Mesones, T. Altamash, D. Salavera, A. Coronas. *Dispositivo experimental de medida de las temperaturas de solubilidad y cristalización de sales en disolventes no-acuosos a alta presión*. VII Congreso Nacional de Ingeniería Termodinámica. Bilbao (Spain) June 2011. ISBN: 84-95416-79-4.

J. Mesones, D. Salavera, A. Coronas. *Determinación experimental y predicción de la temperatura de solubilidad de sales en disolventes no-acuosos a alta presión*. Third International Seminar on Engineering Thermodynamics of Fluids. Tarragona (Spain) July 2011.

J. Mesones, D. Salavera, A. Coronas. *Solubility Measurements of Lithium Nitrate & Sodium Thiocyanate in Ammonia Solutions.* ANQUE International Congress of Chemical Engineering. Sevilla (Spain) June 2012. ISBN: 988-84-695-3536-3.

J. Mesones, D. Salavera, A. Coronas. *Solubility Prediction of Lithium Nitrate and Sodium Thiocyanate in Water and/or Ammonia Solutions with Symmetric Electrolyte NRTL Model*. International Workshop on New Working Fluids for Absorption Heat Pumps and Refrigeration Systems. Tarragona (Spain) July 2013. ISBN: 84-616-5547-8.

Y. Coulier, J. Mesones, A. Lowe, K. Ballerat-Busserolles, J-Y. Coxam. *Experimental determination and modeling of enthalpy of solution of carbon dioxide in aqueous solutions of demixing amines*. International Conference on Chemical Thermodynamics. Durban (South Africa) July 2014.

J. Mesones, D. Salavera, A. Coronas. *Effect of the Addition of $LiNO_3$, LiI and LiCl in the Solubility of LiBr Aqueous Solutions for Absorption Refrigeration Systems*. International Symposium on Solubility Phenomena and Related Equilibrium Processes (ISSP). Karlsruhe (Germany) July 2014.

Participation in Projects

SOLEF - Absorption systems for the simultaneous production of refrigeration and mechanical energy with solar thermal energy or waste heat.
Ministry of Science and Innovation. National Plan I+D +I (ENE2009- 14177).

Nuevos fluidos de trabajo y componentes para bombas de calor de absorción de altas prestaciones.
Ministry of Economy and Competitiveness. National Plan I+D +I (DPI2012-38841-C02-01).

NARILAR - New Working Fluids based on Natural Refrigerant and Ionic Liquids for Absorption Refrigeration.
People International Research Staff Exchange Scheme. Seventh Framework Programme. Marie Curie Actions (PIRSES – GA – 2010) (269321).

Internships

Institute of Chemistry of Clermont-Ferrand. Thermodynamics and Molecular Interactions (France).
Period: September 2013 – December 2013.
Advisor: Dr. Jean-Yves Coxam.
Topic: Experimental measurement of enthalpy of solution and solubility limit of CO_2 in aqueous methylpiperidine solutions.
Scholarship: URV - Grants for short stays in foreign countries (AEE2013).

NCL - National Chemical Laboratory (Pune, India).
NARILAR Project.
Period: November 2011 – December 2011.
Advisor: Dr. Anil Kumar.

Table of Contents

Chapter 1

Introduction, Justification and Objectives

1.1. Global energy situation

1.1.1. Past, present and future of world energy use

Throughout history and especially since the beginning of the industrial revolution, the use of energy in new and different areas has determined a socio-economic, technological and cultural transformation and evolution of the society. In the current world, the energy is so integrated in our life that we hardly notice its presence and the society has become critically dependent of its use. While taking hot shower every morning, using gas for cooking, electricity in our homes or petrol in our cars, we consume energy; also all the elements of common use are fabricated in factories which consume energy.

The energy situation in the world has changed a lot in the last century. In the past 20 years the energy consumption has been doubled, mainly due to the evolution of the developing countries and the unceasing growth of the world population and economy, and the studies performed indicate that the need of energy will continue increasing at a similar rate.

The International Energy Outlook (2013) projects that world energy consumption will grow a 56 % between 2010 and 2040. While in 2010 the total world energy consumption was 524 quadrillion Btu, the prediction for the year 2020 is 630 quadrillion Btu and this amount is predicted to rise up to 820 quadrillion Btu in 2040 (figure 1.1). Most of the growth of the world energy consumption occurs in the non-OECD countries, where demand is driven by strong long-term economic growth and the restrictions in legislation and policies for energy saving are much less restrictive. While the use of energy in non-OECD countries increases by 90 %; in OECD countries, the increase is 17 %.

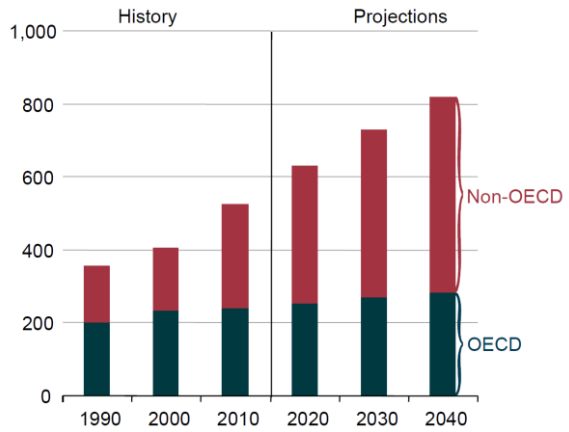

Figure 1.1. World energy consumption, 1990-2040, Quadrillion Btu. (EIA,IEO2013)

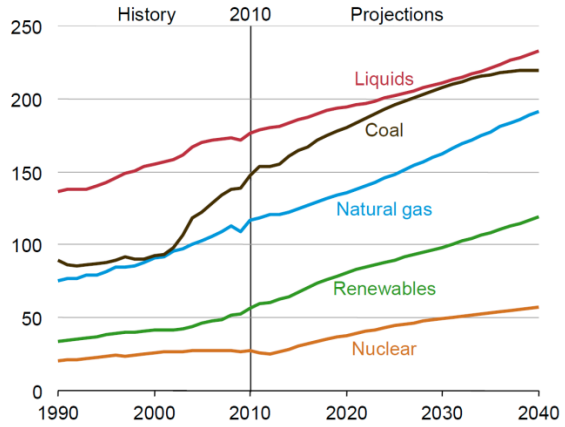

Figure 1.2. World energy consumption by fuel type, 1990-2040. Quadrillion Btu (EIA,IEO2013)

As a result, the world energy consumption from all fuel sources (figure 1.2) will continue increasing in the next years, even at a higher rate than the actual. Fossil fuels (petroleum, coal, or natural gas) will continue supplying most of the worldwide energy, being liquid fuels, which are mostly petroleum-based, the largest source of energy used (mainly in transport and industrial sectors). Renewable and nuclear energy are the energy sources which will reach the fastest growing rate, compared with the current rates. The renewables share of total energy use rises from 11 % in 2010 to 15 % in 2040, and the nuclear share grows from 5 % to 7 %.

Considering that the electrical energy is a secondary energy source produced, its demand is directly related with the consumption of primary energy sources (fossil fuels, nuclear or renewable energies). The total net electricity generated is expected to increase a 93 % in 2040 (IEO 2013). In OECD countries, where electricity markets are well established and consumption markets are mature, the growth of electricity demand presents an average of 1.1 % per year from 2010 to

2040. This value is lower than in the non-OECD countries (excluding Asia), where is expected an average increase of 3.1 % per year (figure 1.3).

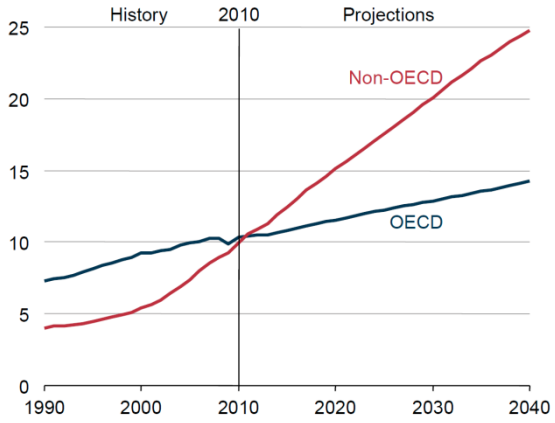

Figure 1.3. OECD and non-OECD net electricity generation 1990-2040. Trillion kilowatthours. (EIA,IEO2013)

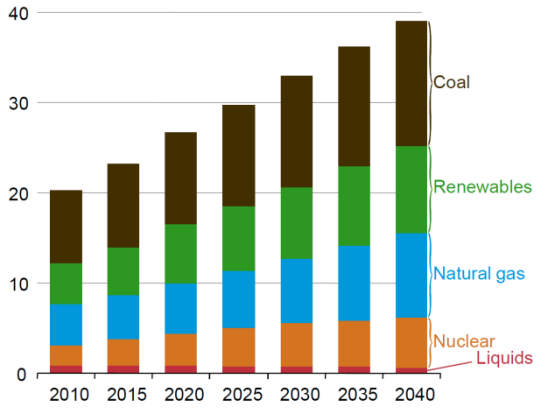

Figure 1.4. World net electricity generation by fuel, 2010-2040. Trillion kilowatthours, (EIA,IEO2013)

As it can be seen in figure 1.4, although the use of coal is, and is expected to be (though could be altered in future policies or international agreements), the largest source of world power generation through 2040, the use of renewable energy supposes the fastest growing source of electricity generation, at 2.8 % per year, followed by natural gas and nuclear energy with a 2.5 %.

Many organizations state that there exists a direct relationship between the continuous increasing emissions of CO_2 coming from fossil fuels (figure 1.5) as a consequence of the increasing energy consumption, and global warming or climate change. For this reason, from the last decade, the union of the high fossil prices, the increasing concern about the security of energy supplies and the environmental consequences of greenhouse gas emissions, have encouraged a boost in government policies focused on the development and sustained use of renewable energy sources.

Coal, main source of the energy produced, is the fossil fuel which contributes maximum to the total world carbon dioxide emissions, representing 44 % in 2010, involving emissions from liquid fuels and natural gas 36 % and 22 % respectively. However, the emissions of CO_2 vary depending if the countries belong to OECD or not. As can be observed in figure 1.6, non-OECD countries present higher emissions with a higher increase per year than OECD countries. While OECD emissions increase only a 0.2 % per year on average, non-OECD emissions increase by an average of 1.9 %.

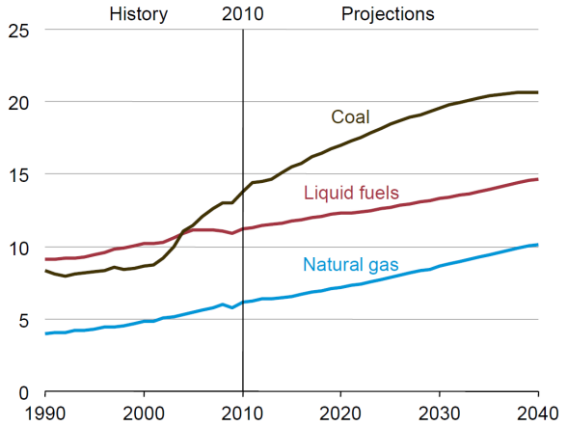

Figure 1.5. World carbon dioxide emissions by fuel type, 1990-2040. Billion metric tons. (EIA,IEO2013)

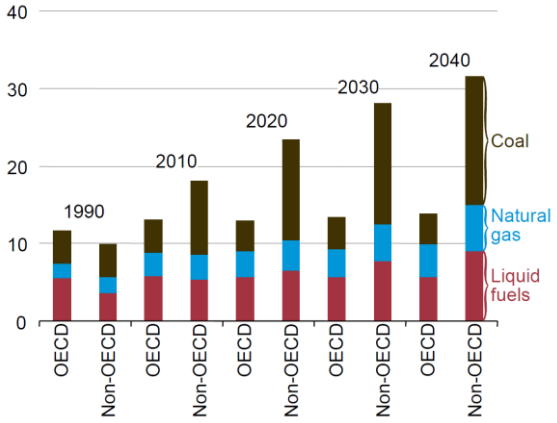

Figure 1.6. OECD and non-OECD world CO_2 emissions by fuel type, 1990-2040. Billion metric tons. (EIA,IEO2013)

1.1.2. Building energy consumption

In 2010, building sector accounted for more than one-fifth of total worldwide consumption of delivered energy. This fast growth is a consequence of the global growth in living standards and economic conditions, which leads to an increasing demand of services and comfort levels. Building represents the most energy consuming sector of OECD Europe, with about 40 % of total final energy requirements in 2010, of which 27 % corresponds to residential and 13% to services or tertiary sector (offices, health sector, education, restaurants, etc). Transport 32 %, industry 25 % and agriculture 2 % represent the rest of the consuming sectors (Energy Efficiency Status Report 2012).

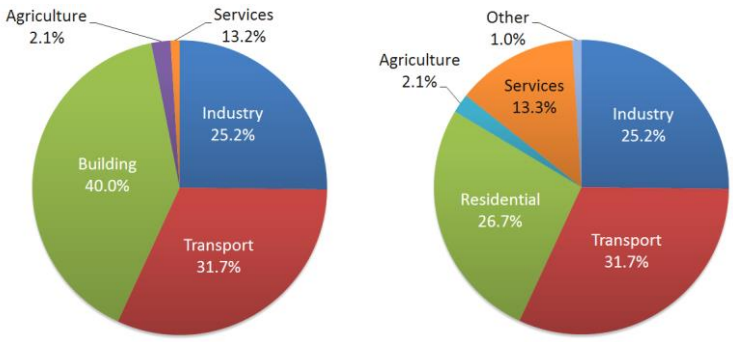

Figure 1.7. European energy consumption breakdown into sectors, 2010 (EESR 2012)

Every year the number of appliances, lighting, cooling and heating increases in buildings and, though they are each time more efficient, they are used more often and for longer periods and

hence every year more energy is required. Electricity supposes the main energy use in residential and commercial buildings, rising in OECD Europe by an annual average rate of 1.4 % and 5.4 % respectively (figure 1.8 and 1.9).

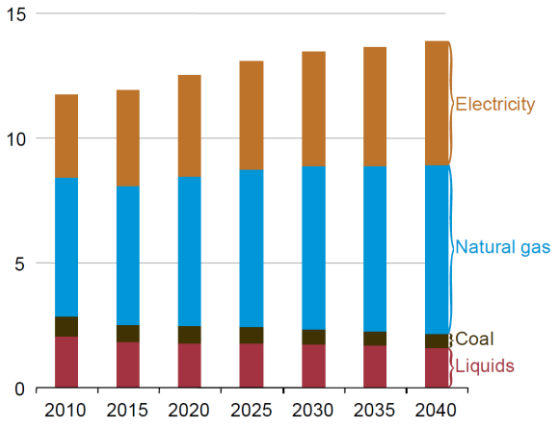

Figure 1.8. OECD Europe residential energy consumption. Quadrillion Btu (EIA,IEO2013)

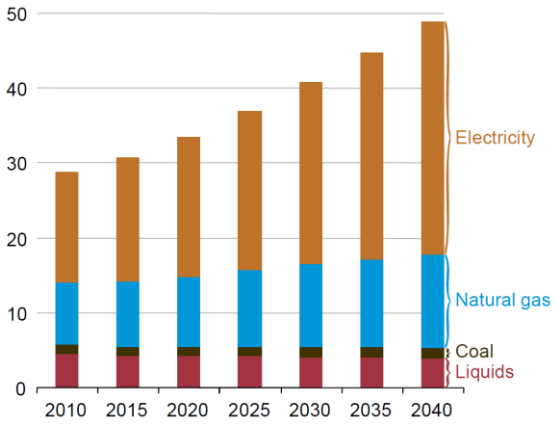

Figure 1.9. OECD Europe commercial energy consumption. Quadrillion Btu (EIA,IEO2013)

From the last decade, a wide array of measures has been adopted at EU level and implemented across individual Member States to actively promote better energy performance of buildings. As a result, the energy consumption in the building sector has increased only around 0.6% per year in households and 1.5 % per year in the tertiary sector since 1990 (Energy Efficiency Trends in Buildings in the EU 2012).

In buildings, one of the elements that requires more electrical energy is the refrigeration based on mechanical vapour compression technology. Under this pretext, the increasing interest in protecting the environment and saving energy has favoured the use of absorption chillers, whose requirements in electricity are much lower and are driven by thermal energy and environmental friendly working fluids.

1.2. Absorption refrigeration cycles

1.2.1. General overview

Most of the industrial processes use thermal energy by burning fossil fuel to produce steam or heat for the purpose and after the process heat is rejected to the surrounding as waste. By using a heat operated refrigeration system, like an absorption refrigeration cycle, this waste heat can be used to drive a refrigeration system.

The origin of absorption refrigeration cycles can be situated in 1755 when William Cullen observed that, regardless of the environmental conditions, ice could be produced by evaporating volatile liquids. From its experiments he published a paper called Essay on Cold Produced by Evaporating Fluids in which at a given temperature of 6 °C a jar filled with ether was placed inside another jar, slightly larger, that contained water. The pressure was decreased to vacuum to force the evaporation of the nitrous ether, which has a higher volatility (boiling point of 17 °C), absorbing thermal energy from water. As a result, almost all the water was found frozen. Few years later, other researchers Gerald Nairne in year 1777 and John Leslie in 1810 carried out similar experiments based on the same principle using water and sulphuric acid to obtain ice.

The first absorption refrigeration cycle, with water/ammonia as working fluid was introduced by Ferdinand Carre in 1859 and was used in the following years as a base design in the absorption refrigeration development. In 1950's a system using lithium bromide/water as working fluid was introduced for air-conditioning and industrial applications. Years later, the double-effect absorption system was introduced as improvement in the performance of the refrigeration cycle.

Absorption refrigeration systems use thermal energy as the driving energy, instead of electrical or mechanical power required for conventional vapour compression devices, therefore the electricity required is drastically reduced. Additionally, the use of absorption refrigeration systems helps to reduce problems related to global environment like the so called greenhouse effect due to CO_2 emissions from the combustion of fossil fuels in utility power plants. The working fluids used in the absorption refrigeration cycles differ from classical vapour compression systems. While vapour compression systems use refrigerants such as hydrofluorocarbons (HFCs) because of their thermophysical properties, the absorption refrigeration cycles uses natural refrigerants such as water, ammonia and salts as absorbents.

Some advantages of absorption cycles in front of compression systems are listed in the following table:

Table 1.1. Comparison between absorption and compression systems

Absorption Systems	Compression Systems
Low grade energy like heat, which can proceed from solar energy.	High grade energy like electricity.
Initial capital cost of installation is higher but operation is cheaper.	Cost of the entire system is cheaper but operation is much more expensive.
Typical refrigerants used are green and cheap.	Halocarbons used as refrigerants as expensive and produce greenhouse effect.
Lower efficiency. Coefficient of performance ≈ 0.5-1.5.	Higher efficiency. Coefficient of performance ≈ 4.5-5.5.
Overall system is larger due to the dimensions of absorber and generator	Lower system dimensions.
Higher reliability and durability. Moving parts are only in the pump. Smooth operation.	Moving parts are in the compressor. More wear, tear and noise.
The system can work on lower evaporator pressures without affecting COP.	The COP decreases considerably with decrease in evaporator pressure.
No effect of reducing the load on performance.	Performance adversely affected at partial loads.
Liquid traces of refrigerant present in piping at the exit of evaporator constitute no danger.	Liquid traces in suction line may damage the compressor.

Although absorption systems are a good alternative due to all the above described advantages, they still have some important drawbacks such as high cost and low efficiency compared to the vapour compression systems, which still dominate all market sectors. Absorption systems are only preferable from the energetic point of view if they use thermal energy from sources such as waste heat, cogeneration or even solar thermal energy. Furthermore, these systems are recommended where electricity is unreliable or costly and where the noise and vibrations from the compressor are not admissible. Consequently, in order to promote the use of absorption systems, current efforts are focussed in the improvement of their characteristics and performance.

1.2.2. Principle of operation

As it can be observed in figure 1.10, single-stage absorption refrigeration systems are similar to mechanical vapour compression systems. Basically, the difference lies in the procedure of fluid compression from low to high pressure. The mechanical compressor is replaced by a chemical compressor, which is composed of absorber, pump, generator and expansion valve.

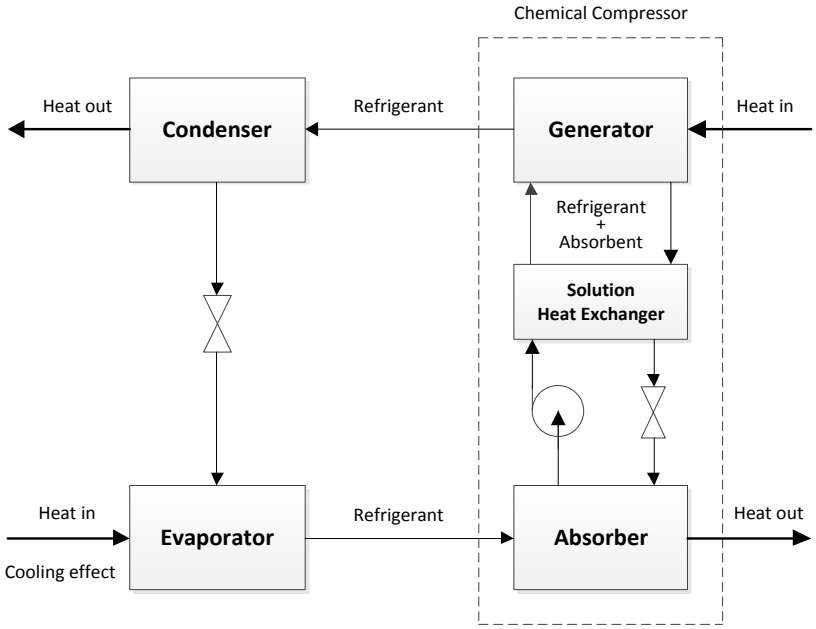

Figure 1.10. Schematic diagram of absorption Refrigeration cycle

The absorber is a heat exchanger in which the refrigerant in vapour phase is absorbed by a highly concentrated liquid solution called as absorbent. As the absorption produces an exothermic reaction, the temperature of the absorber is dissipated and controlled by means induced air or cooling water. The solution diluted in refrigerant is pumped from low pressure to the generator at high pressure with the advantage that requires much less energy to pressurize it than a compressor, reducing drastically the electricity requirements for the cycle operation. The generator is another heat exchanger in which the refrigerant evaporated and desorbed from the solution by applying thermal energy. This is the so called activation energy of the cycle. The remaining solution highly concentrated in absorbent is returned to the absorber at low pressure by means an expansion valve, closing thus the refrigerant/absorbent solution cycle in the chemical compressor.

Between the absorber and the generator, in many cases there is another heat exchanger installed which allows the solution from the absorber to be preheated before entering the generator by the hot solution leaving the generator. Therefore, the coefficient of performance is improved as the heat input at the generator is reduced. Moreover, the size of the absorber can be reduced as less heat is rejected. The rest of the elements, evaporator and condenser have the same role functions as in vapour compression cycles: in the condenser the refrigerant at high pressure changes from vapour phase to liquid phase by releasing thermal energy, then, the pressure is decreased to low pressure by an expansion valve. In the evaporator the refrigerant at low pressure is evaporated by absorbing heat from the fluid or medium where the cooling effect is produced. The high and low pressures of the cycle are determined by the condensation and evaporation saturation temperature respectively.

The coefficient of performance (COP) is a common measure of the efficiency of a refrigeration cycle. It's defined as the ratio of cooling power produced (Q_E) to the energy input in the system (Q_G) plus the pump consumption (W) (eq. 1.1).

$$\mathrm{COP} = \frac{Q_E}{Q_G + W} \tag{1.1}$$

As the work input of the pump is very small as compared to the thermal energy input in the generator, the consumption of the pump is sometimes neglected for the calculation of the COP.

1.2.3. Classification

Absorption refrigeration systems are classified depending upon the different aspects:

- *Heat dissipation technology*

Water-cooled systems: Uses water cooling tower to dissipate the heat released in the absorber (due to the exothermic reaction produced) and in the condensation process of the refrigerant. This method is restricted to industrial or commercial applications.

Air-cooled systems: Uses induced air currents to perform the heat dissipation in the absorber and condenser.

- *Source of heat activation*

Direct-fired systems: The absorption system is activated by an integrated burner with the flame being in direct contact with the generator. Natural gas is the most used fuel.

Indirect-fired systems: The generator is heated by means of a fluid at high temperature such as steam, thermal oil or exhaust gases coming from combustion, solar thermal collectors or industrial processes.

- *Number of activation stages*

Single effect absorption systems: These are the simplest and basic systems. The configuration is the explained in section 1.2.2, obtaining coefficients of performance between 0.6 - 0.7 in the most favourable conditions. They require low temperatures of activation, from (85-90) °C depending of the working fluids used.

Double-effect absorption systems: Systems activated by two generators suppose an improvement in the performance of the cycle with requirements of heat sources > 150 °C. They are used with H_2O/LiBr as working fluids obtaining COP of 1 - 1.2.

Triple-effect absorption systems: These systems are currently developed as prototypes to make use of thermal sources at high temperature (> 200 °C), achieving coefficients of performance up to 1.7. At the temperatures reached in the cycle, conventional working fluid H_2O/LiBr presents problems of decomposition. To overcome this problem, new absorbents such as the so called alkitrate aqueous solution ($LiNO_3$+KNO_3+$NaNO_3$) are studied due to its thermal stability at high temperatures.

GAX absorption systems: In these systems the cycle is activated by only one generator, like single effect systems. However, the absorber and generator are divided in two sections. In the low temperature absorber section the heat released by the absorption process is rejected to surroundings and in the high temperature absorber section the heat released is used to preheat the solution entering the generator. They are used with NH_3/H_2O working fluids at temperatures of activation > 160 °C with coefficients of performance of 1.0.

1.3. Conventional working fluids

The overall performance of absorption refrigeration systems is strongly dependent on the physic-chemical properties of the working fluids. The working fluid in an absorption refrigeration system is a solution consisting of refrigerant and absorbent. The refrigerant is a volatile fluid and the absorbent can be another fluid or a solution in which the solute is a non-volatile inorganic salt and the solvent is the same fluid as the refrigerant. The fundamental requirements for a proper absorbent/refrigerant combination are as follows:

- In liquid phase, the absorbent/refrigerant must have a margin of miscibility within the operating temperature range of the cycle.
- At the same pressure, the difference between the boiling points of pure refrigerant and the solution must be as large as possible.
- The refrigerant must have a high heat of vaporisation and high composition within the absorbent to maintain low circulation rate between the generator and the absorber per unit of cooling capacity.
- Transport properties, which determine the heat and mass transfer, such as viscosity, thermal conductivity or diffusion coefficient, should be favourable.
- If the absorbent is composed by a salt, its solubility has to be good enough to avoid crystallisation at working temperatures and salt compositions.
- The solution refrigerant/absorbent should be chemically stable, non-toxic, non-corrosive, and environmental friendly.

Many mixtures have been proposed as working fluids over the last 50 years (Macriss et al., 1988), however only commercial systems based on H_2O/LiBr for air conditioning and NH_3/H_2O for industrial refrigeration are used nowadays.

1.3.1. Water/Lithium Bromide Systems

In H_2O/LiBr systems, water is the refrigerant and lithium bromide is the absorbent, which performs an excellent absorbance of water due to the strong association of lithium ion Li^+ with the water molecules (highly hygroscopic).

The main advantage of these systems is the high latent heat and the excellent environmental and toxicity properties that water presents, as well as the negligible vapour pressure, low viscosity and non-toxicity of the LiBr solution.

However they present some drawbacks such the necessity to work at vacuum conditions. For example, at typical operating conditions of absorption chillers for air-conditioning applications the low pressure is only 0.680 kPa for water evaporation temperature of 1.5 °C and the higher pressure corresponds to 7.35 kPa for a condensing temperature of 40 °C (Herold et al., 1996). Also, at high compositions the absorbent solution is close to crystallization. At the outlet of the solution/solution heat exchanger, before entering the absorber, there exists a high risk of crystallization due to the unfavourable temperature/composition ratio, i.e. low temperature and high salt composition. Additionally, the equipment large dimensions due to vacuum operation, the lithium bromide solution is corrosive to some metals and since the refrigerant is water, the minimum possible chilled water temperature at its lowest is about 1.5 °C, what limits the application of H_2O/LiBr absorption chillers from being used for air-conditioning uses. These systems require water cooling tower for heat dissipation in the absorber (wet dissipation) in an interval of 25-30 °C with no possibility to perform it by atmospheric air (dry dissipation). Air cooled absorbers could be a big improvement in H_2O/LiBr absorption systems for the non-necessity of cooling towers, but its utilisation is restricted due to the poor heat transfer of air that leads to higher heat exchange areas and temperatures up to (40-45) °C, what attached to a constant low pressure entails to an increase in the salt composition and hence crystallisation of the mixture.

Nevertheless, absorption systems operated with this working fluid allows high energy and economic efficiency using simple and compact equipment. Current technology of water/lithium bromide absorption systems is based on double effect machines activated by direct flame. They are used mainly for medium and high power charges such as industry, hospitals, offices or big buildings, with production of cold water at temperatures of (7-12) °C for fan-coils and (14-18) °C for cold roofs.

1.3.2. Ammonia/Water Systems

In NH_3/H_2O absorption systems, ammonia is the refrigerant and water is the absorbent. The most advantage of these systems is that they can provide chilled temperatures down to -40 °C. Unlike water/lithium bromide systems, ammonia/water absorption systems work with pressure

conditions (e.g. low pressure corresponds to 2.9 bar for NH_3 evaporation temperature of -10 °C and high pressure is 15.6 bar for a condensing temperature of 40 °C) which means equipment with smaller dimensions. Another advantage of working with water as absorbent is the absence of crystallization problems.

Nonetheless, they also present some drawbacks: due to the significant vapour pressure of water, part is evaporated when the ammonia/water solution is heated in the generator. To avoid the presence of water in the condenser and evaporator, the installation of a rectifier column after the generator is required to separate the water from the solution by water condensation, supposing a decrease in the energy efficiency of the cycle and limits the cooling capacity. There are also other drawbacks of ammonia such as the high temperature of activation required, its toxicity and flammability.

The commercial uses of ammonia/water machines are limited to industrial refrigeration or low power air-conditioning units (18 kW) of single-effect or GAX, direct flame and air-cooled systems for air-conditioning applications.

1.4. New working fluids

Conventional refrigerant/absorbent fluids H_2O/LiBr and NH_3/H_2O have been used for many years in commercial absorption systems for air-conditioning and refrigeration applications respectively. However, as explained in the previous section, they present drawbacks that have promoted research efforts focussed in the improvement of their characteristics, performance and applicability. The use of new absorbents such as $LiNO_3$ or NaSCN for systems with ammonia as refrigerant allows the non-necessity of rectification and the capacity to operate with solar thermal energy as activation energy (Libotean, 2007, Infante Ferreira, 1984). Also, other alternative includes the use of NaOH as additive to reduce the necessity of rectification (Steiu et al., 2008, 2009, 2011). In case of absorption systems with water as refrigerant, the use of additives such as ethylenegylcol, ethanolamine or lithium based salts ($LiNO_3$, LiI) improves the solubility of the LiBr solution, inhibiting crystallization and making it capable to work with air-cooled absorbers (Kim et al., 1996; Koo et al, 1999). Additionally, the use of CO_2 as refrigerant and ionic liquids, alcohols or amines as absorbents has been proposed by some authors to be an alternative to conventional absorption systems, obtaining good efficiencies in conventional and absorption/desorption cycles (Sen and Paolucci, 2006; Jones, 2002; Jones, NASA, 2004).

In the next sections are explained in detail these new mixtures, divided by the three different refrigerants studied.

1.4.1. Working fluids with NH_3 as refrigerant

Absorption refrigeration systems based on $NH_3/LiNO_3$ and NH_3/NaSCN as working fluids have been established in literature as a good alternative to the classical ammonia/water systems (Libotean, 2007, Infante Ferreira, 1984; Rivera and Rivera, 2003; Abdulateef et al., 2008,). The most important features of these new mixtures are that they allow activating the system with lower temperatures, which permits to use low grade waste heat or solar energy as thermal energy source by using flat plate collectors (FPC) or evacuated tube collectors (ETC), obtaining temperatures of (40-80) °C and (70-120) °C respectively (Montero, 2012); and, due to the non-volatility of the salt the necessity of rectifier is avoided because only ammonia is present in vapour phase, making the system smaller and cheaper.

While single-effect ammonia/water systems require generation temperatures higher than 115°C to achieve refrigeration temperatures of -10 °C, the temperatures required in ammonia/lithium nitrate and ammonia sodium thiocyanate systems for obtaining the same refrigeration temperatures are 90 °C and 100 °C respectively (Infante Ferreira, 1984). Additionally, the lower working temperatures allow the use of plate heat exchangers, which results in more compact equipment (Zacarías, 2009). These systems also present a slight improvement in the coefficient of performance regarding conventional ammonia/water system (Sun, 1998). The advantages of using the NH_3/NaSCN or $NH_3/LiNO_3$ cycles are very similar but they present some problems such as high viscosity, which limits heat and mass transfer processes in the absorber (Amaris et al., 2014) or even in the case of NH_3/NaSCN, the cycle cannot operate below -10 °C evaporator temperature because of the possibility of crystallization (Sun, 1998).

Another alternative to improve the performance of absorption NH_3/H_2O systems is the addition of a third component to the mixture. Reiner and Zaltash (1991, 1992, 1993) studied different compounds to reduce the necessity of rectification and observed that LiBr, LiCl or $LiNO_3$ strengthen ammonia-water attraction, making absorption easier, and hydroxides such as LiOH or KOH weakens their attraction, obtaining a higher composition of ammonia in vapour phase. In this way, Steiu et al. (2008, 2009, 2011) studied the performance of absorption cycles by adding NaOH to the absorbent. As a result, the ammonia composition in vapour phase leaving the generator is

increased, diminishing the need of rectification in the process. The addition of NaOH also reduces the boiling temperature regarding the binary solution, which it is translated in a lower temperature needed in the generator and an increase in the COP of the cycle. However, due to the fact that the presence of sodium hydroxide worsens the absorption of ammonia, it is necessary to introduce a reverse osmosis separation system to prevent that the hydroxyl arrives to the absorber.

1.4.2. Working fluids with H_2O as refrigerant

In H_2O/LiBr absorption systems, the major drawbacks of working fluid pair H_2O/LiBr are the corrosive nature of lithium bromide and the crystallization risk that presents the solution at high salt compositions. To overcome these problems some authors studied the addition of inorganic compounds to improve the solubility. Some examples are the mixture H_2O/LiBr+Ethylene gylcol+Phenylmethylcarbinol developed by Carrier, using ethylene glycol as crystallisation inhibitor and Phenylmethylcarbinol as heat and mass transfer enhancer; or H_2O/LiBr+Ethanolamine (Rockenfeller and Langeliers 1988; Kim et al., 1996) in which further studies of heat and mass transfer need to be carried out to analyse the performance. Other proposed working fluids to improve solubility and another thermodynamic properties are based on the addition of lithium salts such as H_2O/(LiBr+LiI), H_2O/(LiBr+$LiNO_3$) (Iyoki et al., 1993), H_2O/(LiBr+LiI+LiCl) (Koo and Lee, 1998), or H_2O/(LiBr+$LiNO_3$+LiI+LiCl) (Koo et al, 1999), where lithium iodide decreases crystallisation temperature, lithium nitrate improves both solubility and corrosion and lithium chloride reduces vapour pressure without altering the performance of the cycle.

1.4.3. Working fluids with CO_2 as refrigerant

The use of CO_2 as refrigerant has been successfully used from few years ago in vapour-compression refrigeration systems as an option to overcome the security problems that presents ammonia. Carbon dioxide is environmental friendly, it has non-toxicity, non-flammability and additionally low cost. Due to its very low evaporation point (-57 °C) can provide very low temperatures of refrigeration, making it excellent for cryogenic uses. Also, as the volumetric relation of the CO_2 as compared to ammonia is 10:1, the dimensions of the equipment and the amount of refrigerant required are lower.

Nevertheless, though its properties make it a promising fluid, CO_2 has not been used so far as refrigerant in absorption refrigeration cycles; it has only been done proposals of suitable absorbents and its integration in the absorption systems (Klocker et al, 2001; Zhang and Lior, 2007). Some authors have studied the use of CO_2 in conventional absorption systems using ionic liquids as absorbents (Martín and Bermejo, 2010, Sen and Paolucci, 2006), alcohols or amines (Jones, 2002). Also it has been studied the use of alcohols or amines as absorbents in absorption/desorption cycles called "champagne heat pumps", where the absorber and generator are the only components of the system (Jones, NASA, 2004). These systems can provide proper performances with working pressures from 40 bar to 100 bar to provide cooling to about 4 °C.

1.5. Justification and Objectives

The knowledge of thermophysical properties of the working fluids is essential to design and evaluate the efficiency of absorption refrigeration systems. In particular, the knowledge of the solubility of absorbents consisting in single salts or multicomponent salt mixtures in the refrigerant plays a critical role because they present a partial solubility that impose restrictions in the operability and applications of the refrigeration systems, limiting the working conditions in order to avoid crystallization of the solution refrigerant/absorbent. The higher crystallisation risk occurs before returning the solution into the absorber because is where the relation temperature/composition is the most unfavourable of the cycle: the solution has high salt composition and low temperature.

In this context, the overall objective of this study is to perform an experimental and theoretical study of the solubility of the new absorbents in natural refrigerants (H_2O, NH_3 and CO_2) as alternative of H_2O/LiBr and NH_3/H_2O absorption systems:

- For absorption systems with NH_3 as refrigerant it will be studied the solubility temperature (temperature in which is completely dissolved a fixed composition of the solution under study) of mixtures $NH_3/LiNO_3$ and NH_3/NaSCN, because the solubility data available in literature is scarce, very old and without reported working pressure. For NH_3/NaSCN only is presented a phase diagram, no experimental data is tabulated. Additionally, for $NH_3/(H_2O$+NaOH) no solubility data of NaOH in ammonia+water were found in literature.
- For absorption systems with H_2O as refrigerant it will be made an extension of the solubility study carried out by Koo et al. (1999) with the H_2O/(LiBr+LiNO3+LiI+LiCl) mixture. It will be

optimized the ratio of salts in order to improve the solubility at higher absorbent compositions than presented in literature.

- On the other hand, it will be studied a flow-calorimetric methodology to measure the solubility limit of CO_2 in amines. This technique allows the simultaneous determination of the enthalpies of solution and solubility limits. Specifically it will be used 2-Methylpiperydine and 4-Methylpiperydine solutions because there is no data published in literature. In process of CO_2 capture they present liquid-liquid phase separation at a specific temperature and CO_2 composition that allows separation of the amine from water + carbon dioxide solution, diminishing the energy requirements in the amine recuperation process (Coulier et al., 2010). (*Work carried out in Institute of Chemistry of Clermont-Ferrand, France*).

To success with the main objectives of this work, the followings tasks will be carried out:

- Design and build an experimental device based on the visual-polythermal methodology to measure the solubility temperature of salts in ammonia at moderate-high pressure.
- Develop a methodology for sample preparation in order to work under pressure conditions.
- Validate the experimental device and methodology with $H_2O/LiNO_3$ system at atmospheric pressure and $NH_3/LiNO_3$ system at 20 bar (also for providing new data to literature).
- Measurement of solubility temperature NH_3/NaSCN and $NH_3/(H_2O+NaOH)$ at different salt compositions.
- Development of a new image processing methodology to provide an objective criterion in the solubility measurements.
- Solubility modelling of $H_2O/LiNO_3$, $NH_3/LiNO_3$, and NH_3/NaSCN systems in order to provide a theoretical study of solubility and a comparison of the modelling procedure for aqueous or non-aqueous solvents.
- Solubility temperature measurements, using a rough technique, of the different mole ratios $LiNO_3$/LiBr, LiI/$LiNO_3$ and LiCl/Li in the systems $H_2O/(LiBr+LiNO_3)$, $H_2O/(LiBr+LiNO_3+LiI)$ and $H_2O/(LiBr+ LiNO_3+LiI+LiCl)$ respectively, at total salt mass fractions from 0.65 to 0.69, in order to obtain the ratio with lower solubility temperature at higher composition than studied in literature.

- Measurement in a glass solubility cell based visual-polythermal method (but simpler due to atmospheric pressure conditions) the solubility temperature of the obtained optimum solution of lithium salts in water in a wide range of salt composition.
- Vapour pressure modelling of the optimum solution of lithium salts obtained in order to analyse the effect of the addition of lithium chloride in the vapour pressure.
- Comprehensive study of flow-calorimetric methodology to measure solubility limit of CO_2 in methylpiperydine aqueous solutions.
- Study of the uncertainties associated to the experimental measurements.

1.6. Thesis structure

The methodology followed to reach the objectives listed previously is presented in the different chapters that form this thesis:

In *Chapter 2* it is studied the solubility of working fluids of absorption refrigeration systems with ammonia as refrigerant. First, the design and methodology of a new experimental device is described, based in the visual-polythermal method, to determine the solubility of salts in ammonia at moderate-high pressure to maintain ammonia in liquid phase. It presents the experimental measurements of solubility temperature in a wide range of absorbent composition for the systems: $H_2O/LiNO_3$ for device validation at atmospheric pressure, $NH_3/LiNO_3$ for providing new useful data and device validation under pressure, and NH_3/NaSCN systems to provide also new accurate data to literature. Additionally, it is presented a new image processing method with Matlab software, based on the analysis of the images taken from the inner of the cell with a digital camera, in order to provide an objective criterion in the solubility temperature determination.

On the other hand, it is also measured the solubility temperature of sodium hydroxide in the ternary system $NH_3/(H_2O+NaOH)$. However, for a certain composition of ammonia and water, sodium hydroxide presents a composition that represents its solubility limit in the solution that causes the impossibility to dissolve it by increasing temperature. For this reason, the solubility temperature curve as a function of sodium hydroxide composition could not be performed as usual, instead, the maximum ammonia composition which allows a constant composition of salt in the water + salt solution without salt precipitation was measured.

Chapter 3 presents the solubility modelling of the $H_2O/LiNO_3$, $NH_3/LiNO_3$ and NH_3/NaSCN systems, carried out by means of solid-liquid equilibrium and the activity coefficient models LIQUAC (J. Li et al., 1994) for water solvents and Symmetric Electrolyte-NRTL (Song and Chen, 2009) for ammonia solvents. It is also presented the differences in the modelling procedure when is used aqueous or non-aqueous solvents. Aqueous solvents allow the use of a rigorous method based on the calculation of the Gibbs free energy that avoids the use of experimental solubility data. However, for systems with ammonia as solvent the required thermodynamic properties are not available and it is required the use of experimental solubility data for the modelling.

In *chapter 4* is presented the experimental measurement of solubility temperature of a new working fluid with water as refrigerant and lithium salts as absorbent. Based on the previous studies of Koo et al. (1999) it is analysed by a rough visual-polythermal method how the addition of lithium salts ($LiNO_3$, LiI and LiCl) at different mole salt ratios and mass fractions from 0.65 to 0.69, affects to the solubility of H_2O/LiBr, with the aim to achieve an optimum ratio that obtains a minimum solubility temperature, making it compatible for air-cooled absorbers. The solubility of the resulting optimum mixture is measured with a glass solubility cell in a wide range of absorbent compositions. Finally, the vapour pressure of the optimum mixture obtained is modelled in order to analyse if lithium chloride, as reported in literature, decreases the vapour pressure of the solution and if this effect really justifies its use.

In *chapter* 5 it is studied the solubility of working fluids with carbon dioxide as refrigerant and amines as absorbent. It is measured the solubility limit of CO_2 in aqueous solutions of 2-methylpiperidine and 4-methylpiperidine with flow-calorimetric methodology by means of the determination of the enthalpy of solution of the mixture. The main purpose of these experiments lies in the study of other methodology to measure solubility limit of gases into absorbents.

Finally, in *Chapter 6* there are presented the conclusions of this thesis and the proposed future work.

1.7. References

ASHRAE Handbook: *Fundamentals. Absorption Refrigeration Cycles*. (2009).

Abdulateef, J. M.; Sopian, K.; Alghoul, M.A. *Optimum Design for Solar Absorption Refrigeration Systems and Comparison of the Performances Using Ammonia-Water, Ammonia-lithium Nitrate and Ammonia-Sodium Thiocyanate Solutions.* Int. J. of Mechanical and Materials Eng 1 (2008) 17-24.

Amaris, C.; Bourouis, M.; Vallès, M. *Passive intensification of the ammonia absorption process with $NH_3/LiNO_3$ using carbon nanotubes and advanced surfaces in a tubular bubble absorber*. Energy 68 (2014) 519-528.

Bennani, N.; Prevost, M. *Absorption heat pump cycle: Performance analysis of water-glycerol mixture*. Heat Recovery System and CHP 9 (1989) 257–263.

Bertoldi, P.; Hirl, B.; Labanca, N. *Energy Efficiency Status Report 2012. Electricity Consumption and Efficiency Trends in the EU-27*. European Commission. Institute for Energy and Transport.

Best, R.; Rivera, W.; Cardoso, M.J.; Romero, R.J.; Holland, F.A. *Modelling of single-effect stage and advanced absorption heat transformers operating with H_2O/carrol mixture*. Applied Thermal Eng. 17 (1997) 1111-1122.

Coulier, Y.; Ballerat-Busserollesa, K.; Rodiera, L.; Coxam, J.-Y. *Temperatures of liquid–liquid separation and excess molar volumes of {N-methylpiperidine–water} and {2-methylpiperidine–water} systems*. Fluid Phase Equilib. 296 (2010) 206–212.

Energy Efficiency Trends in Buildings in the EU 2012. Lessons from the ODYSSEE MURE project. Agence de l'Environnement et de la Maîtrise de l'Energie. September 2012.

Herold, K.E.; Radermacher, R.; Klein, S.A. *Absorption Chillers and Heat Pumps.* CRC Press. Florida USA (1996).

International Energy Outlook 2013. U.S. Energy Information Administration. DOE/EIA-0484 (2013).

Infante Ferreira, C.A. *Thermodynamic and Physical Property Data Equations for Ammonia-Lithium Nitrate and Ammonia-Sodium Thiocyanate Solutions*. Solar Energy 32 (1984) 231-236.

Iyoki, S.; Iwasaki, S.; Kuriyama, Y.; Uemura, T. *Solubilities for the Two Ternary Systems Water + Lithium Bromide + Lithium Iodide and Water + Lithium Chloride + Lithium Nitrate at Various Temperatures.* J. Chem. Eng. Data 38 (1993) 396-398.

Iyoki, S.; Yamanaka, R.; Uemura, T. *Physical and thermal properties of the water-lithium bromide-lithium nitrate system*. Int. J. of Refr. 16 (1993) 191-200.

Iizuka, H.; Nagamatsuya, K.; Takahashi, K.; Kuroda, J.; Takigawa, T. *Some Properties of Absorption Fluid containing Ethylene Glycol for Air-cooled Chiller*. Proceedings of the International Gas Research Conference , Tokyo (1989).

Li, J.; Polka, H.-M.; Gmehling, J. *A g^E model for single and mixed solvent electrolyte systems. 1. Model and Results for Strong Electrolytes*. Fluid Phase Equlib. 94 (1994) 89-114.

Jones, J.A. United States Patent. No: US 6,374,630 B1 (2002)

Jones, J.A. Champagne Heat Pump, NASA Technical Support Package (2004), www.techbriefs.com/tsp.

Klocker, K.; Schmidt, E.L.; Steimle, F. *Carbon dioxide as working fluidin drying heat pumps*. Int. J. of Refr. 24 (2001) 100-107.

Kim, J.S.; Park, Y.; Lee, H. *Solubilities and vapor pressures of the water + lithium bromide + ethanolamine system*. J. Chem. Eng. Data 41 (1996) 279 - 281.

Koo, K.-K.; Lee, H.-R. *Solubilities, Vapor Pressures, Densities, and Viscosities of the(Water + Lithium Bromide + Lithium Iodide + Lithium Chloride) System.* J. Chem. Eng. Data 43 (1998) 722-725.

Koo, K.-K.; Lee, H.-R.; Jeong, S.; Oh, Y.-S.; Park, D.-R.; Back, Y.-S. *Solubilities, Vapor Pressures, and Heat Capacities of the Water + Lithium Bromide + Lithium Nitrate + Lithium Iodide + Lithium Chloride System.* Int. J. Thermodynamics. 20 (1999) 589-600.

Libotean, S.; Salavera, D.; Valles, M.; Esteve, X.; Coronas A. *Vapor-liquid equilibrium of ammonia + lithium nitrate + water and ammonia + lithium nitrate solutions from (293.15 to 353.15) K*. J. Chem. Eng. Data 52 (2007) 1050-1055.

Macriss, R.A.; Gutraj, J.M.; Zawacki, T.S. *Absorption fluids data survey: Final report on worldwide data.* Institute of Gas Technology, Illinois 1988.

Martín, A.; Bermejo, M.D. *Thermodynamic analysis of absorption refrigeration cycles using ionic liquid + supercritical CO_2 pairs*. J. of Supercritical Fluids 55 (2010) 852–859.

Montero, A. *Modelización de Sistemas de Refrigeración por Absorción con Captadores Solares de Concentración.* Tesis doctoral Universitat Rovira i Virgili, Tarragona 2012.

Rivera, C.O.; Rivera, W. *Modeling of an intermittent solar absorption refrigeration system operating with ammonia–lithium nitrate mixture*. Solar Energy Materials & Solar Cells 76 (2003) 417–427.

Reiner, R.H. *Evaluation of Ternary AmmoniaWater Fluids for GAX and Regenerative Absorption Cycles*. Report ORNL/CF-91/263; Oak Ridge National Laboratory: Oak Ridge, TN, 1991.

Reiner, R.H.; Zaltash, A. *Corrosion Screening of Potential Fluids for Ammonia Water Absorption Cycles.* Report ORNL/CF-92/41; Oak Ridge National Laboratory: Oak Ridge, TN, 1992.

Reiner, R.H.; Zaltash, A. *Densities and Viscosities of Ternary Ammonia Water Fluids*. ASME Winter Annual Meeting, 1993.

Rockenfeller, U.; Langeliers, J. *Aqueous Absorption Fluids*. Annual Report. Gas Research Institute. Chicago (1988).

Sen, M.; Paolucci, S. *Using Carbon Dioxide and Ionic Liquids for Absorption Refrigeration*. 7th IIR Gustav Lorentzen Conference on Natural Working Fluids, Norway (2006)

Steiu, S.; Salavera, D.; Bruno, J.C., Coronas, A. *A basis for the development of new ammonia–water–sodium hydroxide absorption chillers*. Int. J. of Refr. 32 (2009) 577-587.

Steiu, S.; Bruno, J.C.; Coronas, A.; San Roman, M. F.; Ortiz, I. *Separation of Ammonia/Water/Sodium Hydroxide Mixtures Using Reverse Osmosis Membranes for Low Temperature Driven Absorption Chillers.* Ind. Eng. Chem. Res. 47 (2008) 10020–10026.

Steiu, S.; Martínez-Maradiaga, D.; Salavera, D.; Bruno, J.C.; Coronas, A. *Effect of Alkaline Hydroxides on the VaporLiquid Equilibrium of Ammonia/Water and the Performance of Absorption Chillers.* Ind. Eng. Chem. Res. 50 (2011) 13037–13044.

Song, Y.; Chen, C.-C. *Symmetric Electrolyte Nonrandom Two-Liquid Activity Coefficient Model*. Ind. Eng. Chem. Res. 48 (2009) 7788–7797.

Sun, D.-W. *Comparison of the Performances of NH_3-H_2O, NH_3-$LiNO_3$ and NH_3-NaSCN Absorption Refrigeration Systems*. Energy Convers. and Mgmt 39 (1998) 357-368.

Zacarías, A. Transferencia de masa y calor en absorbedores adiabáticos con aplicación de la disolución nitrato de litio-amoniaco, Ph.D. Thesis, Universidad Carlos III de Madrid (2009).

Zhang, N.; Lior, N. *Development of a Novel Combined Absorption Cycle for Power Generation and Refrigeration*. J. Energy Resour. Technol. 129 (2007) 254-265.

Ziegler, F. *Absorption Cycle Basics revisited.* International Sorption Heat Pump Conference. Denver, USA (2005).

Chapter 2

Solubility of $LiNO_3$, NaSCN and $NaOH+H_2O$ in Ammonia

2.1. Introduction

Systems based on $NH_3/LiNO_3$ and NH_3/NaSCN working pairs can be activated at lower temperature heat sources than the ammonia/water systems at the same working conditions, what permits the use of solar thermal energy or low grade waste heat. Also, due to non-volatility of the salt, the necessity of rectification is avoided. On the other hand, the use of additives like NaOH to the conventional ammonia/water system increases the composition of ammonia in vapour phase at the outlet of the generator, reducing the necessity of rectification in the process.

The study of the solubility of these systems is an important task to establish the optimum composition and temperatures of the solution in the system in order to maximize the efficiency of the cycle avoiding crystallization of the solution before returning to the absorber, where the relation composition/temperature is the most unfavourable, as explained in *Chapter 1*.

Experimental solubility data of $LiNO_3$, NaSCN and ($NaOH + H_2O$) in ammonia available the literature is scarce, old and incomplete. Tsimbalist et al. (1983) studied the solubility of $LiNO_3$ in

NH_3 by isothermal method (no more details were given) at 278.15 K, 288.15 K, 298.15 K and 308.15 K, which corresponded to salt mass fractions 0.6175, 0.6955, 0.7090 and 0.7225 respectively, with no data of working pressure specified. Portnow and Dwilewitch (1937) also reported the solubility of the same mixture in all the range of salt compositions, with no data of the working pressure in the measurements. Blytas and Daniels (1962) measured the solubility of NaSCN in NH_3 by visual-polythermal method in all the range of ammonia composition but no experimental data was tabulated and the working pressure of the experiments was also not indicated. For the system NH_3/(H_2O+NaOH) no results of solubility of sodium hydroxide in water + ammonia solutions were found in literature.

In this study, the experimental measurement of solubility of $LiNO_3$, NaSCN and aqueous solutions of NaOH in liquid ammonia has been done in order to provide new useful data to literature, giving details of operating conditions and working pressure for maintaining the ammonia in liquid phase.

The solubility measurements have been carried out by means of a new experimental device designed and built for this work in GATE-CREVER group, based on visual-polythermal method and capable of working at moderate-high pressures.

The experimental device and methodology have been validated at atmospheric pressure with water/lithium nitrate system and at 20 bar with ammonia/lithium nitrate system. Also, an image processing treatment has been developed and compared with visual procedure for determining the solubility temperature in an attempt to provide a more objective criterion than visual detection.

2.2. Operating methodology and procedure

The methodologies for the experimental measurement of solubility are generally divided in two categories and its choice depends mainly on the characteristics of the components involved in the mixture and the purpose of the measurement:

- *Analytic methods:* The solubility is determined by analysing the composition of the saturated solution at a fixed pressure and temperature. Allow the determination of tie lines but presents technical problems and is more complex.

- *Synthetic methods*: A known composition mixture is prepared and the dependence of the phase behaviour with pressure and temperature is determined. They are suitable for determining phase boundaries.

Likewise, the experimental solubility can be carried out by two different methodologies:

- *Isothermal methods:* Consists in the determination of the solubility of a system at constant temperature, maintaining the solution of known composition oversaturated and with continuous stirring, while aliquots of solvent of known mass are added until there solute is completely solved.
- *Polythermal method:* It is based on the regular heating of an oversaturated solution at constant composition of salt and solvent. With constant stirring, the solute is gradually dissolved as temperature increases. The temperature at which the last crystal of solute is dissolved corresponds to solubility temperature.

The measurement of the solubility, either polythermal or isothermal method, can be carried out by non-visualization or by direct visualization of the experiment. Despite visual methods present some limitations of accuracy, they are good and specially appreciated in laboratory work due to its simplicity and versatility, but they can also be suitable for quick or complete studies of system phase behaviour.

Considering the characteristics of each of the different alternatives to determinate the composition and the solubility of the sample under study, this study has been performed by means of the synthetic method to determine the composition of the sample and the visual-polythermal method to determine the solubility temperature of the salts in water at constant composition of the sample.

The basis of the solubility determination by polythermal and visual methodology consists in the direct visual observation of the dissolution or crystallization of the solute into the solvent by means the procedure of heating and cooling the sample respectively. Since the amount of salt decreases when the temperature increases, the solubility temperature of the sample is reached when the dissolution of the salt crystal of salt is observed.

2.3. Experimental device description

The design and characteristics of a device built for measuring solubility of salts in ammonia under moderate-high pressure conditions becomes more complex than a device designed for working with water or low volatile solvents at atmospheric pressure.

The illumination and observation system is the most critical aspect to take into account when the device is developed. It is necessary to install windows of a special material like sapphire to resist high pressures. In some devices two windows are placed on opposite sides, one to be used for viewing the experiment and the other for illumination. This ensure a very effective visual observation (figure 2.1-a) (Pérez, 2007). The problem of these devices is that the pressurization system is outside the field of view; thus, part of the volume cannot be observed, causing blind volumes where phase change can appear but not be detected.

Another possibility consists of a device with only one window through which illumination and observation of the experiment is done. The pressurization system is located in the opposite side thus allowing the observation of the entire volume (figure 2.1-b) (Pérez, 2007). The experimental device used in this work is based in this configuration.

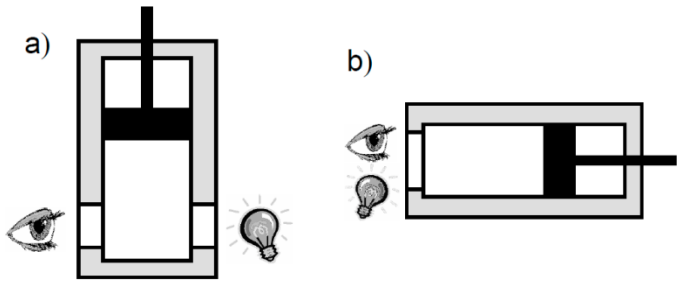

Figure 2.1. Cell configuration types for illumination and observation of solubility measurements under pressure conditions. a) Two opposite windows, b) One window (Pérez, 2007)

The experimental device consists of a stainless steel variable-volume cell with a sapphire window in one of its sides through which the illumination and visual observation of the experiment is carried out. The other side of the cell is connected to a hydraulic line, which is in turn connected to a manual hydraulic pressure generator. The measuring device was designed and built in-house based on the design of Pérez (2007). Figures 2.2 and 2.3 show a diagram and photograph of the equilibrium cell and the entire equipment used to measure solubility temperature of salts in liquid ammonia or mixtures of ammonia and water, respectively.

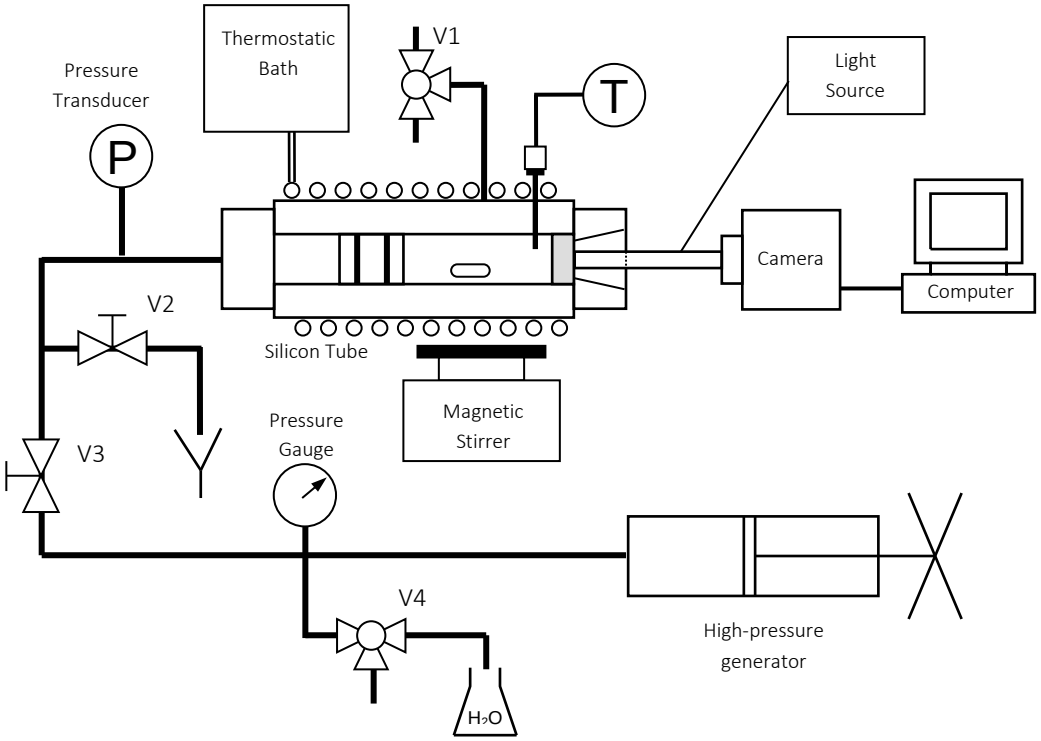

Figure 2.2. Diagram of the device for solubility temperature determination at moderate-high pressure

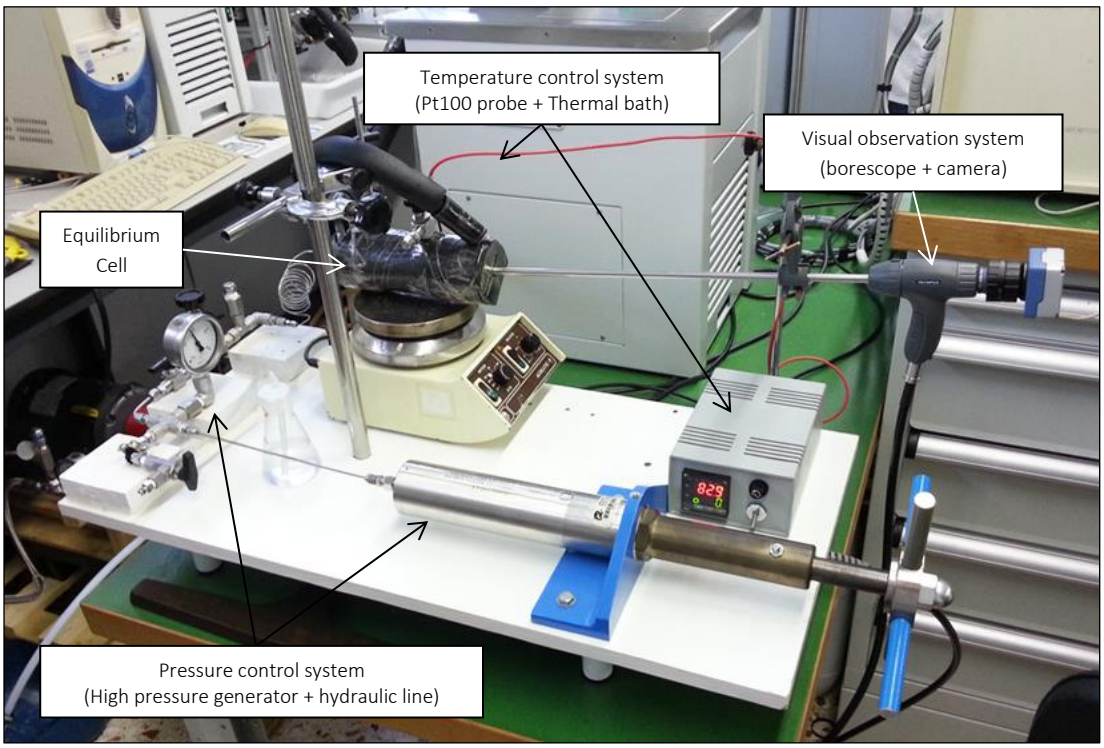

Figure 2.3. Entire equipment for experimental solubility temperature determination at moderate-high pressure

A detailed description of the equilibrium cell, the visual observation system and the temperature and pressure control systems is given in the following sections.

2.3.1. Equilibrium cell

The design of the equilibrium cell is the most important factor to consider because it must reach a number of requirements to obtain a successful experiment. It must be a watertight compartment, must be able to withstand high pressures and temperatures and at the same time must have the capacity to vary its internal volume. A small variation in the characteristics of its components (such as breakage or incorrect placement of the sealing o-rings) results in the loss of the sealing, causing ammonia leaks to the environment or to the hydrostatic line, thus changing the composition of the sample and ruining the experiment. The cylindrical equilibrium cell is built in stainless steel to resist high pressures and temperatures, as well as to make it compatible with the chemicals used, especially with ammonia. The inner chamber which houses the sample under study has a total length of 128 mm with an internal diameter of 14 mm. Figure 2.4 and 2.5 shows a photograph and diagram of the equilibrium cell with the different elements that constitutes it.

Figure 2.4. Equilibrium cell

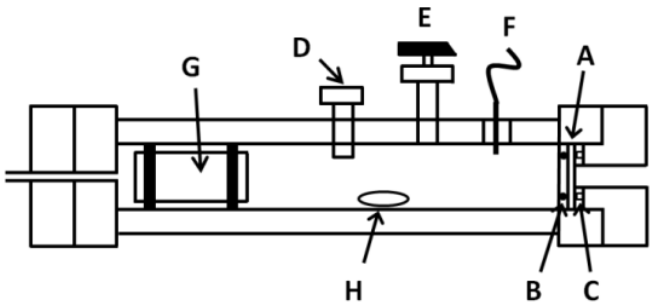

A: Sapphire window
B: EPDM o-ring
C: Teflon seal
D: Piston limit
E: Three-way valve
F: Pt100 probe
G: Piston
H: Magnetic stirrer

Figure 2.5. Schematic diagram of equilibrium cell

A movable piston (figure 2.6), also made of stainless steel and fitted with o-rings of ethylene propylene diene monomer rubber (EPDM), is used to modify the internal volume of the cell and is the responsible of providing the working pressure to the solution by its connection to a hydraulic line, which is in turn connected to the manual hydraulic pressure generator (figure 2.2).

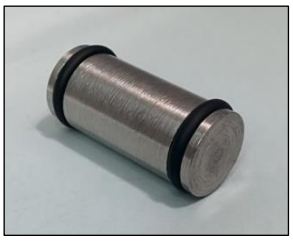

Figure 2.6. Movable piston

The piston dimensions are 30 mm length and diameter 13.7 mm, 0.3 mm narrower than the internal diameter of the equilibrium cell. Two EPDM o-rings with measures 10 mm x 2.5 mm, are placed in two grooves of 2.1 mm depth with the objective of providing mobility and at the same time to isolate the internal chamber of the cell from the hydraulic system to avoid mixing of both fluids. A screw is installed at 58 mm from the sapphire window to establish a limit to the piston movement and prevent an excess of pressure, which could cause the breakage of the o-rings or the sapphire window (figure 2.5-D). Thus, the useful volume of the internal chamber can change from 15.1 cm^3 to 8.9 cm^3.

The visual observation of the experiment is made through a circular sapphire window of 25 mm diameter (useful visualization diameter 10 mm) and 2mm thickness, which allows pressures up to 40 bar. In order to avoid possible ammonia leaks and/or the breakage of sapphire window, the window is located between o-rings of EPDM and teflon (2.5 mm x 14.85 mm).

The insertion of ammonia and water as well as the extraction of air is done by a three-way valve located at the top of the cell. The insertion of salts is done through the opposite side of the sapphire window where a screw cap is located. Finally, a scabbard is placed in the cell to allow an easy insertion and extraction of the platinum temperature probe Pt100 to prevent its breakage when the cell is cleaned.

2.3.2. Visual observation system

Due to the small dimensions of the sapphire window (10 mm diameter), direct visual observation of the experiment is not possible. For this reason, a rigid borescope (Olympus Series 5 R080-044-000-50) with source light (Olympus ILK-7B) is used.

A borescope is an optical device consisting of a rigid or flexible tube with an eyepiece on one end and a lens on the other. A lens captures the image and transmits it to the eyepiece by an optical relay, while surrounding optical fibres transmit light for illumination of remote object. Figure 2.7 depicts a typical rigid borescope.

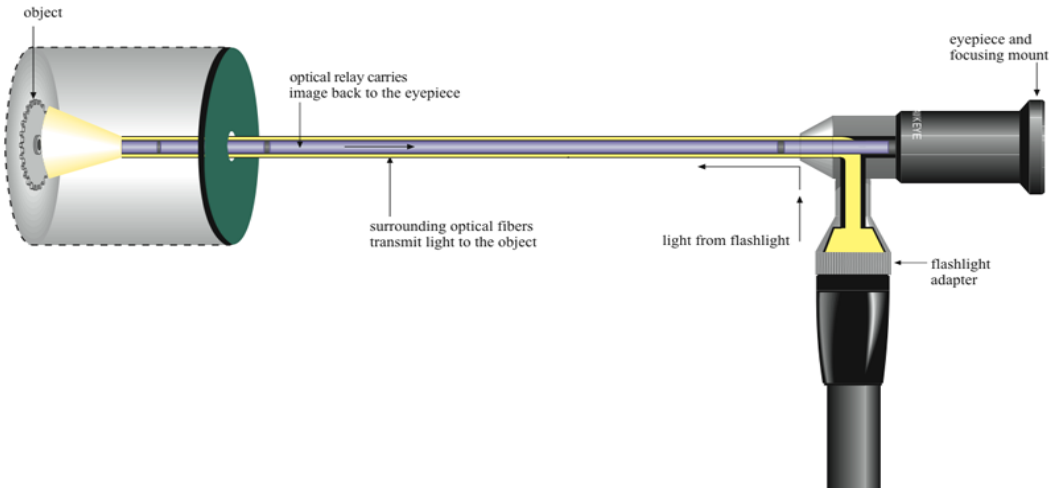

Figure 2.7. Diagram a typical rigid borescope with light source (www.gradientlens.com)

Instead of observing the experiment directly through the eyepiece, a camera Moticam 2000 2.0M is connected to the eyepiece in order to allow visualization and recording of the image with a personal computer using Moticam Images Plus 2.0 software.

Figure 2.8. Digital camera connected to borescope

This configuration also allows the determination of solubility temperature using directly the images taken from the camera, with a special processing in Matlab software. Figure 2.9 illustrates two examples of images taken from Moticam 2000 camera during dissolution of lithium nitrate in ammonia: a) salt in process of dissolution and b) salt completely dissolved.

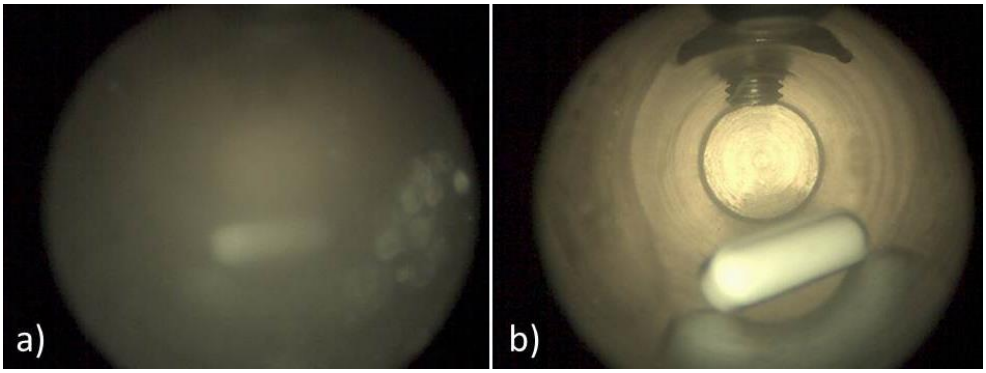

Figure 2.9. Images of the inside of the equilibrium cell: a) Unsolved NaSCN in ammonia at 20 bar. b) Completely solved NaSCN in liquid ammonia at 20 bar

2.3.3. Temperature control system

The temperature of the experiments is controlled externally with the thermal bath Julabo F33-EH (working temperature range between 243 K - 423 K, temperature stability ± 0.03 K and resolution ± 0.1 K) by means of recirculation of thermostatic fluid through silicon tube ($Ø_{int}$ = 8 mm) rolled over the cell and covered by thermal insulator.

The thermostatic fluid used is an aqueous solution of 85 % ethylene glycol because it provides the required range of working temperatures (237-400) K. Temperature is measured by a platinum probe Pt100 inserted to the cell through a scabbard and connected to a temperature indicator Kosmon PXR-4 with resolution ± 0.1 K. To ensure a correct temperature homogenization and a correct distribution and dissolution of the salt, the content of the cell is continuously agitated using a magnetic nucleus placed inside the cell and a magnetic stirrer P-Selecta AGIMATIC-N.

It is important to analyse the temperature homogeneity of the sample because some factors, such as the geometry of equilibrium cell or the non-thermostatization of sapphire window, generate a temperature gradient in the inner of the cell. Furthermore, since the temperature probe is not in direct contact with the sample, there exists a difference of temperature between the real temperature and the temperature reading of the probe. Therefore, the homogeneity has

been evaluated in the following way: the equilibrium cell is filled with water, a reference temperature probe is placed inside through the back of the cell, and the cell is sealed. Next, different experiments are carried out in a range of temperatures from 268 K to 353 K, with the reference probe placed at three different positions (0.5 cm, 3.5 and 8 cm from sapphire window) and constant stirring in the middle of the cell. The maximum temperature difference has been determined to be 0.4 K and has been considered in the calculation of the temperature uncertainty.

The working probe has been calibrated in the same range of temperatures by means of quadratic regression of the average reference temperature in the inner of the cell at the two positions nearest to the working probe (maximum temperature difference of 0.1 K), and the temperature of the working probe. The estimated expanded uncertainty (k = 2) of temperature has been determined to be 0.5 K (details in section 2.6.2)

2.3.4. Pressure control system

The pressure control system consists of a manual high-pressure generator (HiP model #87-6-5) connected to a hydraulic pressurized line with water as hydrostatic fluid. The pressure generator can operate at pressures up to 345 bar and has an internal chamber of 60 cm^3 which houses the hydrostatic fluid and pressurizes it with a piston movement by the rotation of a screw, allowing the increasing or decreasing of the pressure.

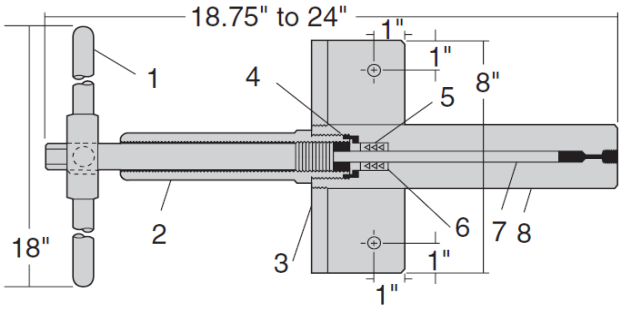

1. Handle
2. Gland nut
3. Support set-up
4. Upper packing washer
5. Gasket
6. Lower gasket washer
7. Axis
8. Body

Figure 2.10. Mechanical scheme of hydraulic pressure generator (HiP specification sheet)

The hydraulic pressure line is made in stainless steel (external diameter 1/8”) and contains a number of accessories which complete the pressure control system (figure 2.11):

- Three-way valve V4, which enables on one hand filling up the line with hydrostatic fluid, and on the other hand, to make vacuum to purge the air from the hydrostatic line in order to prevent the appearance of air bubbles which imply pressure fluctuations.
- Pressure gauge Baumer with pressure limit up to 40 bars (resolution ± 2 bar)
- Gate valve V3, which isolates the high-pressure generator and the fluid charging valve from the equilibrium cell.
- Air purge valve V2.

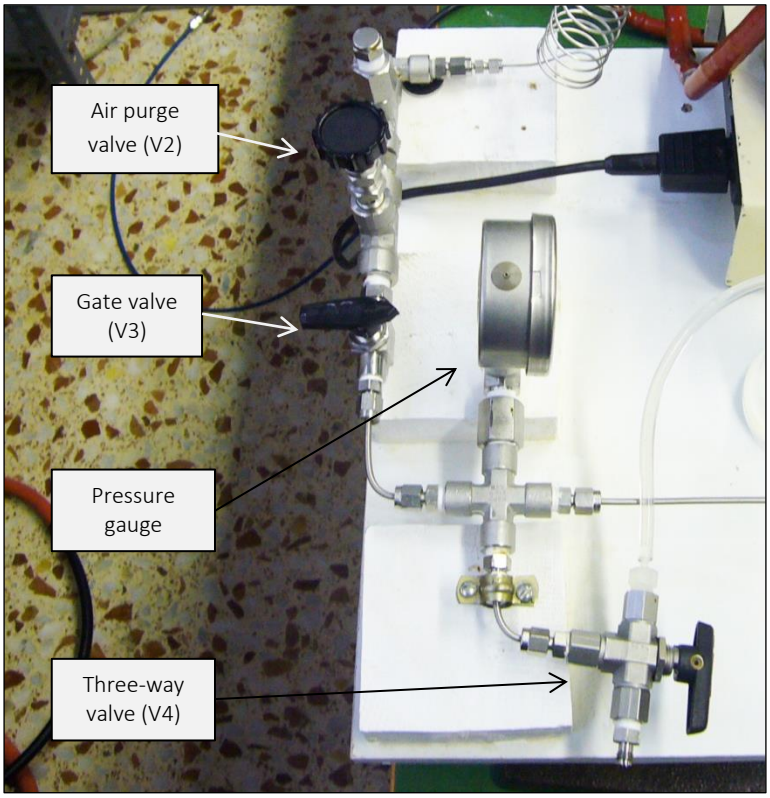

Figure 2.11. Elements of the hydraulic pressure line

The differential pressure between the hydraulic system and the inner of the cell has been evaluated by applying hydraulic pressure against atmospheric pressure. The piston was moved when the hydraulic pressure applied was approximately between 1 bar and 2 bar higher than atmospheric. This differential pressure cannot be considered important, because the objective of pressurizing the cell is to maintain the ammonia in liquid phase and the influence of this difference of pressure on the solid–liquid equilibrium is negligible.

2.4. Experimental methodology

The experimental procedure is divided in four phases: sample preparation and introduction into the equilibrium cell, preparation of the pressure system, solubility temperature measurement, and sample extraction and cell cleaning.

2.4.1. Chemicals

Lithium nitrate (purity ≥ 0.98) is supplied by Fluka. Sodium thiocyanate (purity ≥ 0.98) is supplied by Panreac. Compressed ammonia (purity 0.9998) is supplied by Carburos Metálicos. Milli-Q water (resistivity lower than 18.2 MΩcm) is used to prepare aqueous solutions. All chemicals are used without further purification. The salts are dried in an oven at 373 K for at least 24 h and maintained in a desiccator at room temperature before being used.

2.4.2. Sample preparation and introduction into equilibrium cell

The solution is constituted by two components: the solute which consists of $LiNO_3$, NaSCN or NaOH and the solvent, which can be water (for device validation at atmospheric pressure), ammonia or a mixture of both.

The preparation and insertion of the solute is carried out in the following way: the desired mass of salt is taken in a funnel for solids and is introduced through the back of the cell; then, a magnetic stirrer and the piston are placed inside and the cell is sealed and closed. The quantity of salt introduced into the cell is determined by mass difference with a balance Mettler AE260 DeltaRange (resolution ± 0.0001 g).

The preparation and insertion of the solvent changes depending if the fluid is in liquid phase (water) or vapour phase (ammonia):

a) Water as solvent

In this case, the desired mass of deionised water is taken in a syringe and is introduced into the cell through an injector connected to one side of the three-way valve V1 (figure 2.12).

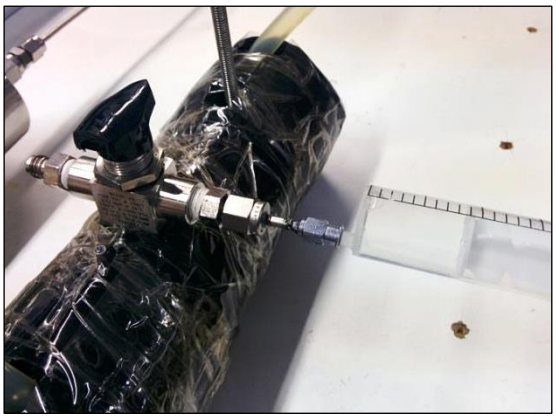

Figure 2.12. Insertion of water into equilibrium cell

Before introducing water, the cell is cooled to ~283 K in order to stabilize the temperature of the solution due to the exothermic reaction produced when water and lithium nitrate are mixed.

Air is purged from the cell and injector by creating vacuum for 5 minutes to avoid the presence of air or death volumes. One side of the three-way valve is connected to the vacuum pump and the opposite side is connected to the injector. On the injector orifice is placed a piece of parafilm, then valve is opened slowly towards the injector to purge the air from it taking care to avoid breakage of the parafilm. When the parafilm starts to deforms the valve is closed and is opened towards the vacuum pump for 1 minute. After that, the valve is closed and the vacuum pump is switched off. Finally, the syringe is connected to the injector breaking the parafilm and the valve is opened towards the syringe to introduce water.

b) Ammonia as solvent

In this second case, an auxiliary cylinder is used to contain and introduce into the cell the desired amount of ammonia. The cylinder is connected to a line with a coil, which is in turn connected to the equilibrium cell and the vacuum pump (figure 2.13).

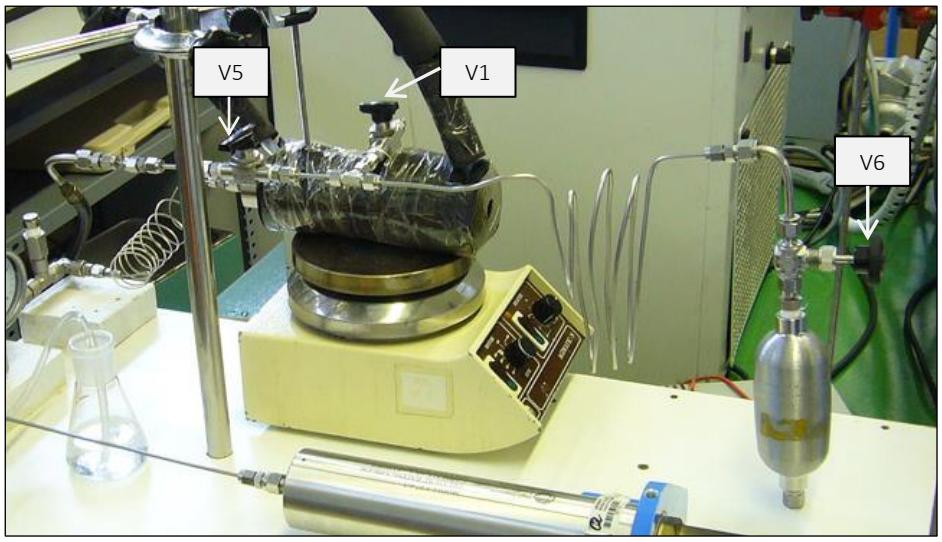

Figure 2.13. Insertion of ammonia into equilibrium cell

First of all, the air of the equilibrium cell and the coil-line is purged by creating vacuum for 5 minutes. Next, it is started the procedure of ammonia insertion into the cell. There are three main steps for introducing ammonia inside the cell and to determine the amount of ammonia introduced:

- Introduction of ammonia from the cylinder

  To introduce the ammonia into the cell it is necessary to produce a higher vapour pressure in the cylinder than the cell. Therefore, the cell is cooled to ~283 K, then the cylinder is heated and the coil is partially submerged in liquid nitrogen with a Dewar vessel. Valve V6 (figure 2.13) is opened slowly and progressively while valve V1 is opened. Cylinder is heated for 10 minutes to ensure that the maximum possible amount of ammonia passes to the cell.

  The low temperature of the cell also helps stabilize the temperature because the mixing of ammonia with salts produces also an exothermic reaction.

- Introduction of the remaining ammonia of the coil-line

  Valve V6 is closed and the Dewar vessel is removed from the coil. The line and coil are heated for 3 minutes and then V1 is closed.

- Introduction of possible ammonia remaining in the line into the cylinder

  With the cylinder at least half covered with liquid nitrogen, valve V6 is opened and the coil-line are heated again to assure all possible remaining ammonia returns to the cylinder.

c) Water + Ammonia as solvent

In the third case, the procedure to introduce both solvents is a mixture of the procedures explained previously, therefore the details are omitted here. First, in one side of the three-way valve is connected the coil-line which is in turn connected to the cylinder and to vacuum pump. Then the air is purged by creating vacuum and the cell is cooled to ~283 K. Next, water is introduced from a syringe connected to an injector connected to the other side of the three-way valve and ammonia is then introduced from the cylinder.

The quantities of the solvent, water or ammonia, introduced into the cell are determined by mass difference of the syringe or the cylinder by means of the balance Mettler Toledo PR2003 DeltaRange (precision ± 0.001 g).

The estimated expanded average uncertainty (k = 2) of mass fraction for systems with water and ammonia has been determined to be 0.0002 and 0.002 respectively (details in section 2.6.1)

2.4.3. Preparation of the pressure system

To avoid pressure fluctuations, it is necessary to purge the air from the hydrostatic line. The vacuum pump is connected to one side of the three-way valve V4 and vacuum is generated for 3 minutes. Since the other side is connected to a tube whereby is introduced water to the circuit, is necessary to extract the air from this tube by sequential movement of the three-way valve. Filling of the hydrostatic line is carried out by moving the three-way valve towards the tube placed inside a vessel with deionized water and turning the screw wheel in anti-clockwise direction.

2.4.4. Solubility temperature measurement

Once the sample is prepared, in case of working with ammonia as solvent, a fixed pressure is set to the desired value and is kept constant along the whole process by means of the high-pressure generator. For this work, a pressure of 20 bars is set to maintain the ammonia in liquid phase.

Being the solution oversaturated of salt and continuously stirred, the procedure for determining the solubility temperature is described as follows:

1) Initially the salt presents compacted blocks that require more temperature to be dissolved, for this reason first solubility temperature measurement is always higher than the real solubility temperature. Hence, a high enough temperature is set until the salt is completely dissolved. The temperature at which the solution is dissolved is maintained for 15 minutes to ensure a complete dissolution.
2) Next, a low temperature is set to cool the sample until reaching the complete precipitation of the solution at temperature T2.
3) The temperature is increased to a value 5 K higher than T2 and later in intervals of 2 K until complete dissolution in the interval T3-T4 is achieved, waiting 15 minutes between each change of temperature to ensure thermal stabilization.
4) The sample is again cooled by setting a temperature 2 K lower than T2 until the precipitation is reached at T4.
5) Temperature is set to T3 and is increased at intervals of 0.5, 0.2 and 0.1 K progressively as the amount and size of the salt decreases, waiting 15 minutes between them to guarantee thermal stabilisation.
6) The temperature in which no crystal is visible in the solution corresponds to the solubility temperature.
7) To assure reproducibility, steps 4-6 are repeated at least two more times.

2.4.5. Sample extraction and cell cleaning

The method of extracting the solution from the cell varies depending on the solvent used, being the procedure carried out in one or another way:

When an experiment is made with ammonia as solvent, pressure needs to be decreased before extracting ammonia by turning the screw counter clockwise. Thus, one end of a flexible tube is connected to the three-way valve V1 (fig. 2.13) and the other end is immersed in a bottle filled with water. When the valve V1 is opened, ammonia becomes vapour phase, and by pressure difference it passes to the bottle with water where is absorbed. Once evacuated most of the

ammonia, equilibrium cell is disassembled by the rear cap and the rest of the residue is emptied in a proper container.

On the other hand, when an experiment is performed with water as solvent, the procedure consists on the disassembling of the equilibrium cell, extracting the mixture through the rear cap and emptying it in the proper container. The equilibrium cell and the piston with o-rings are cleaned by means of hot water with soap and acetone, and finally they are dried.

2.4.6. Image processing

In order to avoid the subjective criterion of the visual method, an image processing has been developed using Matlab software (*Annex A*). This treatment is based on quantification of the pixel colours from the recorded image in the inner of the equilibrium cell, which varies depending whether crystals of salt are present or not, and its comparison to the pixel colours of the recorded image when the salt is completely dissolved.

In this procedure, a blank (base) image is recorded after first complete dissolution of the salt in solvent. Next, the procedure is followed as previously explained. Then, multiple images are systematically recorded at each temperature change along the experiment. Only red channel from RGB (red-green-blue) range of each image is extracted and compared with those of the blank image because shows higher contrast between the salt crystals and the cell. The result shows the presence of the salt unsolved by means of red pixels (figure 2.14). The stirrer is sent to the end of the cell and is stopped when the pictures are taken to avoid the interference in the image processing, being only a specific part of the cell bottom analysed. Solubility temperature is determined when quantification of red pixels in the resultant image is negligible.

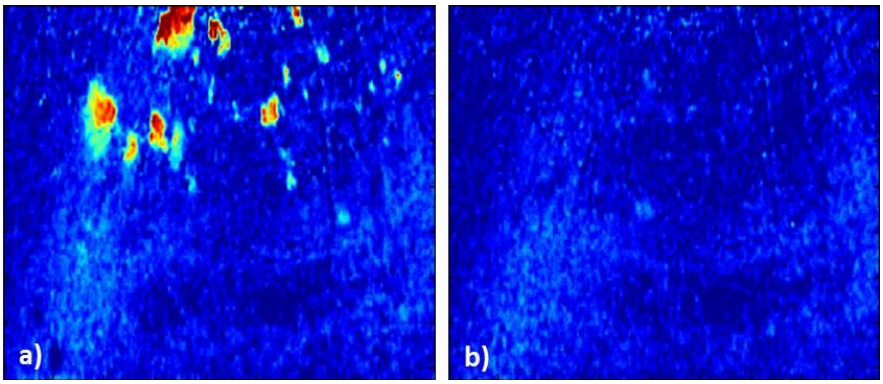

Figure 2.14. Processed sample images: a) Non-solved $LiNO_3$ in water; b) Solved $LiNO_3$ in water.

Few red pixels always appear in the image but cannot be associated with the presence of salt because they also appear in the blank image. Thus, it has been considered the salt completely dissolved in solvent when the image has a maximum of 30 red pixels. The choice of this amount of pixels has been carried out through empirical deductions. For example, in figure 2.15 the number of red pixels, which indicate the presence of salt, are quantified at temperature intervals of 0.1 K, for a $H_2O/LiNO_3$ mixture with a salt mass fraction of 0.6166. Using the criterion selected, it can be concluded from this figure that the temperature at which the salt is dissolved is 323.6 K. Image processing was only performed for the $H_2O/LiNO_3$mixture.

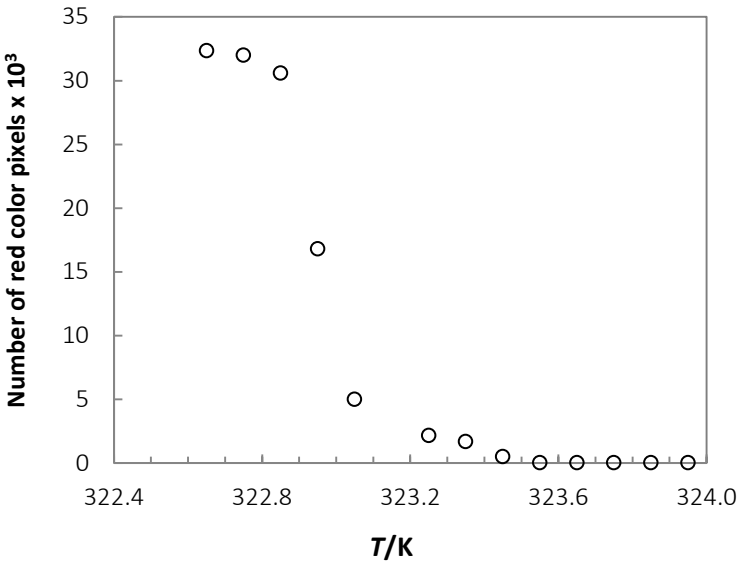

Figure 2.15. Number of red colour pixels at several temperatures for $H_2O/LiNO_3$ mixture with 0.6166 salt mass fraction

2.5. Experimental results

2.5.1. $H_2O/LiNO_3$ system

2.5.1.1. Visual method

In order to test the measurement trueness at atmospheric pressure, solubility of $LiNO_3$ in water has been measured and compared with literature data (Tsimbalist et al, 1983; Donnan and Burt, 1903; Campbell and Bailey, 1958; Berthet and Counioux, 1990; Zeng et al., 2008). Table 2.1 and figure 2.16 show the solubility temperature results and its comparison with reported literature

data in a range of lithium nitrate mass fraction from 0.35 to 0.64, which corresponds to a range of solubility temperatures from 279 K to 340 K.

The solubility temperature increases as usual with the salt composition but not in the same way for the whole range. The experimental data obtained in this work fits very well in all the range of salt compositions measured with reported data of Donnan and Burt (1903). For a salt mass fraction up to 0.60 there is also good agreement with data reported by the rest of authors, but for higher compositions there exist a big discrepancy between the experimental values of this work, Donnan and Burt (1903), and the values of the other authors.

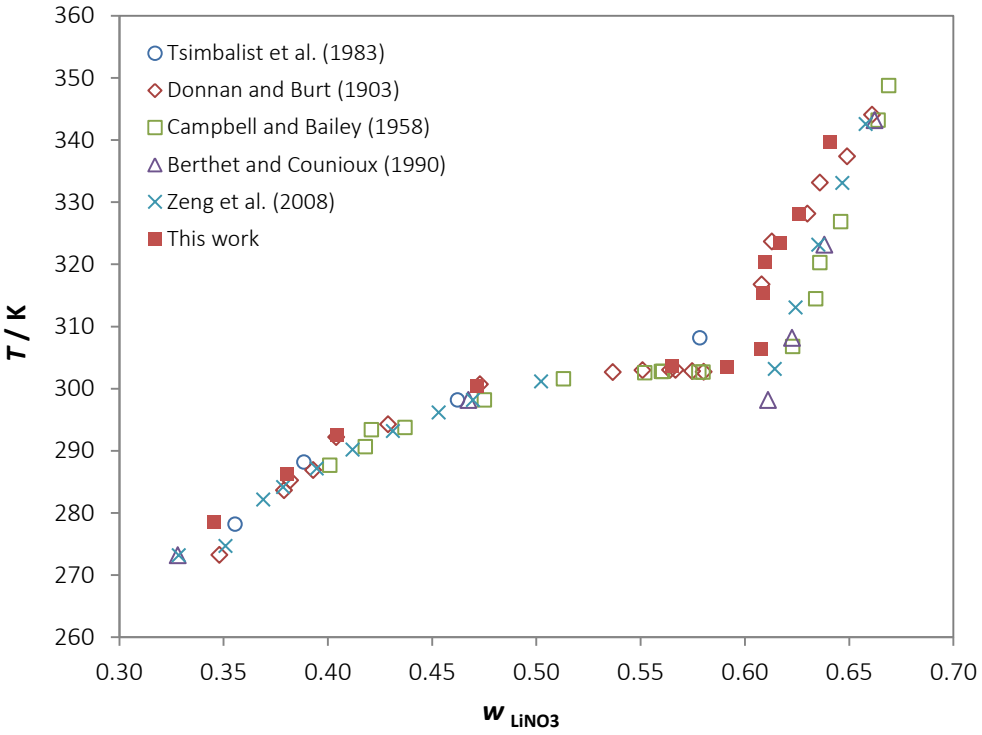

Figure 2.16. Solubility of lithium nitrate in water at atmospheric pressure

The tendency of the points in figure 2.16 presents a turning point associated to a transition between different salt hydration states. For salt mass fractions from 0.345 to 0.600 all the authors agree with the existence of trihydrate solid phase, $LiNO_3 \cdot 3H_2O(s)$, but for higher compositions there are some discrepancies. While Donnan and Burt (1903) reported the existence of hemihydrate solid phase, $LiNO_3 \cdot 0.5H_2O(s)$, in the interval of salt mass fraction from 0.608 to 0.636 and anhydrous solid phase, $LiNO_3(s)$, for higher compositions, the rest of authors dismissed the existence of the hemihydrate solid phase and only reported the existence of the anhydrous phase for salt mass fractions higher than 0.600.

Table 2.1. Solubility temperature of $LiNO_3$ in H_2O

w $LiNO_3$	T / K
0.3455	278.6
0.3806	286.2
0.4026	292.5
0.4715	300.3
0.5653	303.6
0.5913	303.5
0.6078	306.3
0.6086	315.4
0.6098	320.4
0.6166	323.4
0.6259	328.1
0.6382	339.7

2.5.1.2. Image processing method

As explained in section 2.4.6, a new method for measuring solubility temperature based on an image processing has been proposed with the aim of providing a more objective criterion than the visual method. Table 2.2 shows, for the same composition of salt, a comparison of the results obtained of solubility temperature by visual and image processing method.

Table 2.2. Comparison of solubility temperature by visual and image processing methods

w $LiNO_3$	T / K Visual	T / K Image Processing	ΔT
0.3806	286.2	286.0	-0.2
0.4026	293.7	293.5	-0.2
0.4715	300.3	300.2	-0.1
0.6098	320.4	320.4	-0.1
0.6159	323.6	323.5	0.0
0.6166	323.4	323.6	+0.2
0.6259	328.1	328.1	-0.1

There is a good agreement between both methods, with a maximum temperature difference of 0.2 K, which is an acceptable value, being in almost all cases the higher temperature obtained by

the visual method. The reason of this difference lies in the fact that this method cannot detect the minimal illumination changes of the sample when is very close to the solubility point.

2.5.2. $NH_3/LiNO_3$ system

The solubility measurements of $LiNO_3$ in liquid ammonia have been performed to validate the measurements under pressure conditions (20 bar) and also, to provide new useful experimental data since only two old references are available in literature (Tsimbalist et al., 1983 & Portnow and Dwilewitch, 1937). In both references the working pressure is not specified and the data reported by Tsimbalist et al. doesn't represent all the composition range studied.

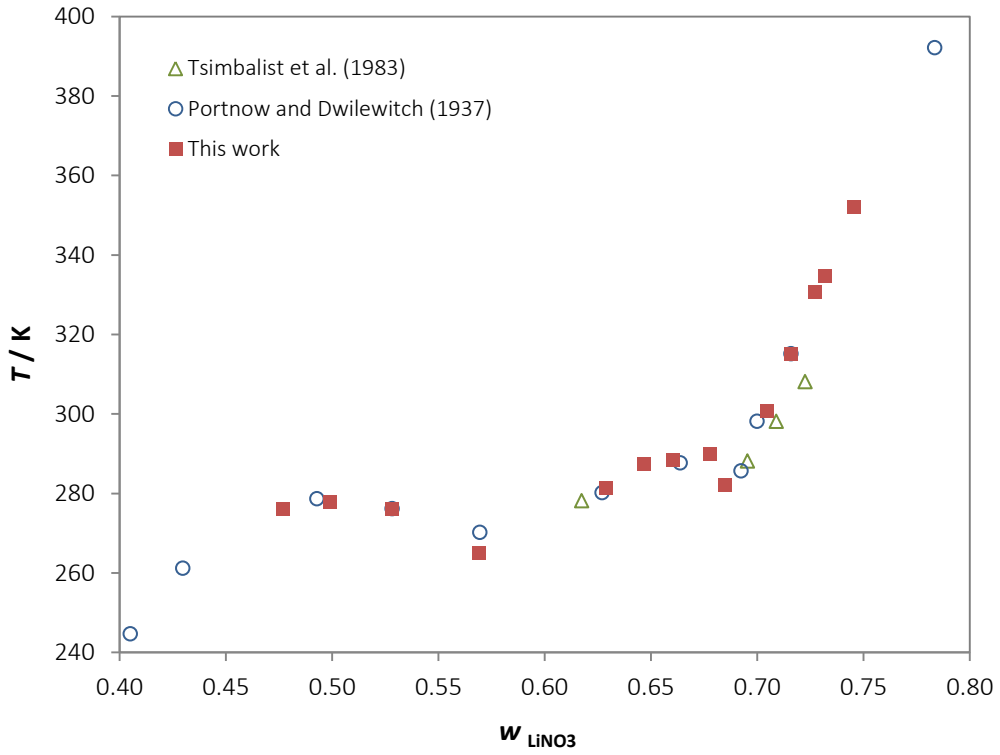

Figure 2.17. Solubility of lithium nitrate in liquid ammonia at 20 bar

Table 2.3 shows tabulated values of the experimental solubility temperature obtained. Figure 2.17 compares the results obtained with those reported in literature in a range of $LiNO_3$ mass fraction from 0.48 to 0.78, which corresponds to a range of solubility temperatures from 276 K to 352 K.

Table 2.3. Solubility temperature of $LiNO_3$ in NH_3 at 20 bar

w $LiNO_3$	*T* / K
0.4768	276.0
0.4988	277.9
0.5284	276.0
0.5689	265.0
0.6291	281.3
0.6470	287.3
0.6603	288.5
0.6780	289.9
0.6847	282.2
0.7047	300.7
0.7160	315.2
0.7272	330.8
0.7319	334.7
0.7458	352.0

As it can be observed in figure 2.17, the experimental points present three well differenced tendencies, which are due to different molecular associations of the salt with the solvent. Portnow and Dwilewitch (1937) reported the existence of three different solid phases in equilibrium depending on the composition of lithium nitrate. First one corresponds to $LiNO_3 \cdot 4NH_3$(s) for a range of salt mass fraction from 0.357 to 0.570, second one to $LiNO_3 \cdot 2NH_3$(s) for salt mass fraction up to 0.692, and the last one to $LiNO_3$(s) for higher mass fractions.

In the areas where the salt is associated to *n* molecules of solvent, there is very good agreement with both literature references. When the solid phase consists only of solid salt there is good agreement with reported values by Portnow and Dwilewitch (1937) but differences with values of Tsimbalist et al. (1983) increase. The reason of this difference could lie in the steep slope of the composition range, that is to say, small differences in ammonia composition lead to considerable variations in solubility temperature, which affects the accuracy of the measurements.

2.5.3. NH_3/NaSCN system

The solubility of sodium thiocyanate in liquid ammonia at 20 bar has been measured in a salt mass fraction range from 0.528 to 0.684, which cover temperature range from 263.8 K to 333.5 K. The results obtained are shown in figure 2.18 and table 2.4.

For this mixture, Blytas and Daniels (1962) reported a phase diagram of temperature versus composition of NaSCN in liquid ammonia, but no experimental data were tabulated and working pressure is unknown. For this reason, reference data shown in figure 2.18 are the values directly extracted by interpolation from the reported plot. The uncertainties associated to the interpolation have been estimated to be 0.9 K for the temperature and 0.009 for mass fraction of sodium thiocyanate.

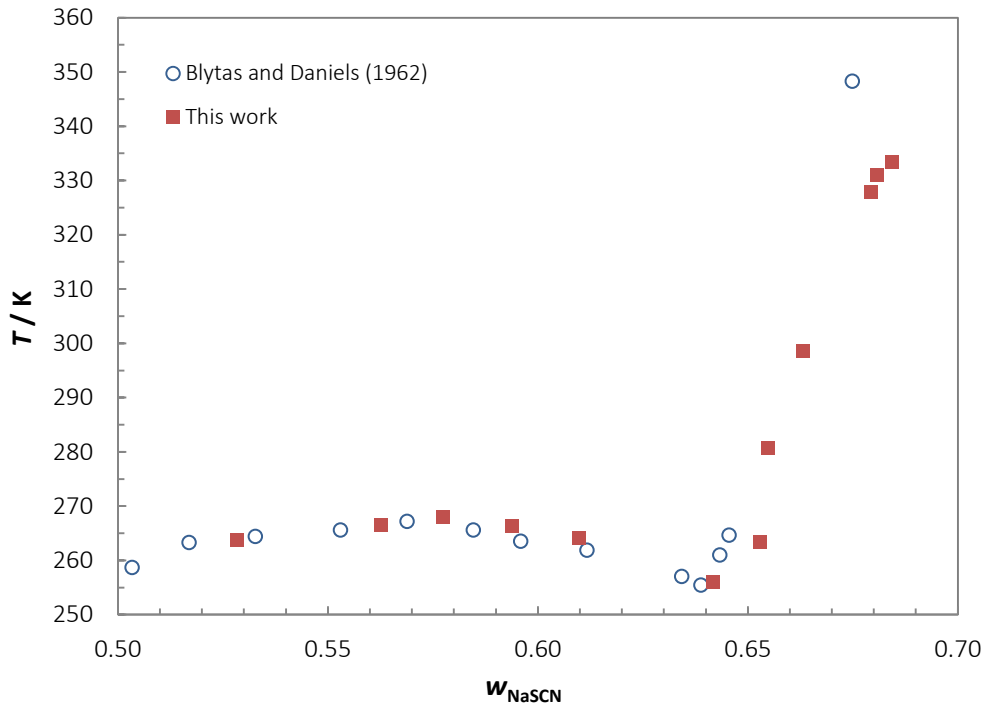

Figure 2.18. Solubility of sodium thiocyanate in liquid ammonia at 20 bar

In this case the points present two different behaviours associated with two different solid phases. Blytas and Daniels (1962) reported the existence of $NaSCN{\cdot}3.5NH_3$(s) solid phase in the range from 0.437 to 0.639 in salt mass fraction with a soft concave curve behaviour, and NaSCN(s) solid phase for higher salt mass fractions with a pronounced straight line tendency.

Table 2.4. Solubility of NaSCN in NH_3 at 20 bar

w NaSCN	*T*/K
0.5283	263.8
0.5627	266.6
0.5774	268.0
0.5940	266.3
0.6099	264.1
0.6418	256.0
0.6529	263.5
0.6549	280.8
0.6632	298.6
0.6793	327.9
0.6809	331.0
0.6843	333.5

For a range of salt mass fraction up to 0.642 there is good agreement with literature data. However, for higher salt compositions it cannot be done a proper comparison due to the scarce and inaccurate data available. It can however be noted that as the composition of salt increases the deviation with the experimental values of this work also increases. The differences at the highest compositions and temperatures could lie in the working pressure of reference data. Blytas and Daniels didn't report any pressure control in their experiments and in those conditions the vapour pressure corresponds to a maximum approximate value of 6 bar (Chaudhari et al., 2011). Thus, if there is no pressure applied in the system, not all the ammonia remains in liquid phase and therefore the composition of salt increases, causing the real point to shift rightwards following the same tendency that the experimental values of this work.

2.5.4. NH_3/(H_2O+NaOH) system

Initially, the purpose of the solubility study of NaOH in H_2O+NH_3 was to measure the solubility temperature at different salt mass compositions. However, the study could not be performed in this way because for a certain composition of ammonia and water, sodium hydroxide presents a composition that represents its solubility limit in the solution that causes the impossibility to dissolve it by increasing temperature. For a solution with a mass fraction 0.3 of ammonia and 0.7 of water + sodium hydroxide, a sodium hydroxide mass fraction of 0.05 supposed the impossibility to

be crystallized at a temperature of 262 K, and at a sodium hydroxide mass fraction of 0.06 supposed the impossibility to be dissolved at temperatures up to 363 K.

The most probable hypothesis of this behaviour can be explained as follows: The solubility of sodium hydroxide in water is based on the attraction forces of the Na^+ ion and dipoles of water (figure 2.19). When these forces are sufficiently intense to break interionic forces of the salt it is produced the dissolution. On the other hand, NH_3 interacts with water molecules creating NH_4OH and hydrogen bonds between free hydrogen radicals of ammonium and water (figure 2.20). The Na^+ cation and the NH_4^+ compete for the association to water molecules, and due to the limited amount of water available, it results in a limited number of Na^+ that can be dissolved in water. Thus, this limit corresponds to the limit of solubility of sodium hydroxide in a certain composition of water and ammonia mixture.

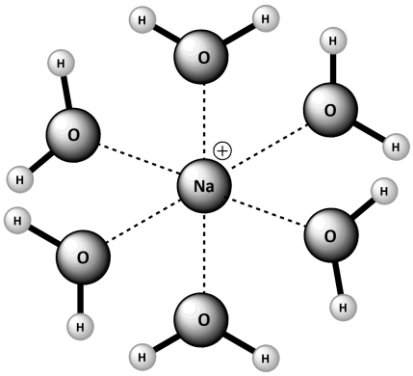

Figure 2.19. Ions Na^+ in water solution

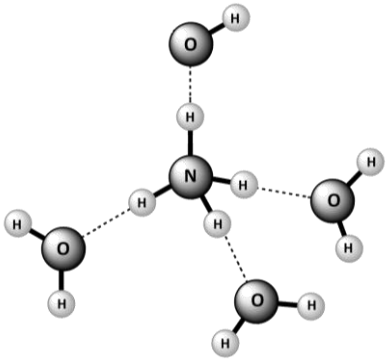

Figure 2.20. NH_4OH in water solution

Given the impossibility of measuring the solubility temperature of different compositions of NaOH in a solution with constant composition of NH_3 and (H_2O+NaOH), it has been performed a study to determine the maximum composition of ammonia which allows a certain composition of salt in the water + salt solution without salt precipitation. The results obtained for a range of NaOH mass fraction from 0.02 to 0.15 are shown in figure 2.21.

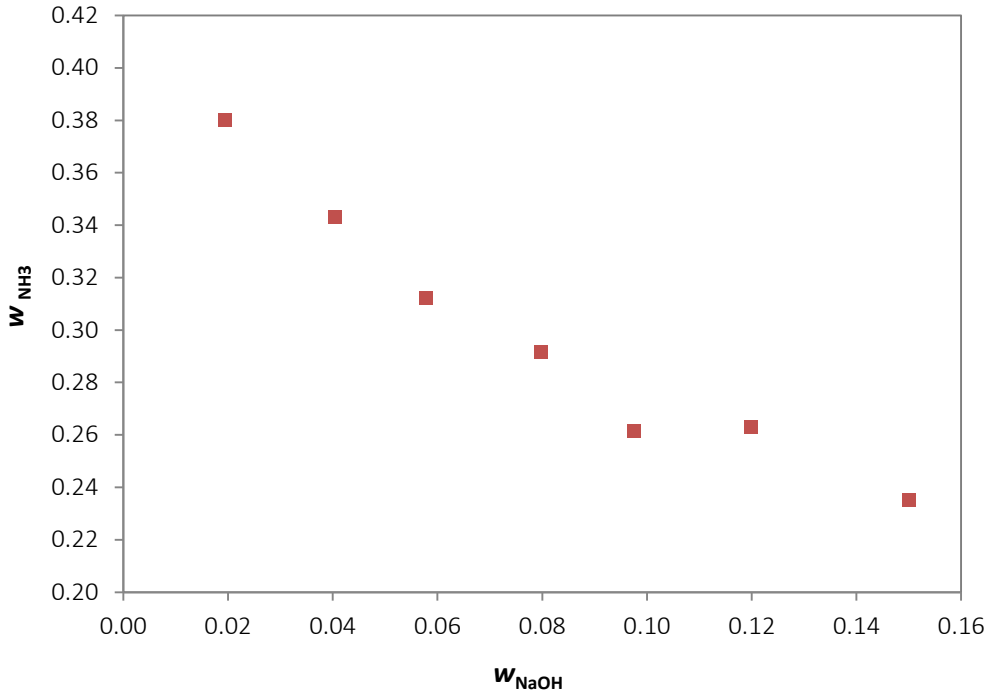

Figure 2.21. Solubility of ammonia in water + sodium hydroxide solutions. T = 288 K

Table 2.5. Solubility of NH_3 in H_2O+NaOH solutions. T = 288 K

w NaOH	*w* NH_3
0.0194	0.3801
0.0404	0.3426
0.0578	0.3118
0.0799	0.2918
0.0975	0.2615
0.1198	0.2631
0.1504	0.2354

For each NaOH composition analysed, the corresponding value of ammonia composition represents the solubility limit of the solution. Higher mass fractions of ammonia or sodium hydroxide cause the precipitation of the solution, being impossible to solubilise with temperature. At the beginning of the experiment, the temperature was set to (286-288) K to facilitate the insertion of ammonia in the equilibrium cell and later the temperature was increased up to 363 K but no change was found in the solubility of the NaOH, for this reason, a constant temperature of 288 K was maintained for all the experiments.

At the system conditions, all the solutions present a vapour pressure near to atmospheric (Salavera et al., 2005), thus, it is not necessary to increase the pressure of the system. To assure and prove this fact an experiment was done in which the ammonia was in a composition very near to precipitation point. Then the pressure was increased up to 20 bar and as there was no change in solubility it was concluded that there was no ammonia in the vapour phase.

2.6. Uncertainty of measurements

2.6.1. Mass fraction uncertainty

The uncertainties corresponding to the salt mass fraction of the different systems analysed are associated to the uncertainty sources provided by the manufacturer of the balances Mettler AE260 DeltaRange and Mettler Toledo PR2003 DeltaRange (resolution, calibration, linearity, accuracy and reproducibility) used to measure the mass of the components of the mixture.

Table 2.6 lists the uncertainties obtained for each system. It includes the maximum and average uncertainty of all the samples prepared.

Table 2.6. Maximum and average mass fraction uncertainties of analysed systems

	$H_2O/LiNO_3$	$NH_3/LiNO3$	$NH_3/NaSCN$	$NH_3/(H_2O+NaOH)$	
	w $LiNO_3$	*w* $LiNO_3$	*w* NaSCN	*w* NH_3	*w* NaOH
Maximum	0.0003	0.0024	0.0021	0.0026	0.0002
Average	0.0002	0.0017	0.0017	0.0021	0.0002

2.6.2. Temperature uncertainty

The uncertainty of the temperature corresponds to the uncertainties associated to the resolution and calibration and of the thermometer Kosmon PXR-4 connected to a probe Pt100, as well as the homogeneity, stability and repeatability of the temperature measurements along the experiments. The expanded uncertainty (k = 2) obtained is 0.5 K. A detailed explanation of the uncertainty calculation is presented in *Annex B*.

2.7. Conclusions

In this work, it has been designed and built a new experimental device based on the visual-polythermal method for the determination of solubility temperature of inorganic salts in liquid ammonia or mixtures of ammonia and water at pressures up to 40 bar.

The experimental device and methodology have been validated at atmospheric pressure with the system $H_2O/LiNO_3$ in a range of lithium nitrate mass fractions from 0.35 to 0.64 which corresponds to a range of solubility temperatures from 279K to 340 K. The experimental solubility data obtained is in good agreement with reported literature data for mass fractions of lithium nitrate up to 0.60, obtaining lower deviations than the experimental temperature uncertainty value (0.5 K) compared with reported data of Donan and Burt (1903). However, for higher mass fractions there is a remarkable deviation of experimental solubility with those reported by most of the authors, obtaining only good agreement with reported data of Donnan and Burt.

The experimental device has been evaluated under pressure conditions by the measurement of solubility temperature of $LiNO_3$ in ammonia. It also provides new useful information because the reported data is scarce, old and at unknown working pressure. Solubility data have been analysed in a range of salt mass fraction from 0.48 to 0.78 which corresponds to a range of solubility temperatures from 276 K to 352 K. The solubility results are in good agreement with those reported in literature, obtaining in most of the points lower temperature deviations than the uncertainty temperature of the equipment.

The solubility temperature of sodium thiocyanate in liquid ammonia at 20 bar has been measured in a salt mass fraction range from 0.53 to 0.69, which cover a solubility temperature range from 263.8 K to 329.8 K. The results could not be properly compared with those reported by Blytas and Daniels (1962) because they only reported a phase diagram of temperature versus composition and no experimental data were tabulated. The solubility temperature uncertainty of the interpolation of the points (0.9 K) was bigger than the experimental solubility temperature uncertainty.

Due to the solubility limit that NaOH presents in the water and ammonia solutions, it was analysed the maximum composition of ammonia which allows a constant composition of sodium hydroxide in the water + salt solution without salt precipitation. The results were performed for a salt mass fraction range from 0.02 to 0.15, obtaining a limit of ammonia from 0.38 to 0.235.

To avoid the subjective criteria in the determination of the solubility temperature by the visual method, a new method based on the image processing treatment has been developed. In this treatment, the pixel colours of the recorded image in the inner of the equilibrium cell are quantified and compared to the pixel colours of the recorded image when the salt is completely dissolved. The comparison of the results obtained in the system $H_2O/LiNO_3$ by the visual method and the image processing method shows a maximum difference in solubility temperature of 0.2 K which is an acceptable value and is under the measurement uncertainty. Thus it can be concluded that the image processing method is suitable to perform measurements of solubility temperature.

From the results obtained at atmospheric and moderate-high pressure, it can be concluded that the experimental device and the visual and image processing methodologies are suitable for measuring the solubility of salts in aqueous and non-aqueous solvents at pressures up to 20 bar.

2.8. References

Blytas, G.C.; Daniels, F. *Concentrated Solutions of NaSCN in Liquid Ammonia. Solubility, Density, Vapor Pressure, Viscosity, Thermal Conductance, Heat of Solution and Heat Capacity.* J. Amer. Chem. Soc. 84 (1962) 1075-1083.

Berthet, J.; Counioux, J.J.; Floreancing, A.; Cohen-Adad, R. *Les isothermes −25, 0, 25, 35, 50 et 70°C du système ternaire H_2O–$LiNO_3$–$Al(NO_3)_3$.* Bull. Soc. Chim. Fr. 616 (1990).

Campbell, A.N.; Bailey, R.A. *The system lithium nitrate-ethanol-water and its component binary systems*. Canadian J. Chem. 36 (1958) 518-536.

Chaudhari, S.K.; Salavera, D.; Coronas, A. *Densities, Viscosities, Heat Capacities, and Vapour Liquid Equilibria of Ammonia + Sodium Thiocyanate Solutions at Several Temperatures.* J. Chem. Eng. Data 56 (2011) 2861–2869.

Donnan, F.G.; Burt, B.C. *The solubilities and transition-points of lithium nitrate and its hydrates*. J. Chem. Soc. Trans. 83 (1903) 335.

Pérez, E. *Equilibrio de fases y solubilidades en fluidos supercríticos*. Tesis doctoral, Universidad Complutense de Madrid, 2007.

Salavera, D.; Chaudhari, S.K.; Esteve, X.; Coronas, A. *Vapor-Liquid Equilibria of Ammonia + Water + Potassium Hydroxide and Ammonia + Water + Sodium Hydroxide Solutions at Temperatures from (293.15 to 353.15) K*. J. Chem. Eng. Data 50 (2005) 471-476.

Seidell, A. *Solubilities of Inorganic and Metal Organic Compounds*. 4th ed., Van Nostrand Company, New York, 1958.

Tsimbalist, A.O.; Prudnikov, A.I.; Orekhov, I.I. *Solubility in a Lithium Nitrate - Ammonia - Water System.* Zh. Prikl. Khim. 56 (1983) 167.

Zeng, D.; Ming, J.; Voigt, W. *Thermodynamic study of the system ($LiCl + LiNO_3 + H_2O$).* J. Chem. Thermodyn. 40 (2008) 232– 239.

Chapter 3

Solubility Modelling of $H_2O/LiNO_3$, $NH_3/LiNO_3$ and NH_3/NaSCN Systems

3.1. Introduction

A variety of models for the description of electrolyte solutions have been developed over the last decades. However, only few models allow a reliable description of solvent activity coefficients up to high salt compositions. In this context, once the solubility temperature of $H_2O/LiNO_3$, $NH_3/LiNO_3$ and NH_3/NaSCN systems has been experimentally measured in *Chapter 2*, in order to make a comparison of the modelling procedure for aqueous or non-aqueous solvents, in the following study the solid-liquid equilibrium has been modelled by means the activity coefficient models LIQUAC (for systems with water as solvent), and Electrolyte Nonrandom Two-Liquid (E-NRTL) (for systems of ammonia as solvent).

For system $H_2O/LiNO_3$ the solubility modelling has been performed in a salt mass fraction range between 0.323 and 0.666, for $NH_3/LiNO_3$ system between 0.41 and 0.75, and for NH_3/NaSCN between 0.51 and 0.69. The modelling of $NH_3/(H_2O+NaOH)$ couldn't be performed due the impossibility to measure the solubility temperature at different salt compositions (explanation in Chapter 2).

3.2. Solid-liquid equilibrium

In aqueous or non-aqueous electrolyte systems the solid phase can be associated with various numbers of solvent molecules (in case of water are called hydrates). The equilibrium between the solvent and the solid phase in dissolution, which consists of v_+ cations C, v_- anions A, and n molecules of m solvent, can be expressed as the following reaction:

$$C_{v_+}A_{v_-} \cdot n_{\,\mathrm{m}}(s) \leftrightarrow v_+C + v_-A + n_{\,\mathrm{m}}\,(l) \tag{3.1}$$

The condition of chemical equilibrium corresponds to an expression that relates the Gibbs free energy (ΔG) with chemical potential (μ) and in which the sum of the chemical potential of the reactants is equal to the sum of the chemical potentials of the products:

$$\Delta G = v_+\,\mu_c + v_-\,\mu_a + n\,\mu_{\mathrm{m}} - \mu_{\mathrm{cv_+\,av_-\cdot n\,m}} = 0 \tag{3.2}$$

$$\mu_{\mathrm{Cv_+Av_-\cdot n\,m\,(s)}} = v_+\,\mu_{\mathrm{c}} + v_-\,\mu_{\mathrm{a}} + n\,\mu_{\mathrm{m\,(l)}} \tag{3.3}$$

For the thermodynamic study of the non-ideal solutions it is necessary an expression of chemical potential of the components of a real solution similar to the chemical potentials of an ideal solution. This is achieved by the introduction of the a dimensionless function activity a_i:

$$\mu_i = \mu_i^{\mathrm{o}} + RT\ln(a_i) \tag{3.4}$$

where μ_i^o is the chemical potential in the standard state and the activity is defined as:

$$a_i = \gamma_i \cdot x_i \tag{3.5}$$

The activity coefficient γ_i represents a measure of the real behaviour deviation regarding ideal behaviour in which γ_i = 1. The comparison between the expressions of chemical potential of a component in an ideal solution and in a real solution shows that, in ideal solutions the activity corresponds to the mole fraction ($a_i = x_i$) and the activity of a component in its standard state is the unit ($a_i^{\mathrm{o}} = 1$).

The definition of activity is completed by choosing the standard state of the components of the solution, for which are taken as reference the models of ideal solution. There are two agreements for the election of the standard state:

a) Asymmetric convention

Activity coefficients of solvent and electrolyte tend to unity (hypothetic ideal behaviour) when mole fraction of solvent tend to unity and mole fraction of electrolyte tend to zero, what means solvent is considered pure solvent and the electrolyte is in infinite dilution. This basis is defined to be used with aqueous solvents.

$$\gamma_{\mathrm{m}}\,(x_{\mathrm{m}}\,\rightarrow 1)=1 \tag{3.6}$$

$$\gamma_{\mathrm{c}}\,(x_{c}\,,x_{\mathrm{a}}\,\rightarrow 0)=\gamma_{\mathrm{a}}\,(x_{\mathrm{c}}\,,x_{\mathrm{a}}\,\rightarrow 0)=1 \tag{3.7}$$

b) Symmetric convention

Activity coefficients of solvent and electrolyte tend to unity when the mole fractions of the solvent and electrolyte tend also to unity. Thus, the reference state of solvent is the pure solvent and the electrolyte is considered pure molten salt. With this convention, infinite dilution for electrolyte is not required and for this reason can be used for non-aqueous solvents like ammonia.

$$\gamma_{\mathrm{m}}\,(x_{\mathrm{m}}\,\rightarrow 1)=1 \tag{3.8}$$

$$\gamma_{\mathrm{c}}\,(x_{\mathrm{c}}\,,x_{\mathrm{a}}\,\rightarrow 1)=\gamma_{\mathrm{a}}\,(x_{\mathrm{c}}\,,x_{\mathrm{a}}\,\rightarrow 1)=1 \tag{3.9}$$

By means of the use of equations 3.3 and 3.4 and taking into account that the activity of a solid is 1, the chemical potentials can be expressed as functions of the standard state chemical potentials, the composition, and the activity coefficients as follows:

$$\mu^{\mathrm{o}}_{\mathrm{Cv_{+}Av_{-}\cdot\,n\,m}}=\left[v_{+}\,\left(\mu^{\mathrm{o}}_{\mathrm{c}}+RT\ln(a_{c})\right)\right]+\,\left[v_{-}\,\left(\mu^{\mathrm{o}}_{\mathrm{a}}+RT\ln(a_{a})\right)\right]+\,\left[n\,\left(\mu^{\mathrm{o}}_{\mathrm{m}}+RT\ln(a_{\mathrm{m}})\right)\right] \tag{3.10}$$

The standard state chemical potentials of the previous equation can be ordered on the left hand side of the equation and the activities on the right hand side:

$$-\,\frac{\mu^{\mathrm{o}}_{\mathrm{Cv_{+}Av_{-}\cdot\,n\,m}}+v_{+}\mu^{\mathrm{o}}_{\mathrm{c}}+v_{-}\mu^{\mathrm{o}}_{\mathrm{a}}}{RT}=\ln({a_{\mathrm{c}}}^{v+}\,{a_{\mathrm{a}}}^{v-}\,{a_{\mathrm{m}}}^{n}) \tag{3.11}$$

The numerical value of the left hand side of the equation can thus be calculated. However, to solve the right side of the equation it is necessary a model to calculate the activity coefficients as functions of composition and temperature. Equation 3.11 can be expressed in terms of Gibbs free energy in standard state in the following way:

$$\exp\left(-\frac{\Delta G^{o}(T)}{RT}\right) = (a_{c})^{\nu_{+}}\,(a_{a})^{\nu_{-}}\,(a_{m})^{n} \tag{3.12}$$

The relation between the Gibbs free energy in standard state in conditions of equilibrium ($\Delta G = 0$) with the equilibrium constant, which in the solid-liquid equilibrium is the solubility product constant K_{sp} , is expressed as :

$$\Delta G = \Delta G^{o} + RT \ln K_{sp} \tag{3.13}$$

$$\ln K_{sp} = \frac{-\Delta G^{o}}{RT} \tag{3.14}$$

Considering these relations, equation 3.12 is expressed in terms of solubility product constant K_{sp} and the final equation of solid-liquid equilibrium is obtained:

$$K_{sp} = (a_{c})^{\nu_{+}}\,(a_{a})^{\nu_{-}}\,(a_{m})^{n} \tag{3.15}$$

$$K_{sp} = (x_{c}\,\gamma_{c})^{\nu_{+}}\,(x_{a}\gamma_{a})^{\nu_{-}}\,(x_{m}\gamma_{m})^{n} \tag{3.16}$$

Equating this expression of K_{sp} to the expression of solubility product constant which depends of temperature, it will be possible to calculate the solubility temperature of the solutions under study:

$$(x_{c}\,\gamma_{c})^{\nu_{+}}\,(x_{a}\gamma_{a})^{\nu_{-}}\,(x_{m}\gamma_{m})^{n} = K_{sp}[f(T)] \tag{3.17}$$

The expression of solubility product constant K_{sp} in function of temperature can be obtained by means of two different methodologies:

a) Rigorous method

This method is chosen for modelling solutions with water as solvent. It is based on the direct calculation of the Gibbs free energy in the standard state at the temperature of the system. In Gibbs-Helmholtz equation the temperature dependency of solubility product is expressed as follows:

$$K_{ps} = \exp\left[\frac{-\Delta G^{o}(T_{r})}{RT_{r}} - \frac{\Delta H^{o}(T_{r})}{R}\left(\frac{1}{T} - \frac{1}{T_{r}}\right) + \frac{\Delta Cp^{o}(T_{r})}{R}\left(ln\frac{T}{T_{r}} + \frac{T_{r}}{T} - 1\right)\right] \tag{3.18}$$

Where T_{r} is reference temperature (298.15 K). Standard Gibbs energy $\Delta G^{o}(T_{r})$, standard enthalpy $\Delta H^{o}(T_{r})$ and standard heat capacity $\Delta c_{p}^{o}(T_{r})$ are defined as follows:

$$\Delta G^o(T_r) = v_+ \, \Delta_f G_c^o(T_r) + \, v_- \, \Delta_f G_a^o(T_r) + n \, \Delta_f G_m^o(T_r) - \Delta_f G_{ca \cdot n\, m(s)}^o(T_r) \quad (3.19)$$

$$\Delta H^o(T_r) = v_+ \, \Delta_f H_c^o(T_r) + \, v_- \, \Delta_f H_a^o(T_r) + n \, \Delta_f H_m^o(T_r) - \Delta_f H_{ca \cdot n\, m(s)}^o(T_r) \quad (3.20)$$

$$\Delta c_p{}^o(T_r) = v_+ \, c_{p,c}^o(T_r) + \, v_- \, c_{p,a}^o(T_r) + n \, c_{p,m}^o(T_r) - c_{p,ca \cdot n\, m(s)}^o(T_r) \quad (3.21)$$

It should be pointed out that the standard state corresponds to the hypothetic ideal solution in mole scale.

b) Approximate method

It is chosen for modelling solutions with ammonia as solvent because required standard Gibbs energy of formation, enthalpies of formation and heat capacities of the salts and ions are not available for non-aqueous solvents like ammonia, thus, Gibbs-Helmholtz equation cannot be used.

As the activity coefficients for the solutions with ammonia as solvent are calculated with symmetric electrolyte NRTL model with Aspen Properties software, the solubility product constant is also obtained with Aspen Properties with the following equation:

$$K_{sp} = \exp\left(A + \frac{B}{T} + C \cdot \ln T + D \cdot T\right) \quad (3.22)$$

With this method the solubility product constant is obtained from regression of experimental solubility data to obtain the four parameters *A, B, C, D* of the equation.

3.3. LIQUAC activity coefficient model for modelling SLE in aqueous electrolyte systems

The knowledge of electrolyte systems started in the last century with Debye and Hückel theory (1923), which was the first electrolyte model that delivered a reliable behaviour of infinite dilute solutions. From this theory, a wide range of models were developed to overcome the limitations of highly dilute compositions of the original theory, such as Pitzer (1973) or Bromley (1973) models.

Current models combine Debye–Hückel theory with the local composition models to represent a reliable behaviour of electrolyte systems at low and high salt mass fractions. In this group appear models such as electrolyte-NRTL (Chen et al., 1982, 1986), extended UNIQUAC (Sander et al., 1986), LIQUAC (Li et al., 1994, 2005) based on UNIQUAC model (Abrams and Prausnitz, 1975), electrolyte group-contribution UNIFAC (Kikic et al. 1991) or LIFAC (Yan et al., 1999) based on UNIFAC model (Fredenslund et al., 1975). In this study, LIQUAC model has been chosen for modelling activity coefficients of aqueous electrolyte systems ($H_2O/LiNO_3$) because obtains a reliable prediction of systems with strong electrolytes up to high salt compositions (Kiepe et al., 2006).

Li et al. (1994) developed an excess Gibbs energy model for single and mixed solvents with strong electrolytes based on the results of statistical thermodynamics and taking into account the interactions between the ions and molecules present in electrolyte solutions. The contributions of the short-range interactions were described by the UNIQUAC model; therefore, the model was called LIQUAC.

LIQUAC model is based on the asymmetric convention and takes into account the interactions which occur in electrolyte solutions. The model calculates the Gibbs energy as the sum of three contributions which represent long-range (LR), middle-range (MR) and short-range (SR) interactions:

$$G^{\mathrm{E}} = G^{\mathrm{E}}_{\mathrm{LR}} + G^{\mathrm{E}}_{\mathrm{MR}} + G^{\mathrm{E}}_{\mathrm{SR}} \tag{3.23}$$

Long-range interactions represent charge-charge interaction contribution caused by Coulomb electrostatic forces. $G^{\mathrm{E}}_{\mathrm{LR}}$ can thus be calculated in terms of the extended Debye-Hückel theory. Middle-range interactions represent contributions of the indirect effects between pair species of charge interactions such as charge-dipole and charge-induced dipole and it is calculated using a Pitzer type virial equation. Short-range interactions represent the contribution of non-charge interactions and can be described using the UNIQUAC approach with minimum modifications. From equation 3.23, the activity coefficients of the molecular and ionic species are derived as follows:

$$ln\,\gamma_i = \frac{1}{RT}\frac{\partial G^E}{\partial n_i} \tag{3.24}$$

In the following lines is described in detail the LIQUAC model of a single-solvent aqueous electrolyte system to obtain the activity coefficient of the solvent and the cation and anion of the electrolyte solute.

3.3.1. Activity coefficient of solvent

Activity coefficient of solvent *m* can be expressed as the sum of the three contributions mentioned before, long-range, middle-range and short-range:

$$\ln \gamma_{\mathrm{m}} = \ln \gamma_{\mathrm{m}}^{\mathrm{LR}} + \ln \gamma_{\mathrm{m}}^{\mathrm{MR}} + \ln \gamma_{\mathrm{m}}^{\mathrm{SR}} \tag{3.25}$$

- *Long-range LR contribution*

LR term is calculated using Debye-Hückel theory modified by Fowler and Guggenheim (1949).

$$\ln \gamma_{\mathrm{m}}^{\mathrm{LR}} = \left(\frac{2AM_{\mathrm{m}}}{b^3}\right)\left[1 + b\sqrt{I} - \left(1 + b\sqrt{I}\right)^{-1} - 2\ln(1 + b\sqrt{I})\right] \tag{3.26}$$

where M_{m} is molecular mass of solvent in kg·mol^{-1}. I is the ionic strength of electrolyte and A, b are Debye-Hückel parameters calculated as:

$$I = 0.5 \sum_i m_i z_i^2 \tag{3.27}$$

$$A = 1.327757 \cdot 10^5 \frac{\rho^{0.5}}{(DT)^{1.5}} \tag{3.28}$$

$$b = 6.35969 \cdot 10^5 \frac{\rho^{0.5}}{(DT)^{1.5}} \tag{3.29}$$

$$D = \varepsilon_{r,A} + \varepsilon_{r,B}\left(\frac{1}{T} - \frac{1}{\varepsilon_{r,C}}\right) \tag{3.30}$$

m_i and z_i^2 are molality and charges of ions of the electrolyte respectively, D is dielectric constant of solvent, ρ is the density and ε_r is dielectric relative constant of solvent.

- *Middle-range MR contribution*

Interactions between equally charged ions and between solvent molecules are not considered. With these considerations, the MR contribution leads to the following expression:

$$\ln \gamma_{\mathrm{m}}^{\mathrm{MR}} = \sum_{\mathrm{ion}} B_{\mathrm{m,ion}}(I)\, m_{\mathrm{ion}} - \sum_{\mathrm{ion}} \left[B_{\mathrm{m,ion}}(I) + I B'_{\mathrm{m,ion}}(I)\right] m_{\mathrm{ion}} - M_{\mathrm{m}} \sum_{\mathrm{c}} \sum_{\mathrm{a}} \left[B_{\mathrm{c,a}}(I) + I B'_{\mathrm{c,a}}(I)\right] m_{\mathrm{c}}\, m_{\mathrm{a}} \tag{3.31}$$

$$B_{\mathrm{m,ion}}(I) = b_{\mathrm{m,ion}} + c_{\mathrm{m,ion}} \exp\left(-1.2\sqrt{I} + d_{\mathrm{m,ion}}\, I\right) \tag{3.32}$$

$$B_{\mathrm{c,a}}(I) = b_{\mathrm{c,a}} + c_{\mathrm{c,a}} \exp\left(-\sqrt{I} + d_{\mathrm{c,a}}\, I\right) \tag{3.33}$$

$$B'_{\mathrm{m,ion}}(I) = c_{\mathrm{m,ion}} \left[\left(\frac{-0.6}{\sqrt{I}}\right) + d_{\mathrm{m,ion}}\right] exp\left(-1.2\sqrt{I} + d_{\mathrm{m,ion}}\, I\right) \tag{3.34}$$

$$B'_{\mathrm{c,a}}(I) = c_{\mathrm{c,a}} \left[\left(\frac{-0.6}{\sqrt{I}}\right) + d_{\mathrm{c,a}}\right] exp\left(-\sqrt{I} + d_{\mathrm{c,a}}\, I\right) \tag{3.35}$$

$b_{i,j}$, $c_{i,j}$, and $d_{i,j}$ are temperature-depend parameters, being $i,j = j,i$. Parameters $d_{\mathrm{c,a}}$ and $d_{\mathrm{m,ion}}$ are set to 0.125 and 0.250 respectively following the recommendations of Kiepe et al. (2006). To extend the capability of MR term to a wider temperature range, the parameters are improved as follows (Li et al., 2011):

$$b_{i,j} = {b_{i,j}}^{(0)} + {b_{i,j}}^{(1)} \left(\frac{1}{T} - \frac{1}{298.15}\right) + {b_{i,j}}^{(2)} \ln \frac{T}{298.15} \tag{3.36}$$

$$c_{i,j} = {c_{i,j}}^{(0)} + {c_{i,j}}^{(1)} \left(\frac{1}{T} - \frac{1}{298.15}\right) + {c_{i,j}}^{(2)} \ln \frac{T}{298.15} \tag{3.37}$$

${b_{i,j}}^{(0)}, {c_{i,j}}^{(0)}, {b_{i,j}}^{(1)}, {c_{i,j}}^{(1)}, {b_{i,j}}^{(2)}, {c_{i,j}}^{(2)}$ are adjustable parameters.

- *Short-range SR contribution*

SR contribution is calculated by the UNIQUAC model as follows:

$$\ln \gamma_{\mathrm{m}}^{\mathrm{SR}} = \ln \gamma_{\mathrm{m}}^{\mathrm{C}} + \ln \gamma_{\mathrm{m}}^{\mathrm{R}} \tag{3.38}$$

$$\ln \gamma_{\mathrm{m}}^{\mathrm{C}} = 1 - V_{\mathrm{m}} + \ln V_{\mathrm{m}} - 5 q_{\mathrm{m}} \left[1 - \frac{V_{\mathrm{m}}}{F_{\mathrm{m}}} + \ln\left(\frac{V_{\mathrm{m}}}{F_{\mathrm{m}}}\right)\right] \tag{3.39}$$

$$\ln \gamma_{\mathrm{m}}^{\mathrm{R}} = q_{\mathrm{m}} \left\{1 - \ln\left(\frac{\sum_i q_i x_i \Psi_{i,\mathrm{m}}}{\sum_i q_i x_i}\right) - \sum_i \left[\frac{q_i x_i \Psi_{\mathrm{m},i}}{\sum_k q_k x_k \Psi_{k,i}}\right]\right\} \tag{3.40}$$

$$V_{\mathrm{m}} = \frac{r_{\mathrm{m}}}{\sum_i r_i\, x_i} \tag{3.41}$$

$$F_{\mathrm{m}} = \frac{q_{\mathrm{m}}}{\sum_i q_i\, x_i} \tag{3.42}$$

$$\Psi_{i,j} = \exp\frac{-a_{i,j}}{T} \tag{3.43}$$

r and q corresponds to Van der Waals volume and surface area of solvent respectively.

$a_{i,j}$ represents UNIQUAC interaction parameters, being $a_{i,j} \neq a_{j,i}$, covering i and j all ions and solvents.

3.3.2. Activity coefficient of ions

Activity coefficients of cations and anions, based on asymmetric convention and molality scale, are obtained by means of the sum of the contributions by the next equation:

$$\ln \gamma_i' = \left(\ln \gamma_i^{\mathrm{LR}} + \ln \gamma_i^{\mathrm{MR}} + \ln \gamma_i^{\mathrm{SR}}\right) - \ln\left(M_{\mathrm{m}} \sum_{\mathrm{ion}} m_{\mathrm{ion}}\right) \tag{3.44}$$

γ_i' is the asymmetric rational activity coefficient and is defined as the ratio of the value of the activity coefficient at the relevant composition and the value of the activity coefficient at infinite dilution γ_i^{∞}.

Contributions of long, middle and short range are defined as:

- *Contribution of large-range LR*

$$\ln \gamma_i^{\mathrm{LR}} = -\frac{z_i^2 A\sqrt{I}}{1 + b\sqrt{I}} \tag{3.45}$$

- *Contribution of middle-range MR*

$$\ln \gamma_i^{\mathrm{MR}} = \frac{1}{M_{\mathrm{m}}} \sum_{\mathrm{m}} B_{i,\mathrm{m}}(I) + \left[\frac{z_i^2}{2M_{\mathrm{m}}}\right] \sum_{\mathrm{m}} \sum_{\mathrm{ion}} B'_{\mathrm{m,ion}}(I)\, m_{\mathrm{ion}} + \sum_{\mathrm{ion}} B_{i,\mathrm{ion}}(I)\, m_{\mathrm{ion}} + \left[\frac{z_i^2}{2}\right] \sum_{\mathrm{c}} \sum_{\mathrm{a}} B'_{\mathrm{c,a}}(I)\, m_{\mathrm{c}} m_{\mathrm{a}} - \frac{B_{i,\mathrm{m}}(I=0)}{M_{\mathrm{m}}} \tag{3.46}$$

- Contribution of short-range MR

$$\ln \gamma_i^{SR} = \ln \gamma_i^{C} - \ln \gamma_i^{C}(B) + \ln \gamma_i^{R} - \ln \gamma_i^{R}(B) \tag{3.47}$$

$$\ln \gamma_i^C = 1 - V_i + \ln V_i - 5q_i \left[1 - \frac{V_i}{F_i} + \ln\left(\frac{V_i}{F_i}\right)\right] \tag{3.48}$$

$$\ln \gamma_i^R = q_i \left\{1 - \ln \sum_i \left(\frac{\sum_i q_i x_i \Psi_{i,j}}{\sum_i q_i x_i}\right) - \sum_i \left[\frac{q_i x_i \Psi_{j,i}}{\sum_k q_k x_k \Psi_{k,i}}\right]\right\} \tag{3.49}$$

$$\ln\left[\gamma_i^C(B)\right] = 1 - \frac{r_i}{r_{\mathrm{m}}} + \ln\left(\frac{r_i}{r_{\mathrm{m}}}\right) - 5q_j \left[1 - \frac{r_i q_{\mathrm{m}}}{r_{\mathrm{m}} q_i} + \ln\left(\frac{r_i q_{\mathrm{m}}}{r_{\mathrm{m}} q_i}\right)\right] \tag{3.50}$$

$$\ln[\gamma_i^R(B)] = q_j\left[1 - \Psi_{j,s} - \ln \Psi_{s,j}\right] \tag{3.51}$$

Established necessary expressions to calculate activity coefficients of solvent and ions of the electrolyte, equating equation 3.16, based on asymmetric convention and molality scale for solvent and mole fraction scale for ions, with the solubility product equation of Gibbs-Helmholtz (eq. 3.18), it is obtained equation 3.52 whereby with an iterative calculus it can be obtained the solubility temperature or the composition of salt that can be dissolved in a certain temperature.

$$\exp\left[\frac{-\Delta G^o(T_r)}{RT_r} - \frac{\Delta H^o(T_r)}{R}\left(\frac{1}{T} - \frac{1}{T_r}\right) + \frac{\Delta Cp^o(T_r)}{R}\left(\ln\frac{T}{T_r} + \frac{T_r}{T} - 1\right)\right] = \\ = (m_{\mathrm{c}}\gamma_{\mathrm{c}})^{\nu_+}(m_{\mathrm{a}}\gamma_{\mathrm{a}})^{\nu_-}(x_{\mathrm{m}}\gamma_{\mathrm{m}})^n \tag{3.52}$$

3.4. Symmetric E-NRTL activity coefficient model for modelling SLE in electrolyte systems with ammonia as solvent

3.4.1. Description of the model

As it was explained in section 3.3, in literature can be found some widely referenced activity coefficient models for electrolyte solutions such as Pitzer, extended UNIQUAC, LIQUAC, OLI MSE model (Wang et al., 2002) or electrolyte NRTL models. However, some of them have some lacks, for example, Pitzer model is only applicable to dilute aqueous electrolyte systems and requires high number of binary and ternary interaction parameters, extended UNIQUAC model has inconsistent treatments in both reference state and concentration scale and OLI MSE model fails in the inconsistent treatment of ion-ion and ion-molecule interactions with the viral expansion-type equation and molecule-molecule interactions with UNIQUAC equation.

In this work, electrolyte nonrandom two-liquid model based in the symmetric reference state (Song and Chen, 2009) has been chosen for modelling solubility of the systems with ammonia as

solvent ($NH_3/LiNO_3$ and NH_3/NaSCN) because allows working with aqueous and non-aqueous solvents and also requires less interaction parameters than the other models. Furthermore, this model is included in Aspen Properties software and therefore its application becomes much easier.

Chen et al. (1982, 1986) proposed the electrolyte-NRTL model for the representation of the Gibbs excess energy of single liquid electrolyte systems and multicomponent systems. Initially, it was proposed as an asymmetric activity coefficient model, with the reference state chosen to be the electrolyte in aqueous infinite dilution, what makes it non appropriate for non-aqueous solvents.

Song and Chen (2009) proposed a formulation of the symmetric electrolyte-NRTL to overcome the limits of applicability, making it feasible for non-aqueous electrolyte systems and mixed-solvent electrolyte systems. The model is based on a symmetric reference state, which considers the pure liquid for solvents and pure fused salts for electrolytes (eq. 3.8-3.9).

The basis of the model consists in the interactions which exist between molecular and ionic species to describe the thermodynamic properties of the solution. These interactions are constituted by two contributions: local interactions and long-range interactions. Local interactions are those which exist at the immediate neighbourhood of any species (molecule-molecule and ion-molecule). Long-range interactions exist beyond the immediate neighbourhood of ionic species (ion-ion). The contribution of local interactions is represented by the local composition NRTL model. In the case of long-range interactions instead it is used the symmetric Pitzer-Debye-Hückel (PDH) model (Pitzer 1980, 1986).

The excess Gibbs free energy of electrolyte systems is represented in the following equation as the basis the E-NRTL model:

$$G^{ex} = G^{ex,\mathrm{lc}} + G^{ex,\mathrm{PDH}} \tag{3.53}$$

$G^{ex,\mathrm{lc}}$ and $G^{ex,\mathrm{PDH}}$ represent contributions from local and long-range interactions, respectively. Activity coefficients of the molecule (solvent), cation and anion (electrolyte) are derived from equation 3.53 as follows:

$$\ln \gamma_i = \frac{1}{RT}\left(\frac{\partial G^{\mathrm{ex}}}{\partial n_i}\right)_{T,P,n_{j\neq i}} = \frac{1}{RT}\left(\frac{\partial G^{\mathrm{ex,lc}}}{\partial n_i}\right)_{T,P} + \frac{1}{RT}\left(\frac{\partial G^{\mathrm{ex,PDH}}}{\partial n_i}\right)_{T,P} \tag{3.54}$$

$$\ln \gamma_i = \ln \gamma_i^{\mathrm{lc}} + \ln \gamma_i^{\mathrm{PDH}} \tag{3.55}$$

where n_i is the mole number of component i, which represents the molecular component m (solvent), the cation c and anion a (electrolyte species).

- *Local interaction contribution based on Electrolyte NRTL model*

In Electrolyte NRTL model there are two main assumptions. First one is based on the local electroneutrality between the central molecular component and the rest of the species in the immediate neighbourhood. The other one is based on the like-ion repulsion when ionic species are surrounding respective central ionic species.

The excess Gibbs free energy $G^{ex,\mathrm{lc}}$ for an electrolyte system can be written as:

$$\frac{G^{ex,\mathrm{lc}}}{nRT} = \sum_{\mathrm{m}} X_{\mathrm{m}} \left(\frac{\sum_i X_i G_{i\mathrm{m}} \tau_{i\mathrm{m}}}{\sum_i X_i G_{i\mathrm{m}}} \right) + \sum_{\mathrm{c}} X_{\mathrm{c}} \left(\frac{\sum_{i \neq \mathrm{c}} X_i G_{i\mathrm{c}} \tau_{i\mathrm{c}}}{\sum_{i \neq \mathrm{c}} X_i G_{i\mathrm{c}}} \right) + \sum_{\mathrm{a}} X_{\mathrm{a}} \left(\frac{\sum_{i \neq \mathrm{a}} X_i G_{i\mathrm{a}} \tau_{i\mathrm{a}}}{\sum_{i \neq \mathrm{a}} X_i G_{i\mathrm{a}}} \right) \quad (3.56)$$

Each one of the terms of the right side of the equation 3.56 corresponds to the contribution when molecular component, cation and anion respectively are in the centre. $X_i = C_i x_i$ where C_i is the charge number z_i for ionic species and is the unity for the solvent.

Activity coefficients of the solvent, cation and anion are derived and expressed as:

$$\ln \gamma_i^{\mathrm{lc}} = \frac{1}{RT} \left(\frac{\partial G^{\mathrm{ex,lc}}}{\partial n_i} \right)_{T,P,n_{j \neq i}} \quad (3.57)$$

Which once normalized corresponds to:

$$\ln \gamma_{\mathrm{m}}^{\mathrm{lc}} \left(x_{\mathrm{m}} \to 1 \right) = 0 \quad (3.58)$$

$$\ln \gamma_{\mathrm{c}}^{\mathrm{lc}} = \ln \gamma_{\mathrm{c}}^{\mathrm{lc},I_x} - \ln \gamma_{\mathrm{c}}^{\mathrm{lc},I_x^0} \quad (3.59)$$

$$\ln \gamma_{\mathrm{a}}^{\mathrm{lc}} = \ln \gamma_{\mathrm{a}}^{\mathrm{lc},I_x} - \ln \gamma_{\mathrm{a}}^{\mathrm{lc},I_x^0} \quad (3.60)$$

$$\frac{1}{z_{\mathrm{c}}} \ln \gamma_{\mathrm{c}}^{\mathrm{lc},I_x} = \sum_{\mathrm{m}} \frac{X_{\mathrm{m}} G_{\mathrm{cm}}}{\sum_i X_i G_{i\mathrm{m}}} \left(\tau_{\mathrm{cm}} - \frac{\sum_i X_i G_{i\mathrm{m}} \tau_{i\mathrm{m}}}{\sum_i X_i G_{i\mathrm{m}}} \right) + \frac{\sum_{i \neq \mathrm{c}} X_i G_{i\mathrm{c}} \tau_{i\mathrm{c}}}{\sum_{i \neq \mathrm{c}} X_i G_{i\mathrm{c}}} + \sum_{\mathrm{a}} \frac{X_{\mathrm{a}} G_{\mathrm{ca}}}{\sum_{i \neq \mathrm{a}} X_i G_{i\mathrm{a}}} \left(\tau_{\mathrm{ca}} - \frac{\sum_{i \neq \mathrm{a}} X_i G_{i\mathrm{a}} \tau_{i\mathrm{a}}}{\sum_{i \neq \mathrm{a}} X_i G_{i\mathrm{a}}} \right) \quad (3.61)$$

$$\frac{1}{z_{\mathrm{a}}}\ln\gamma_{\mathrm{a}}^{\mathrm{lc},I_x}=\sum_{\mathrm{m}}\frac{X_{\mathrm{m}}G_{\mathrm{am}}}{\sum_i X_i G_{\mathrm{im}}}\left(\tau_{\mathrm{am}}-\frac{\sum_i X_i G_{\mathrm{im}}\tau_{\mathrm{im}}}{\sum_i X_i G_{\mathrm{im}}}\right)+\frac{\sum_{i\neq \mathrm{a}} X_i G_{i\mathrm{a}}\tau_{i\mathrm{a}}}{\sum_{i\neq \mathrm{a}} X_i G_{i\mathrm{a}}}+$$
$$+\sum_{\mathrm{c}}\frac{X_{\mathrm{c}}G_{\mathrm{ac}}}{\sum_{i\neq \mathrm{c}} X_i G_{i\mathrm{a}}}\left(\tau_{\mathrm{ca}}-\frac{\sum_{i\neq \mathrm{c}} X_i G_{i\mathrm{c}}\tau_{i\mathrm{c}}}{\sum_{i\neq \mathrm{c}} X_i G_{i\mathrm{c}}}\right) \tag{3.62}$$

$$\ln\gamma_{\mathrm{c}}^{\mathrm{lc},I_x^0}=\ln\gamma_{\mathrm{c}}^{\mathrm{lc},I_x}\,(x_{\mathrm{m}}\to 0) \tag{3.63}$$

$$\ln\gamma_{\mathrm{a}}^{\mathrm{lc},I_x^0}=\ln\gamma_{\mathrm{a}}^{\mathrm{lc},I_x}\,(x_{\mathrm{m}}\to 0) \tag{3.64}$$

where I_x is defined as the ionic strength and I_x^0 represents the ionic strength at the reference state.

In the above equations appears two parameters, G and τ, which are related to each other by the nonrandomness NRTL factor parameter α with the following equation.

$$G=\exp(-\alpha\,\tau) \tag{3.65}$$

The adjustable model parameters include the asymmetric binary interaction energy parameter, τ, and the symmetric non-random factor parameter, α. In the case of study, with single electrolyte systems, these parameters correspond to molecule-electrolyte pairs ($\alpha_{\mathrm{m,ca}}=\alpha_{\mathrm{ca,m}}$ while $\tau_{\mathrm{m,ca}}\neq\tau_{\mathrm{ca,m}}$ where *m* represents molecule and ca the ion pair).

- *Long-range interaction contribution based on extended PDH model*

To take into account the long-range ion-ion interactions it is used the symmetric Pitzer-Debye-Hückel model. The following equation describes the excess Gibbs free energy $G^{ex,\mathrm{PDH}}$ in the symmetric PDH model for single electrolyte systems:

$$\frac{G^{ex,\mathrm{PDH}}}{nRT}=-\frac{4A_\varphi I_x}{\rho}\ln\left[\frac{1+\rho I_x^{\frac{1}{2}}}{1+\rho(I_x^0)^{\frac{1}{2}}}\right] \tag{3.66}$$

The Debye-Hückel parameter A_φ, ionic strength I_x and ionic strength in standard state I_x^0 are defined with the following equations:

$$A_\varphi=\frac{1}{3}\left(\frac{2\pi N_{\mathrm{A}}}{\vartheta}\right)^{1/2}\left(\frac{Q_{\mathrm{e}}^2}{\varepsilon k_{\mathrm{B}}T}\right)^{3/2} \tag{3.67}$$

$$I_x = \frac{1}{2}\sum_{\mathrm{c}} z_{\mathrm{c}}^2\, x_{\mathrm{c}} + \frac{1}{2}\sum_{\mathrm{a}} z_{\mathrm{a}}^2\, x_{\mathrm{a}} \tag{3.68}$$

$$I_x^0 = \frac{1}{2}\sum_{\mathrm{c}} x_{\mathrm{c}}^{\mathrm{o}}\, z_{\mathrm{c}}^2 + \frac{1}{2}\sum_{\mathrm{a}} x_{\mathrm{a}}^{\mathrm{o}}\, z_{\mathrm{a}}^2 \tag{3.69}$$

where N_{A} is Avogadro's number, Q_{e} is the electron charge, k_{B} is the Boltzmann constant, ϑ is the molar volume, ε the dielectric constant of the solvent and z_i is the charge number.

A general expression of the activity coefficient of each component of the solution is derived as follows:

$$\ln \gamma_i^{\mathrm{PDH}} = \frac{1}{RT}\left(\frac{\partial G^{\mathrm{ex,PDH}}}{\partial n_i}\right)_{T,P,n_{j\neq i}} \tag{3.70}$$

Activity coefficient of solvent (molecule) is described with the following expression:

$$\ln \gamma_{\mathrm{m}}^{\mathrm{PDH}} = \frac{2A_\varphi I_x^{2/3}}{1+\rho I_x^{1/2}} \tag{3.71}$$

In the case of cation and anion, activity coefficient is described as follows:

$$\ln \gamma_i^{\mathrm{PDH}} = -A_\varphi \left\{ \left(\frac{2z_i^2}{\rho}\right) \ln\left[\frac{1+\rho I_x^{\frac{1}{2}}}{1+\rho (I_x^0)^{\frac{1}{2}}}\right] + \frac{z_i^2 I_x^{\frac{1}{2}} - 2I_x^{\frac{3}{2}}}{1+\rho I_x^{\frac{1}{2}}} - \frac{2I_x (I_x^0)^{-\frac{1}{2}}}{1+\rho (I_x^0)^{\frac{1}{2}}} \left(n\frac{\partial I_x^0}{\partial n_i}\right) \right\} \tag{3.72}$$

$$n\frac{\partial I_x^{\mathrm{o}}}{\partial n_i} = \frac{1}{2}\sum_j z_j^2 \left(n\frac{\partial x_j^{\mathrm{o}}}{\partial n_i}\right) \tag{3.73}$$

$$n\frac{\partial x_j^{\mathrm{o}}}{\partial n_i} = \frac{\delta_{ij} - x_j^{\mathrm{o}}}{\sum_{\mathrm{c}} x_{\mathrm{c}} + \sum_{\mathrm{a}} x_{\mathrm{a}}} \tag{3.74}$$

3.4.2. Modelling with Aspen Properties software

The calculation of the activity coefficients with Electrolyte-NRTL model and the solid-liquid equilibrium has been performed with Aspen Properties software, which from version 7.3 (2011) incorporates the new symmetric formulation of the model.

- *Fitted model parameters*

Aspen Properties doesn't incorporate in its database binary electrolyte parameters of systems with ammonia as solvent, which are required for the calculation of the activity coefficients (γ_i). Thus, first of all, electrolyte pair parameters are calculated from the vapour-liquid equilibrium with regression of experimental data. Asymmetric binary interaction energy parameters, $\tau_{m,ca}$ and $\tau_{ca,m}$, are related with temperature by means of equations 3.75 and 3.76, being T^{ref}= 298.15 K.

$$\tau_{m,ca} = C_{m,ca} + \frac{D_{m,ca}}{T} + E_{m,ca}\left[\frac{(T^{ref} - T)}{T} + \ln\left(\frac{T}{T^{ref}}\right)\right] \quad (3.75)$$

$$\tau_{ca,m} = C_{ca,m} + \frac{D_{ca,m}}{T} + E_{ca,m}\left[\frac{(T^{ref} - T)}{T} + \ln\left(\frac{T}{T^{ref}}\right)\right] \quad (3.76)$$

$C_{m,ca}$ & $C_{ca,m}$, $D_{m,ca}$ & $C_{ca,m}$ and $E_{m,ca}$ & $E_{ca,m}$ are the fitting parameters.

Symmetric non-random factor α is fixed to 0.1, according to the recommendations of Mock et al. (1986) for non-aqueous solvents.

- *Solid phases and reactions in equilibrium*

The databank of Aspen Properties doesn't include solid phases in equilibrium of the systems analysed, therefore, in addition to the solvent, anions and cations, the solid phases have to be introduced manually as new elements. It is also necessary to introduce the electrolyte dissociation reactions and salt dissolution/precipitation reactions of the new solid-phases introduced:

For ammonia / lithium nitrate system:

Salt	$LINO_3$	$\leftrightarrow$	$Li^+ + NO_3^-$
Salt	$LINO_3 \cdot 2NH_3$	$\leftrightarrow$	$Li^+ + NO_3^- + 2\ NH_3$
Salt	$LINO_3 \cdot 4NH_3$	$\leftrightarrow$	$Li^+ + NO_3^- + 4\ NH_3$
Dissociation	$LINO_3$	$\rightarrow$	$Li^+ + NO_3^-$

For ammonia / sodium thiocyanate system:

Salt	NaCNS	$\leftrightarrow$	$Na^+ + CNS^-$
Salt	$NaCNS \cdot 3.5NH_3$	$\leftrightarrow$	$Na^+ + CNS^- + 3.5\ NH_3$
Dissociation	NaCNS	$\rightarrow$	$Na^+ + CNS^-$

- *Solid-liquid equilibrium*

By the equality of the expression of K_{sp} $[f(x,\gamma)]$ (eq. 3.16) with the solubility product constant equation that Aspen Properties uses as approximate method (eq. 3.77) it is obtained the solid-liquid equilibrium (eq. 3.78).

$$\ln(K_{\mathrm{sp}}) = \mathrm{A} + \frac{\mathrm{B}}{T} + \mathrm{C}\cdot\ln T + \mathrm{D}\cdot T \tag{3.77}$$

$$(x_{\mathrm{c}}\,\gamma_{\mathrm{c}})^{\nu_+}\,(x_{\mathrm{a}}\gamma_{\mathrm{a}})^{\nu_-}\,(x_{\mathrm{m}}\gamma_{\mathrm{m}})^{n} = \exp\left(\mathrm{A} + \frac{\mathrm{B}}{T} + \mathrm{C}\cdot\ln T + \mathrm{D}\cdot T\right) \tag{3.78}$$

Parameters of the equation 3.77 are obtained by regression of experimental solubility data for each solid phase in equilibrium. To determine solubility temperature it is used the solubility index of a salt, defined as the ratio of the activity of the salt by its solubility product, and is expressed as:

$$\text{Solubility index} = \frac{(a_{\mathrm{c}})^{\nu_+}\,(a_{\mathrm{a}})^{\nu_-}\,(a_{\mathrm{m}})^{n}}{\exp\left(\mathrm{A} + \frac{\mathrm{B}}{T} + \mathrm{C}\cdot\ln T + \mathrm{D}\cdot T\right)} \tag{3.79}$$

The solubility index of salt is unity when the solution is supersaturated (salt exists as solid) and less than unity when the solution is unsaturated (dissolved). Thus, the temperature in which the solubility index changes from 1.00 to 0.99 will correspond to solubility temperature of the solution.

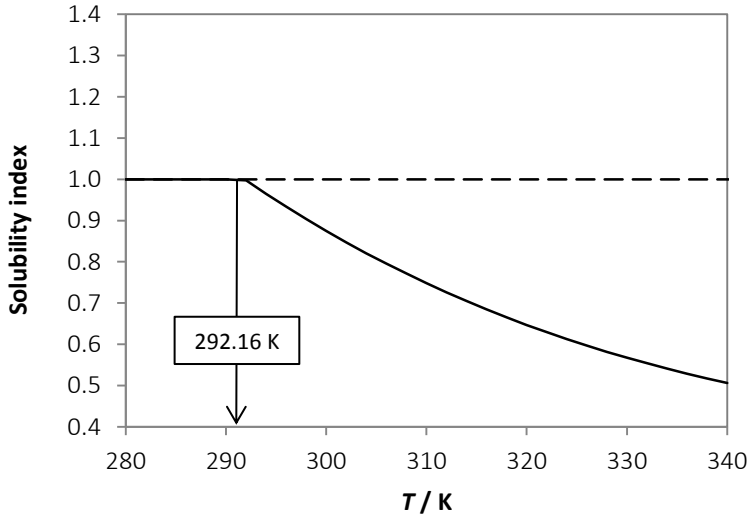

Figure 3.1. Solubility index of ammonia solution with 0.66 in NaSCN mass fraction

Figure 3.1 shows an example of the behaviour of the solubility index of an ammonia solution with 0.66 in NaSCN mass fraction, which corresponds to a solubility temperature of 292.16 K.

3.5. Results of solubility temperature modelling

3.5.1. LIQUAC model - $H_2O/LiNO_3$ system

As defined in the theoretical basis, LIQUAC activity coefficient model requires a series of constants and parameters, such as adjustable binary interaction parameters, relative dielectric constants of water, superficial area or Van der Waals volume of the ions and solvent.

Binary interaction parameters $a_{i,j}$, $b_{i,j}$, $c_{i,j}$ have been obtained in a iterative procedure by the comparison of experimental vapour pressure (Campbell et al., 1956) and the calculated vapour pressure from vapour-liquid equilibrium using LIQUAC activity coefficient model. Due to the non-volatility of lithium nitrate, only water is considered in the phase equilibrium:

$$\emptyset_{\mathrm{w}}\, y_{\mathrm{w}}\, P = x_{\mathrm{w}}\, \gamma_{\mathrm{w}}\, \emptyset_{\mathrm{w}}^{\mathrm{s}}\, P_{\mathrm{w}}^{\mathrm{s}} \exp\left[\frac{v_{\mathrm{w}}(P - P_{\mathrm{w}}^{\mathrm{s}})}{RT}\right] \tag{3.80}$$

The left side of the equation corresponds to vapour phase and the right side to the liquid phase. $\emptyset_{\mathrm{w}}$ is the fugacity coefficient of water, y_{w} and x_{w} are the mole fraction of water in vapour and liquid phase respectively, P is the pressure, γ_{w} is the activity coefficient of water, $\emptyset_{\mathrm{w}}^{\mathrm{s}}$ is the fugacity coefficient of water at saturation pressure, $P_{\mathrm{w}}^{\mathrm{s}}$ is saturation vapour pressure of water and v_{w} is the molar volume of water. The fugacity coefficient is calculated with the equation of state of Redlich-Kwong:

$$P = \frac{R\,T}{v - b} - \frac{a}{T^{1/2} v\,(v + b)} \tag{3.81}$$

$$\emptyset_{\mathrm{w}} = \exp\left[(Z - 1) - \ln\,(Z - \mathrm{B}) - \frac{\mathrm{A}}{\mathrm{B}} \ln\left(1 + \frac{\mathrm{B}}{\mathrm{Z}}\right)\right] \tag{3.82}$$

Parameters *a, b, A* and *B* are calculated with the following expressions:

$$a = \frac{0.42748\, R^2\, T_c^{2.5}}{P_{\mathrm{c}}\, T^{0.5}} \tag{3.83}$$

$$b = \frac{0.08664\, R\, T_{\mathrm{c}}}{P_{\mathrm{c}}} \tag{3.84}$$

$$\mathrm{A} = \frac{a\, P}{R^2 T^2} \tag{3.85}$$

$$\mathrm{B} = \frac{b\, P}{R\, T} \tag{3.86}$$

where T_c and P_c are the critical points of temperature and pressure respectively.

The optimal parameters are those which minimize the objective function, based on the sum of the squared deviations between the experimental and calculated vapour pressure:

$$\mathrm{OF} = \sum_{i=1}^{n} \left(\frac{P_{\mathrm{calc}} - P_{\mathrm{exp}}}{P_{\mathrm{exp}}} \right)^2 \tag{3.87}$$

where n is the number of experiments, P_{calc} is the calculated pressure and P_{exp} is the experimental pressure. The binary interaction parameters obtained are shown in the following table:

Table 3.1. Fitted binary interaction SR and MR parameters

i	j	a_{ij}	a_{ji}	b_{ij}^0	b_{ij}^1	b_{ij}^2
H_2O	Li^+	-478.061	4904.084	0.0009954	-0.000611	-0.0007159
H_2O	NO_3^-	40.565	3811.265	0.0003899	-0.000648	-0.0007152
Li^+	NO_3^-	3300.919	1133.808	0.0922517	-0.007533	0.0004002
i	j	c_{ij}^0	c_{ij}^1	c_{ij}^2	d_{ij}	
H_2O	Li^+	-0.011815	-23.78393	0.005681	0.25	
H_2O	NO_3^-	-0.006724	-0.601466	0.003159	0.25	
Li^+	NO_3^-	0.649695	0.000659	-3.622443	0.125	

In order to check the feasibility of the calculated parameters, the calculated vapour pressure has been compared with experimental data and it has been evaluated with the calculus of the root mean square deviation (RMSD) and maximum deviation (σ):

$$\mathrm{RMSD}\ (\%) = \sqrt{\frac{1}{n} \sum \left(\frac{P_{\mathrm{calc}} - P_{\mathrm{exp}}}{P_{\mathrm{exp}}} \right)^2} \times 100 \tag{3.88}$$

$$\sigma\ (\%) = \frac{P_{\mathrm{calc}} - P_{\mathrm{exp}}}{P_{\mathrm{exp}}} \times 100 \tag{3.89}$$

Figure 3.2 shows the vapour pressure obtained of $H_2O/LiNO_3$ system and its comparison with reported values by Campbell et al. (1956) at different temperatures.

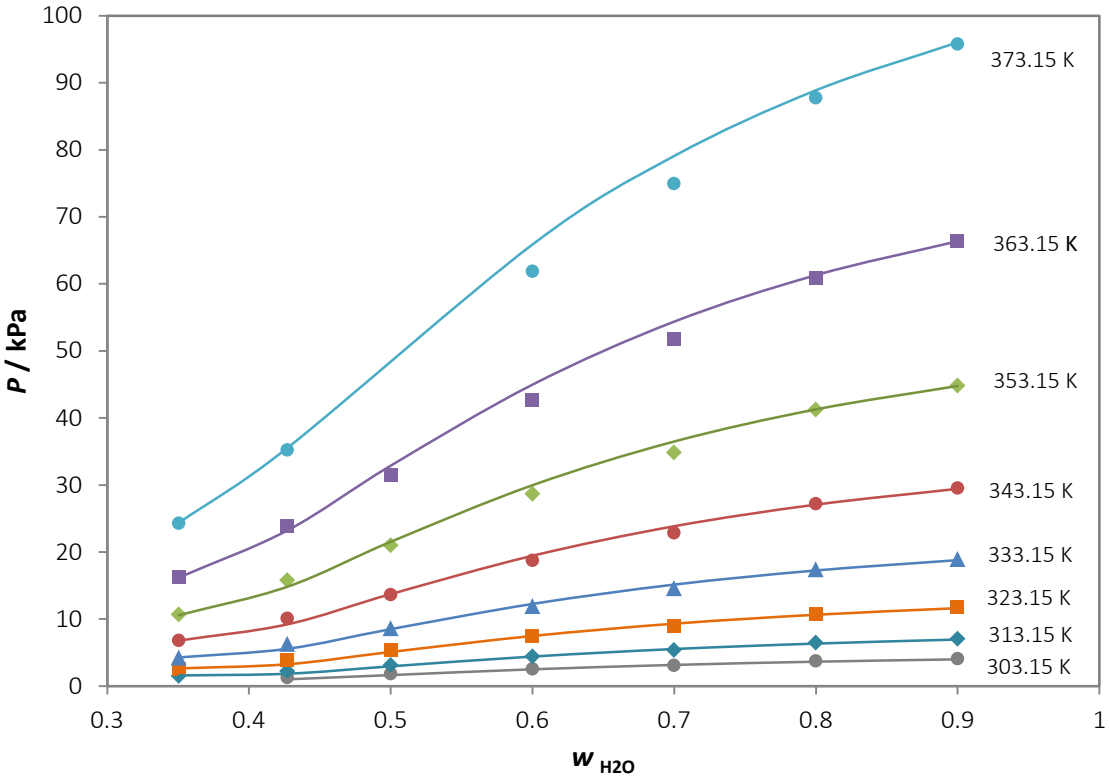

Figure 3.2. Vapour pressure of lithium nitrate aqueous solutions at different temperatures. Lines: modelling. Points: reported experimental values (Campbell et al., 1956)

As it can be observed, there is good agreement between experimental and calculated values at temperatures up to 353 K, for higher temperatures the bigger differences are in the range of 0.6 – 0.7 in mass fraction of water. The RMSD obtained is 5.4 % and the maximum relative deviation is 19 %.

The relative dielectric constants of water are obtained from Aspen Properties databank.

Table 3.2. Water relative dielectric constants (Aspen Properties databank)

$\varepsilon_{r,A}$	78.54
$\varepsilon_{r,B}$	31989.38
$\varepsilon_{r,C}$	298.15

Superficial area (q) and Van der Waals volume (r) of the anion, cation and water are obtained from Kiepe et al. (2006):

Table 3.3. Superficial area (*q*) and Van der Waals volume (*r*) (Kiepe et al., 2006)

	q	*r*
Li^+	0.2556	0.1292
NO_3^-	1.9745	1.6925
H_2O	1.4	0.92

Gibbs energy of formation and enthalpy of formation in standard state of all the species can be obtained from NBS tables of Wagman et al. (1982). However, the heat capacity of solid phases is not available. To overcome this problem, two empirical rules have been adopted:

a) Dulong–Petit (1819) rule expresses that for all solid elemental substances, the product of relative atomic mass (number-ratio representing the relative atomic mass of the substance) and the specific heat capacity, obtains a roughly constant value of 25 $J \cdot mol^{-1} \cdot K^{-1}$. This expression is called atomic heat.

b) Koop's rule establishes that the heat capacity of all solid compounds corresponds to the sum of the atomic heats of the constituent atoms.

With these two rules and considering that the heat capacity of H_2O as water of crystallization in solid substances is 41.033 $J \cdot mol^{-1} \cdot K^{-1}$ according Li et al. (2011), in table 3.4 there are shown the results obtained:

Table 3.4. $\Delta_f G^o$, $\Delta_f H^o$, C_p^o of ions, water and solid phases in equilibrium

	$\Delta_f G^o$	$\Delta_f H^o$	C_p^o
Li^+ (aq)	-293.31	-278.49	68.60
NO_3^- (aq)	-108.74	-205.00	-86.60
H_2O (l)	-237.13	-285.83	75.29
$LiNO_3 \cdot 3H_2O$ (s)	-1103.50	-1374.40	212.10
$LiNO_3 \cdot 0.5H_2O$ (s)	-501.50	-631.68	56.50
$LiNO_3$ (s)	-381.10	-483.13	89.00

With all the parameters and constants obtained, the calculation of the solubility of lithium nitrate in water is accomplished by an iterative calculus changing the lithium nitrate molality in order to obtain the equality of both expressions of K_{sp} (eq. 3.52).

Additionally, Gibbs energy of formation, enthalpy of formation and heat capacity in standard state of solid phases have been optimized from original values by including it as a modifiable values in the iterative calculus, as in the procedure followed by Li et al. (2011).

Table 3.5. Optimized $\Delta_f G^o$, $\Delta_f H^o$, C_p^o of solid phases in equilibrium

	$\Delta_f G^o$	$\Delta_f H^o$	C_p^o
$LiNO_3 \cdot 3H_2O$ (s)	-1099.04	-1351.80	212.12
$LiNO_3 \cdot 0.5H_2O$ (s)	-495.30	-589.85	56.00
$LiNO_3$ (s)	-372.22	-423.90	91.81

Finally, figure 3.3 shows the results obtained of solubility of lithium nitrate in water. The modelling has been carried out considering the three different solid phases in equilibrium depending on the composition of lithium nitrate, obtaining three well differenced tendencies in the curves (section 2.5.1).

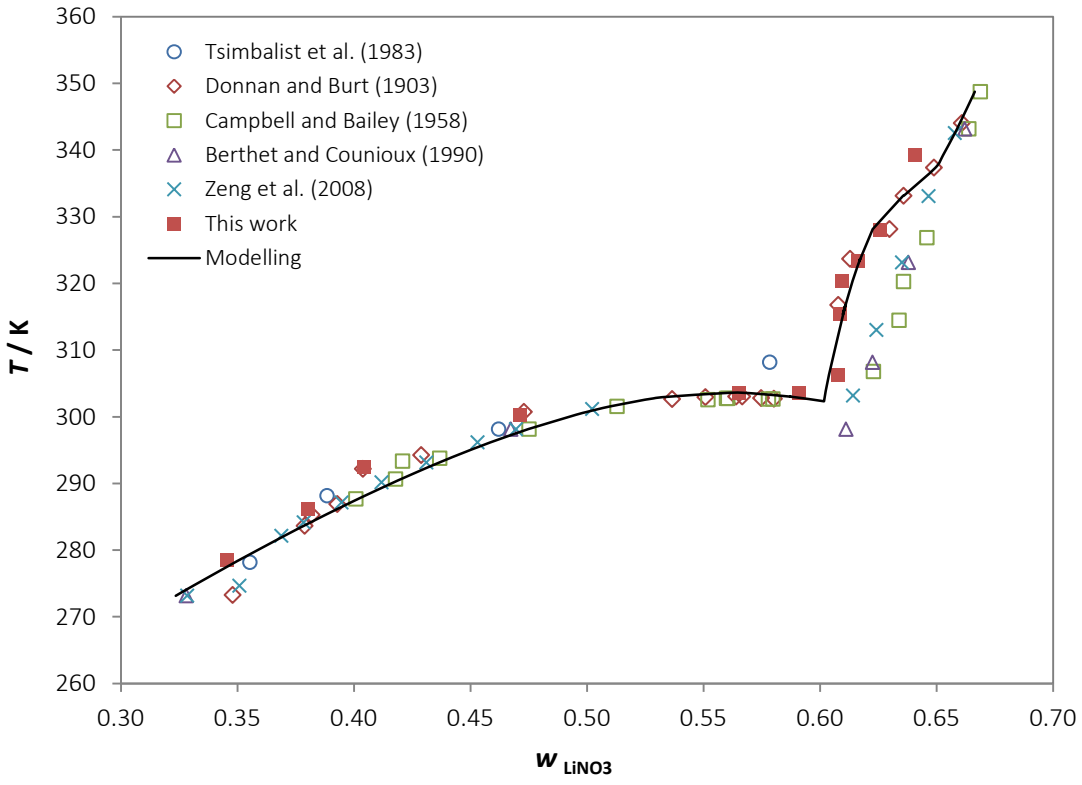

Figure 3.3. Modelling of solubility temperature of lithium nitrate aqueous solutions

The results obtained in the modelling can be considered correct, there is good agreement with experimental values obtained in this work, following the same tendency in the different solid

phases. The root mean square deviation and the maximum relative deviation regarding experimental data of this work are 2.9 % and 6.9 % respectively.

3.5.2. Symmetric Electrolyte-NRTL model — $NH_3/LiNO_3$ & $NH_3/NaSCN$ systems

Aspen Properties doesn't incorporate in its databank the binary interaction energy parameters of symmetric electrolyte NRTL model, $\tau_{m,ca}$ and $\tau_{ca,m}$, for systems with ammonia as solvent. Thus, the parameters $C_{i,j}$, $D_{i,j}$, and $E_{i,j}$, (eq. 3.75 - 3.76) need to be obtained by regression of vapour pressure experimental data, considering the restrictions of vapour-liquid phase equilibrium (only ammonia un vapour phase) by minimizing an objective function of maximum likelihood type, which is calculated as follows:

$$\mathrm{OF} = \sum_{i=1}^{n}\left[\left(\frac{P_{\mathrm{calc},i} - P_{\mathrm{exp},i}}{\sigma_{P,i}}\right)^2 + \left(\frac{T_{\mathrm{calc},i} - T_{\mathrm{exp},i}}{\sigma_{T,i}}\right)^2 + \sum_{j=1}^{m}\left(\frac{w_{\mathrm{calc},i,j} - w_{\mathrm{exp},i,j}}{\sigma_{x,i,j}}\right)^2\right] \qquad (3.90)$$

where n is the number of experiments, σ is the standard deviation, m is the number of species in solution and w is the mass fraction in liquid phase. Table 3.6 shows the results of the parameters obtained:

Table 3.6. Electrolyte pair parameters C, D, E

Species		Electrolyte pair parameters		
Molecule i or electrolyte i	Molecule j or electrolyte j	C	D	E
NH_3	Li^+ NO_3^-	19.462	-9756.582	104.890
Li^+ NO_3^-	NH_3	-7.768	63.557	-89.114
NH_3	Na^+ SCN^-	23.035	-10000	0.629
Na^+ SCN^-	NH_3	-1.650	-774.322	-4.741

Figure 3.4 shows the vapour pressure obtained of $NH_3/LiNO_3$ system and its comparison with reported values by Libotean et al. (2007) at different temperatures and compositions.

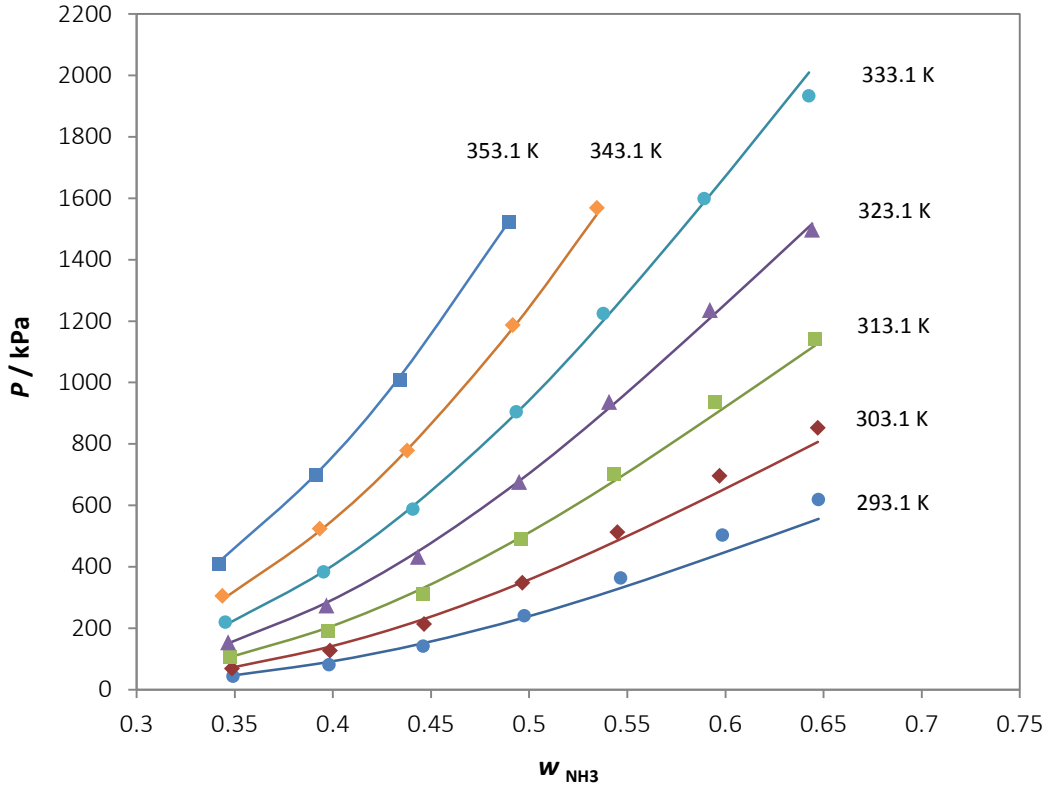

Figure 3.4. Experimental and calculated values of vapour pressure of $LiNO_3$ in ammonia solutions. Lines: modelling. Points: reported experimental data (Libotean et al., 2007)

Experimental and calculated values of vapour pressure present good agreement, with root mean square deviation (RMSD) of 5.1 % and maximum relative deviation of 12 %. The maxim deviation corresponds to calculated values at lower temperatures and higher compositions of ammonia.

In the case of NH_3/NaSCN system, the comparison of experimental and calculated vapour pressure is shown in figure 3.5. There is also good agreement between reported values by Chaudhari et al. (2011) and calculated values at different temperatures and salt compositions, with RMSD of 2.9 % and maximum relative deviation of 8.5 %.

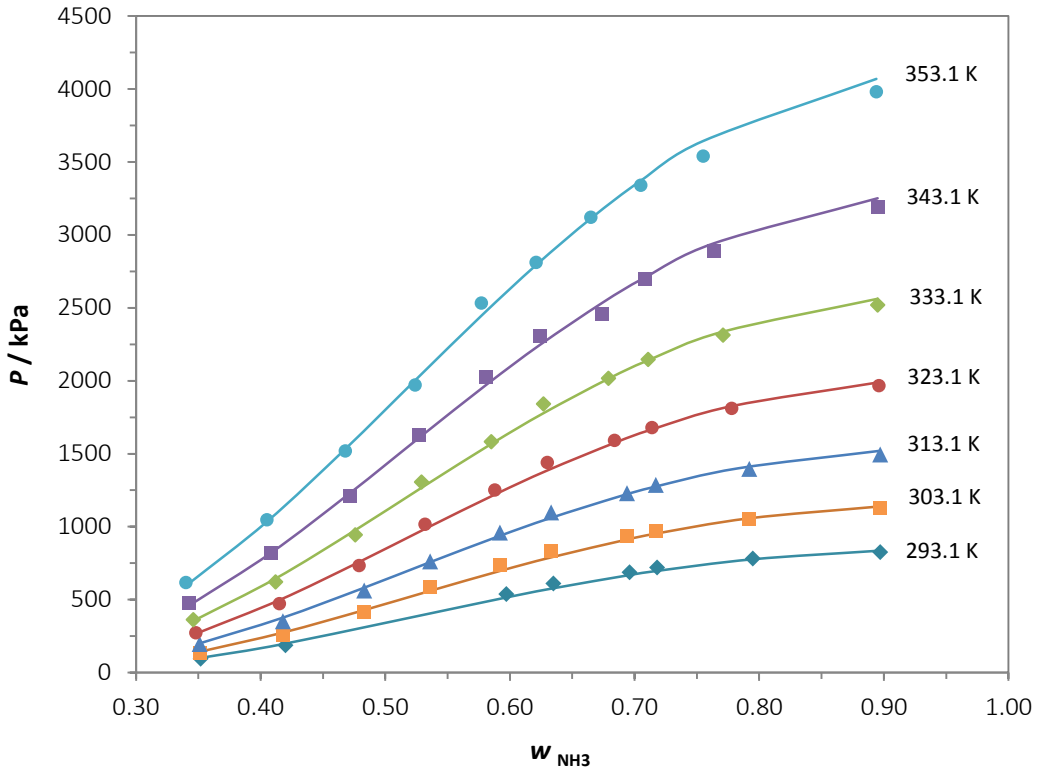

Figure 3.5. Experimental and calculated values of vapour pressure of NaSCN in ammonia solutions. Lines: modelling. Points: reported experimental data (Chaudhari et al., 2011)

Parameters *A, B, C, D* of solubility product constant K_{sp} based on the approximate method (eq. 3.77) of each solid phase in equilibrium are obtained by the regression of experimental solubility data by minimizing the objective function of maximum likelihood type (eq. 3.91).

$$\mathrm{OF} = \sum_{i=1}^{n}\left[\left(\frac{T_{\mathrm{calc},i} - T_{\mathrm{exp},i}}{\sigma_{T,i}}\right)^2 + \sum_{j=1}^{m}\left(\frac{x_{\mathrm{calc},i,j} - x_{\mathrm{exp},i,j}}{\sigma_{x,i,j}}\right)^2\right] \tag{3.91}$$

The following tables show the parameters obtained for each solid phase in equilibrium:

Table 3.7. Parameters of solubility product constant equation for NH_3/$LiNO_3$ system

Solid phase	*A*	*B*	*C*	*D*
$LiNO_3 \cdot 4NH_3$	-592.97	-10000	113.65	-0.185
$LiNO_3 \cdot 2NH_3$	-242.59	-10000	41.68	0.027
$LiNO_3$	-749.70	10000	123.41	-0.035

Table 3.8. Parameters of solubility product constant equation for NH_3/NaSCN system

Solid phase	*A*	*B*	*C*	*D*
NaSCN·3.5NH_3	-1289.81	10000	236.725	-0.4009
NaSCN	-947.01	-2060.77	184.880	-0.4032

Finally, with the binary interaction energy parameters required for the calculation of activity coefficients and the required parameters of the solubility product constant, the solid-liquid equilibrium can be carried out. As a result of the calculation of the solubility index, figures 3.6 and 3.7 present the results of modelling of solubility temperature of $NH_3/LiNO_3$ and NH_3/NaSCN systems respectively.

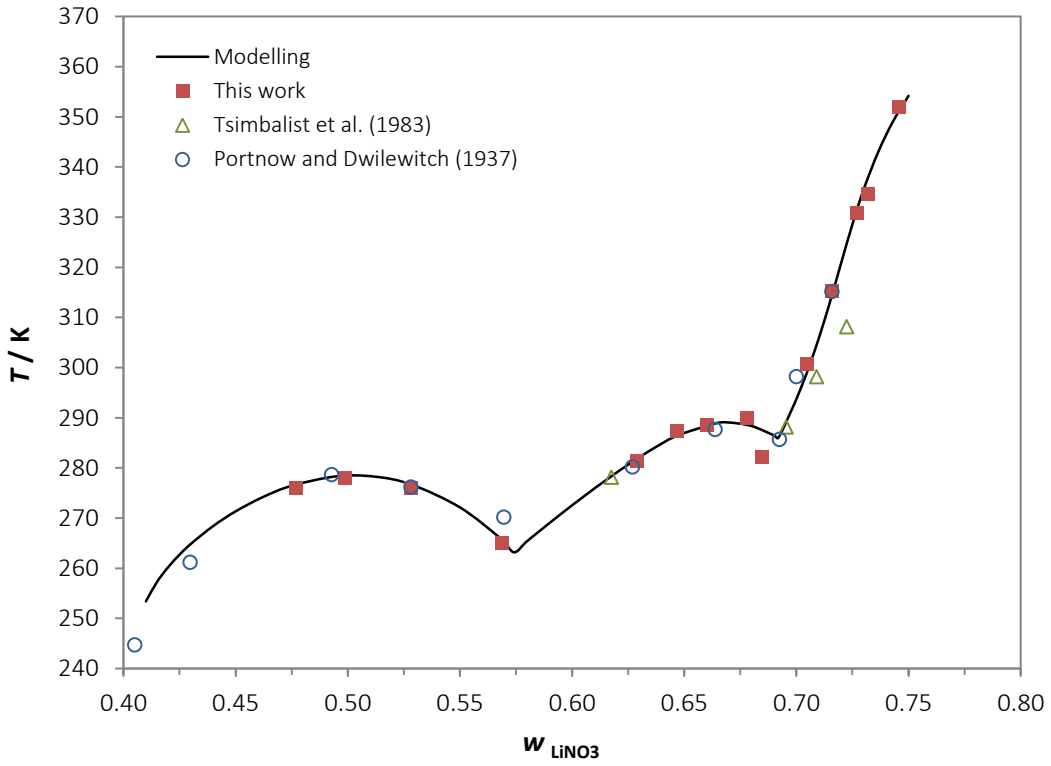

Figure 3.6. Modelling of solubility temperature of lithium nitrate in liquid ammonia at 20 bar

The modelling of solubility temperature of lithium nitrate in liquid ammonia presented in figure 3.6 shows very good agreement with experimental data of this work and from reported literature data. The RMSD and the maximum relative deviation obtained regarding experimental data of this work are 0.6 % and 2.0 % respectively.

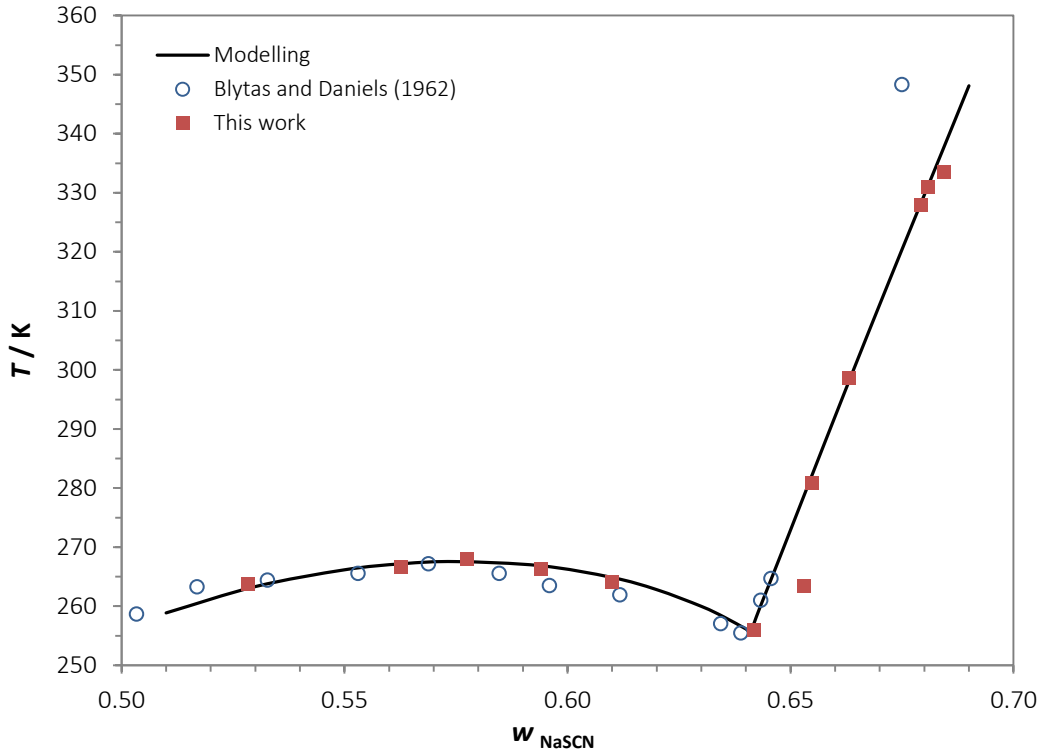

Figure 3.7. Modelling of solubility temperature of sodium thiocyanate in liquid ammonia at 20 bar

As it can be seen, the modelling of solubility temperature of sodium thiocyanate in liquid ammonia (figure 3.7) also presents a very good agreement with the experimental data of this work and with those values reported in literature. From the comparison of calculated and experimental solubility temperature presented in this work it is obtained a maximum relative deviation of 5.7 % and root mean square deviation of 1.7 %.

3.6. Conclusions

The modelling of solubility temperature of the systems $H_2O/LiNO_3$, $NH_3/LiNO_3$ and NH_3/NaSCN have been carried out by means of the solid-liquid equilibrium and thermodynamic models LIQUAC and Symmetric Electrolyte-NRTL.

The activity coefficient allows the representation of the behaviour of a real solution regarding an ideal solution in the chemical equilibrium; however, it is necessary to establish the criterion of the reference state of the components of the solution for its calculation. In the case of water as solvent it is used the asymmetric convention, in which the electrolyte is considered in infinite

dilution. In the case of ammonia as solvent it is used the symmetric convention, in which the electrolyte is represented as the pure molten salt.

The obtainment of the solubility product constant that allows the calculation of the solubility temperature of the solutions under study was obtained by a rigorous method for systems with water as solvent and an approximate method for systems with ammonia as solvent. The rigorous method is based on the direct calculation of the Gibbs free energy in the standard state by using Gibbs-Helmholtz equation, permitting the non-necessity of experimental solubility data for its calculation. On the other hand, the approximate method, due to the fact that the Gibbs free energy in the standard state ions is not available for non-aqueous solvents, is based on an expression with parameters that are obtained from regression of experimental solubility data.

The required binary interaction parameters of LIQUAC and symmetric electrolyte NRTL models have been obtained from the modelling of vapour liquid equilibrium and its comparison with reported vapour pressure literature data, obtaining root mean square deviation below 5.5 % and maximum deviations below 17 %.

For system $H_2O/LiNO_3$, the solubility modelling has been performed in a salt mass fraction range between 0.32 and 0.67, for $NH_3/LiNO_3$ system, between 0.41 and 0.75, and for NH_3/NaSCN between 0.51 and 0.69. From the results obtained, with root square mean deviations and maximum relative deviations regarding experimental data of this work lower than 3 % and 7 % respectively, it can be concluded that the modelling allows the obtainment of reliable results, but in the case of mixtures with ammonia as solvent it is required the use of experimental solubility data, what make it not as predictive as in the case of systems with water as solvent.

3.7. Nomenclature

a	activity
A	Debye-Hückel parameter
$a_{i,j}$	UNIQUAC interaction parameter between species i and j
b	Debye-Hückel parameter
B	second virial coefficient
$b_{i,j}$	middle-range interaction parameter between species i and j
$c_{i,j}$	middle-range interaction parameter between species i and j
Cp	heat capacity ($J \cdot mol^{-1} \cdot K^{-1}$)
D	dielectric constant
$d_{i,j}$	middle-range interaction parameter between species i and j
G	Gibbs energy ($J \cdot mol^{-1}$)
H	enthalpy ($J \cdot mol^{-1}$)
I	ionic strength, ionization potential
K_{sp}	solubility product constant
k_{B}	Boltzmann constant
M	molar mass ($kg \cdot mol^{-1}$)
N_{A}	Avogadro's number
m	molality ($mol \cdot kg^{-1}$)
n	mole number
P	pressure (kPa)
Q_{e}	electron charge
q	surface area parameter
R	general gas constant ($J \cdot mol^{-1} \cdot K^{-1}$)
r	volume parameter
T	temperature (K)
w	mass fraction
x	liquid mole fraction
y	vapour mole fraction
z	charge

Greek Letters

μ	chemical potential
γ	activity coefficient (mole fraction scale)
γ'	activity coefficient (molality scale)
ρ	density ($g \cdot cm^{-3}$)
ϑ	molar volume

ε_r	dielectric relative constant
τ	asymmetric binary interaction energy parameters
α	NRTL symmetric non-randomness factor parameter
$\emptyset$	fugacity coefficient
σ	deviation

Subscripts

a	anion
c	cation
i	component i
j	component j
m	solvent
r	reference property
w	water

Superscripts

o	Standard state
E	excess property
lc	local interaction contribution (electrolyte NRTL model)
LR	long range
MR	middle range
PDH	long-range interaction contribution (Pitzer-Debye-Hückel model)
s	saturated state
SR	short range

3.8. References

Abrams, D.S.; Prausnitz, J.M. *Statistical Thermodynamics of Liquid Mixtures: A New Expression for the Excess Gibbs Energy of Partly or Completely Miscible Systems*. AIChE J. 21 (1975) 116-128.

Bromley, L.A. *Thermodynamic properties of strong electrolytes in aqueous solutions.* AIChE J. 19 (1973) 313-320.

Campbell, A.N.; Fishman, J.B.; Rutherford, G.; Schaefer, T.P.; Ross, L. *Vapor pressures of aqueous solutions of silver nitrate, of ammonium nitrate, and of lithium nitrate.* Canadian J. Chem. 34 (1956) 151-159.

Chaudhari, S.K.; Salavera, D.; Coronas, A. *Densities, Viscosities, Heat Capacities, and VaporLiquid Equilibria of Ammonia + Sodium Thiocyanate Solutions at Several Temperatures.* J. Chem. Eng. Data 56 (2011) 2861–2869.

Chen, C.-C.; Britt, H.I.; Boston, J.F.; Evans, L.B. *Local Composition Model for Excess Gibbs Energy of Electrolyte Systems. Part I: Single Solvent, Single Completely Dissociated Electrolyte Systems*. AIChE J. 28 (1982) 588–596.

Chen, C.-C.; Evans, L.B. *Local Composition Model for the Excess Gibbs Energy of Aqueous Electrolyte Systems*. AIChE J. 32 (1986) 444–454.

Debye, P.; Hückel, E. T*he Theory of Electrolytes. I. Lowering the freezing point and related Phenomena*. Phys. Z. 24 (1923) 185-206.

Dulong, P.L.; Petit, A.T. *Recherches sur quelques points importants de la Théorie de la Chaleur*. Annales de Chimie et de Physique. 10 (1819) 395–413.

Fowler, R.H.; Guggenheim, E.A. *Statistical thermodynamics*. Cambridge University Press: Cambridge, U.K., 1949.

Fredenslund, A.; Jones, R.L.; Prausnitz, J.M. *Group-contribution estimation of activity coefficients in nonideal liquid mixtures*. AIChE J. 21 (1975) 1086–1099.

Kiepe, J.; Noll, O.; Gmehling, J. *Modified LIQUAC and Modified LIFAC. A Further Development of Electrolyte Models for the Reliable Prediction of Phase Equilibria with Strong Electrolytes*. Ind. Eng. Chem. Res. 45 (2006) 2361-2373.

Kikic, I.; Fermeglia, M.; Rasmussen, P. *UNIFAC prediction of vapor-liquid equilibria in mixed-solvent-salt systems*. Chem. Eng. Sci. 46 (1991) 2775-2780.

Li, J.; Polka, H.-M.; Gmehling, J. *A g^E model for single and mixed solvent electrolyte systems. 1. Model and Results for Strong Electrolytes*. Fluid Phase Equlib, 94 (1994) 89-114.

Li, J.; Polka, H.-M.; Gmehling, J. *A g^E model for single and mixed solvent electrolyte systems. 2. Results and Comparison with others Models*. Fluid Phase Equilib. 94 (1994) 115-127.

Li, J.; Lin, Y.; Gmehling, J. *A g^E Model for Single and Mixed-Solvent Electrolyte Systems. 3. Prediction of Salt Solubilities in Aqueus Electrolyte Systems*. Ind. Eng. Chem. Res. 44 (2005) 1602-1609.

Li, M.-Y.; Wang, L.S.; Gmehling, J. *Thermodynamics of Phase Equilibria in Aqueous Strong Electrolyte Systems.* Ind. Eng. Chem. Res. 50 (2011) 3621–3631.

Libotean, S.; Salavera, D.; Valles, M.; Esteve, X.; Coronas, A. *Vapor-Liquid Equilibrium of Ammonia + Lithium Nitrate + Water and Ammonia + Lithium Nitrate Solutions from (293.15 to 353.15) K.* J. Chem. Eng. Data 52 (2007) 1050-1055.

Mock, B.; Evans, L.B.; C.-C. Chen. Thermodynamic representation of phase equilibia of mixed-solvent electrolyte systems. AIChE Journal, 32 (1986) 1655-1664.

Pitzer, K.S. *Thermodynamics of Electrolytes. I: Theoretical and General Equations*. J. Phys. Chem. 77 (1973) 268-277.

Pitzer, K.S. *Electrolytes. From Dilute Solutions to Fused Salts*. J. Am. Chem. Soc. 102 (1980) 2902–2906.

Pitzer, K.S.; Simonson, J.M. *Thermodynamics of Multicomponent, Miscible, Ionic Systems: Theory and Equations.* J. Phys. Chem. 90 (1986) 3005–3009.

Sander, B.; Fredenslund, A.; Rasmussen, P. *Calculation of vapor-liquid equilibria in mixed solvent/salt systems using an extended UNIQUAC equation*. Chem. Eng. Sci. 45 (1986) 1171- 1183.

Song, Y.; Chen, C.-C. *Symmetric Electrolyte Nonrandom Two-Liquid Activity Coefficient Model*. Ind. Eng. Chem. Res. 48 (2009) 7788–7797.

Wagman, D.; Evans, W.H.; Parker, V.B.; Schumm, R.H.; Halow, I.; Bailey, S.M.; Churney, K.L.; Nuttall, R.L. *The NBS tables of chemical thermodynamic properties. Selected values for inorganic and C_1 and C_2 organic substances in SI units*. J. Phys. and Chem. Reference Data 11 (1982).

Wang, P.; Anderko, A.; Young, R.D. *A Speciation-Based Model for Mixed-Solvent Electrolyte Systems*. Fluid Phase Equilib. 203 (2002) 141–176.

Yan, W.; Topphoff, M.; Rose, C.; Gmehling, J. *Prediction of vapor–liquid equilibria in mixed-solvent electrolyte systems using the group contribution concept.* Fluid Phase Equilib. 162 (1999) 97–119.

Chapter 4

Solubility of LiBr + $LiNO_3$ + LiI + LiCl in Aqueous Solutions

4.1. Introduction

Throughout last years, many studies on the new absorbents have been carried out to improve the solubility of H_2O/LiBr mixture, used in absorption refrigeration chillers for air-conditioning applications in order to make it compatible with air-cooled absorbers, which involves higher absorbent compositions. As shown in the *Chapter 1*, these new proposed absorbents can be based on either organic or inorganic compounds added into the mixture. However, in this study only the addition of lithium salts to the original H_2O/LiBr mixture is analysed.

Iyoki et al. (1993) proposed two different alternatives to the H_2O/LiBr mixture with the aim of improving its properties. The first one consisted in the addition of LiI to improve the solubility and the second one consisted in the addition of $LiNO_3$ to improve the solubility and to decrease the corrosivity of the mixture. The solubility study of the mixture H_2O/(LiBr+LiI) was performed by visual-polythermal method in a range of salt mass fraction from 0.56 to 0.686, with an optimum salt mole ratio 4:1, determined in a previous study (Iyoki et al., 1990) at a constant absorbent mass fraction of 0.625. The solubility of H_2O/(LiBr+$LiNO_3$) was studied in a range of total salt mass

fraction from 0.615 to 0.811, with the optimum salt mole ratio of 4:1 obtained at constant salt mass fraction of 0.70. The results showed that the H_2O/(LiBr+LiI) mixture provides better solubility than the H_2O/(LiBr+$LiNO_3$) mixture regarding the original water/lithium bromide mixture (Salavera et al., 2004) (figure 4.1).

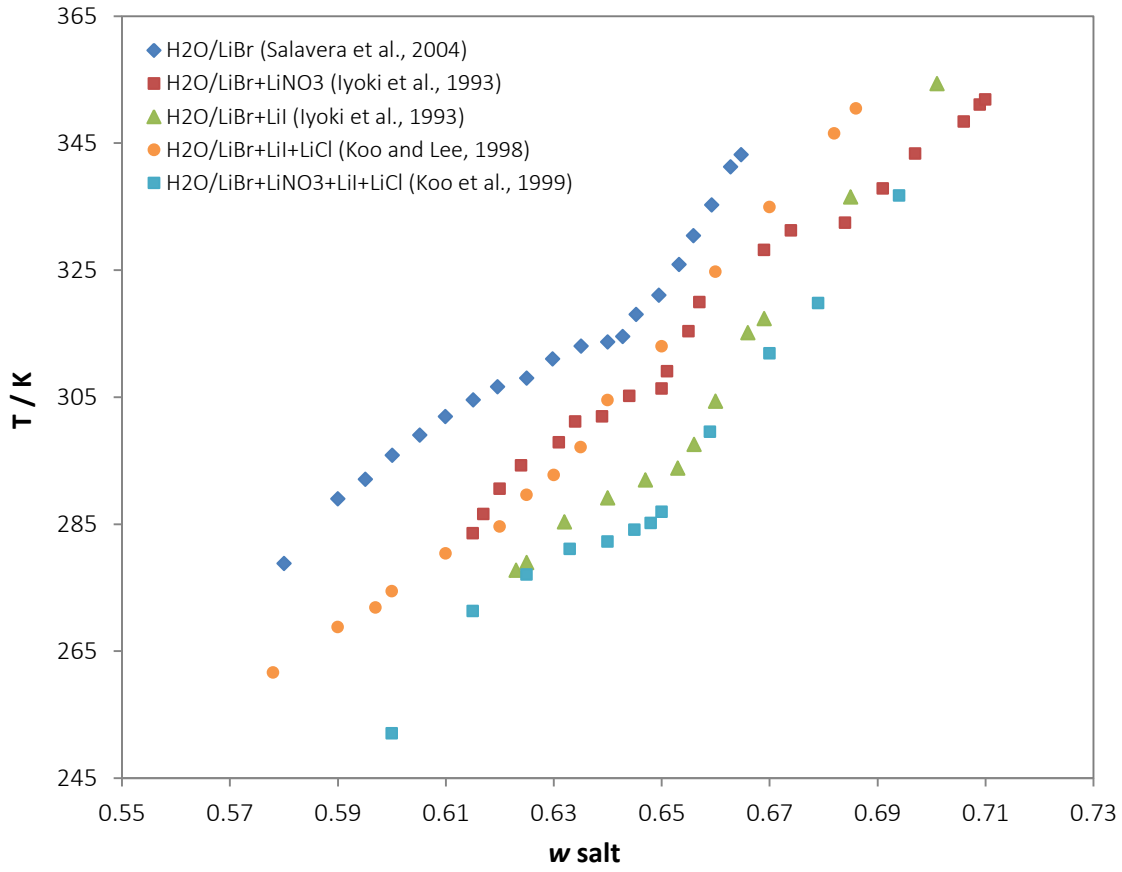

Figure 4.1. Solubility temperature of some mixtures of water with lithium salts. Experimental data reported in literature

Koo and Lee (1998), based on the H_2O/(LiBr+LiI) mixture of Iyoki et al. (1993), proposed the addition of LiCl to decrease the vapour pressure because it was considered higher than desired for a working fluid (Iyoki et al., 1990). The effect of lithium chloride in the solubility was measured by visual-polythermal method in a range of salt mass fraction from 0.56 to 0.686. The proposed optimum salt mole ratio was 4.5:1:2 obtained at 0.60 total salt mass fraction. However, they only showed solubility results of LiBr/LiI ratios, no results of solubility and vapour pressure at different LiCl salt ratios were presented. The addition of LiCl supposed a considerable worsening in the solubility regarding the same mixture without LiCl (figure 4.1) but still supposed a solubility improvement regarding H_2O/(LiBr+$LiNO_3$) mixture for salt mass fractions higher than 0.66.

Koo et al. (1999) suggested the H_2O/(LiBr+$LiNO_3$+LiI+LiCl) mixture which collects the improvements of the mixtures introduced previously by Iyoki et al. and Koo et al. (1998). Also using visual-polythermal method, the solubility of the mixture was studied in a range of total salt mass fraction from 0.60 to 0.694 with salt mole ratio of 5:1:1:2. The determination of the optimum salt mole ratio was carried out in experiments at different salt mole ratios of LiBr/$LiNO_3$, LiI/$LiNO_3$ and LiI/LiCl at total salt mass fractions of 0.58, 0.60 and 0.625. However, no results of solubility at different ratios of LiCl/Li were shown. The results showed an improvement in the solubility as compared to the other lithium salt mixtures proposed previously in the literature (figure 4.1).

Recently, some authors (Salavera et al., 2004, 2005; Yoon et al., 2005) have considered the lithium salts mixture proposed by Koo et al. (1999) as a good alternative to improve the solubility and reduce corrosivity of the conventional water-lithium bromide solution. Consequently, they studied its thermophysical properties and heat/mass transfer performance in the absorber. However, this mixture should be discussed and reconsidered because some aspects, such as the solubility for concentrated solutions higher than 62.5 % of salt or the effect of the addition of LiCl to the solubility of the mixture, were not taken into account.

Within this background and considering that the mixture proposed by Koo et al. (1999) is the one that obtains better solubility, the objective of this work is to accomplish an extension of the solubility study of Koo et al. (1999) by analysing the optimum salt mole ratio at higher absorbent compositions.

In the first study it has been analysed, by rough visual-polythermal method using sample tubes, how the separate addition of $LiNO_3$, LiI and LiCl at different salt mole ratios $LiNO_3$/LiBr, LiI/$LiNO_3$ and LiCl/Li respectively affects to the solubility of H_2O/LiBr. The experiments have been done at total salt mass fractions of 0.65, 0.675 and 0.69 with the aim to obtain the mole ratio of salts that has the minimum solubility temperature of the mixture. The order of lithium salts addition has been established following the experimental procedure Koo et al. (1999), with the aim of obtaining the main solubility improvement with $LiNO_3$ diminishing as much as possible the amount of LiI because of the high economic cost that suppose regarding the other salts. The addition of LiCl has been left to the final stage because according to the literature it is not expected to improve the solubility, its addition is made with the aim of decreasing the vapour pressure of the mixture.

In this way, it has also been modelled with Aspen Properties software, using asymmetric Electrolyte-NRTL activity coefficient model, the vapour pressure of the mixture when the different lithium salts are added, especially lithium chloride in order to analyse whether its addition to decrease the vapour pressure of the optimum mixture obtained is justified.

Once obtained the optimum mole ratio of lithium salts, the solubility temperature of the new composition mixture has been precisely measured, by visual-polythermal methodology using a glass solubility cell, in a range of salt mass fraction from 0.61 to 0.70.

4.2. Operating principle and procedure

The principle of measurement of the solubility temperature of the studied mixtures is a synthetic and visual—polythermal method. The procedure is based on the variation of the temperature of the experiment, maintaining constant the pressure and composition of the sample, until the visual determination of the dissolution of the last crystal of solute. The temperature at which the last crystal of salt is dissolved corresponds to the solubility temperature.

4.3. Experimental device

Depending on the working solvent, the characteristics and configurations of the devices for the solubility determination based on the direct visualization of the experiment changes. In case of aqueous solvents at atmospheric working pressure, the devices are quite simple, mainly made of glass for an optimal visualisation of the experiment.

This section describes the apparatus used for the determination of the optimum lithium salts ratios (LiBr:$LiNO_3$:LiI:LiCl) in aqueous solution and the apparatus used for the precise solubility temperature determination of the optimal mixture obtained.

4.3.1. Sample tubes

Rough solubility measurements of lithium salt mole ratios have been carried out by means of standard sample tubes (figure 4.2) of 17.4 cm^3 (1.5 cm diameter, 16.1 cm height) immersed in a thermal bath Julabo F33-EH with working temperature range from 240 K to 423 K, temperature

stability ± 0.03 K and resolution ± 0.1 K (figure 4.3). Ethylene glycol, with a range of temperatures from 233 K to 403 K in liquid phase, is used as thermostatic fluid to provide the required range of temperatures to perform all the measurements.

Figure 4.2. Sample tubes with lithium salts in aqueous solution

Figure 4.3. Sample tubes immersed in thermal bath to temperature control

Although this methodology has not been previously validated, it has been chosen because the purpose of these experiments is not to obtain a very accurate value of solubility temperature, but to obtain the behaviour and tendency of the different ratios of lithium salts in order to find the mixture with better solubility. In addition, it allows multiple simultaneous solubility measurements, thus saving experimentation time.

4.3.2. Glass solubility cell

The accurate solubility temperature measurements of the optimum mole ratio of lithium salts obtained has been performed by means of a glass solubility cell. The solubility cell available in Group of Research on Applied Thermal Engineering – CREVER is the same that reported by Salavera et al. (2004). The experimental device (figure 4.4) has total dimensions (without orifices) of 12.6 cm height and 9.8 cm diameter, and is entirely made of pyrex glass with three concentric chambers.

Figure 4.4. Solubility cell

Figure 4.5. Equipment used for measuring solubility of salts in water at atmospheric pressure

The internal chamber, with an approximate volume of 40 cm^3, houses the sample under study and it is constituted by two orifices through which can be introduced the solute and solvent and the temperature probe for measuring the temperature of the experiment. The intermediate chamber allows the temperature control of the experiment by means of the recirculation of thermostatic fluid, which enter the cell through the bottom orifice and exit through the top orifice to ensure that the cell is always filled, avoiding dead volumes. The external chamber has vacuum atmosphere to thermally isolate the intermediate chamber from the outside and to avoid condensation at the wall when the temperature is lower than the room temperature, allowing an optimal visualization of the experiment.

The temperature control is carried out with a thermal bath Julabo EH-F33 by means of ethylene glycol recirculation. The temperature is measured by a platinum temperature Pt100 with uncertainty 0.005 K, connected to a calibrated thermometer ASL F100 with resolution ± 0.001 K in a range from 273.15 K to 423.15 K. In order to ensure the correct homogenization of the solution and temperature, the content of the solubility cell is continuously stirred using a magnetic bar placed inside the solution and activated by a magnetic stirrer P-Selecta AGIMATIC-N placed under the solubility cell.

The estimated expanded uncertainty (k = 2) of temperature has been determined to be 0.2 K (details in section 4.6.2)

4.4. Experimental methodology

In the following section it is explained the experimental methodology used for the solubility temperature determination, which is divided in three parts: the preparation of the aqueous solutions of lithium salts (LiBr, $LiNO_3$, LiI and LiCl), the solubility temperature measurement and the emptying and cell cleaning.

4.4.1. Chemicals

Lithium bromide (purity ≥ 0.99) is supplied by Sigma-Aldrich. Lithium iodide (purity 99.9 %) is supplied by Sigma-Aldrich. Lithium nitrate (purity ≥ 0.98) is supplied by Fluka. Lithium chloride (purity ≥ 0.99) is supplied by Panreac. Milli-Q water (resistivity lower than 18.2 MΩcm) is used to prepare aqueous solutions. All chemicals are used without further purification. The salts are dried in an oven at 373 K for at least 24 h and maintained in a desiccator at room temperature before being used.

4.4.2. Sample preparation

The preparation of the sample, constituted by the salt/s and the solvent, depends on whether the experiment is performed in the sample tubes or in the solubility cell.

a) Sample tubes

The required mass of lithium salts for the mixture under study is measured separately in a funnel for solids and is directly introduced into the sample tube. The required amount of water is determined by mass in an appropriate syringe and is directly introduced into the sample tube.

The quantity of lithium salts and water introduced is determined by mass difference of the funnel and the syringe in balance Mettler AE260 DeltaRange (resolution ± 0.1 mg).

b) Solubility cell

The solubility cell is placed inside a mass balance Mettler Toledo PR2003 DeltaRange (resolution ± 0.001 g). In one of the orifices of its internal chamber is placed a funnel whereby are introduced and directly determined the required mass of lithium salts. The deionised water is introduced through the same orifice with a syringe.

The desired most concentrated solution is prepared first to reduce the amount of salt required for the experiments and to simplify the procedure of the sample preparation. Finally, by the addition of the required water into the solution, the rest of the desired diluted compositions of the mixture will be obtained.

The estimated expanded uncertainty (k = 2) of mass faction has been determined to be 0.0003 for the most concentrated solution and 0.0009 for the most diluted solution (details in section 4.6.1)

4.4.3. Solubility temperature measurement procedure

The determination of the solubility temperature of the mixtures is practically similar for the measurements in the sample tubes or in the solubility cell. The only difference is the accuracy in which the solubility temperature is obtained. The solubility measurements for the determination of the optimum mole ratio of lithium salts are performed with an accuracy of ± 1 K. On the other hand, the solubility temperature determination of the optimum ratio obtained is precisely measured with an accuracy of ± 0.1 K.

Before starting the procedure, since the mixture of water with lithium salts produces an exothermic reaction, after the addition of water to the lithium salts the solution has to be immediately cooled to control the reaction temperature. Once the oversaturated solution is stable and with continuous stirring, the procedure for determining the solubility temperature is described as follows:

1) The first solubility temperature measurement is always higher than the real solubility temperature because at the beginning salt presents compacted blocks that require more temperature to be dissolved. For this reason, a high temperature is set until the salt is dissolved. The reached temperature is maintained for 15 minutes to ensure a complete dissolution.
2) Next, a low temperature is set to cool the sample until reaching the precipitation of the solution at temperature T2.
3) Temperature is increased at a value 5 K higher than T2 and later in intervals of 2 K until complete dissolution is reached in the interval T3-T4, waiting 15 minutes between each change of temperature to ensure thermal stabilization.

4) The sample is cooled again until the precipitation is reached at T5.
5) For the third dissolution the temperature is set at T3. Then, if the experiment is to obtain the optimum salt ratio, the temperature is increased in intervals of 1 K. If the experiment is for obtaining the precise solubility temperature of the optimum mixture, the temperature is increased in intervals of 0.5 K, which are lowered to 0.2, and 0.1 K progressively as the amount and size of the salt decrease. For both cases, 15 minutes are waited between each temperature change to assure thermal stabilization.
6) The solubility temperature is reached when no crystal is visualized in the solution.
7) Finally, the steps 4-6 are repeated at least two times more to assure reproducibility.

4.4.4. Sample extraction and cleaning

Once the experiments are finalized, the sample extraction procedure consists of disassembling the measuring device from the thermal bath, extracting the solution from the sample tube or from the orifices of the solubility cell and emptying it in the proper container. Both devices are cleaned with soapy water, acetone and finally dried in a drying oven at 373 K.

4.5. Experimental results

4.5.1. Determination of the optimum mole ratio of lithium salts

The procedure for the determination of the optimum mole ratio of lithium salts has been carried out in three different stages at total salt mass fraction of 0.65, 0.675 and 0.69. These compositions suppose an extension and improvement of the study of Koo et al. (1999) for absorption chillers with air-cooled absorbers, in which the absorbent compositions achieves higher values than absorbers refrigerated by water cooling tower.

In a *first stage*, it is analysed how the addition of $LiNO_3$ affects to the solubility of the mixture H_2O/LiBr. In these experiments, firstly the solubility temperature of water/lithium bromide is measured and then the solubility temperature of the system H_2O/(LiBr+$LiNO_3$) by adding lithium nitrate at $LiNO_3$/LiBr mole ratios from 0 to 0.20 for 0.65 total salt mass fraction and from 0 to 0.23 for 0.675 and 0.69 total salt mass fractions. Figure 4.6 shows the experimental solubility results of this work and the results of crystallization temperature obtained by Koo et al. (1999) at total salt

mass fractions of 0.58, 0.60 and 0.625. The solubility temperature decreases as the ratio $LiNO_3$/LiBr increases until certain ratio in which a minimum is reached and is produced a pronounced turning point, from which the solubility increases again.

In the results of Koo et al. (1999), the minimum crystallization temperature obtained corresponds to a mole ratio of 0.2. However, the experimental results obtained in this work are quite different. For a total salt mass fraction of 0.65, the ratio with the minimum solubility temperature is the same that obtained by Koo et al. (1999), with a decrease in the solubility temperature of 22 K regarding H_2O/LiBr mixture. At total salt mass fraction of 0.675 and 0.69, the minimum solubility temperature obtained for both mass fractions correspond to a salt mole ratio $LiNO_3$/LiBr of 0.15, with a decrease of the solubility temperature of 27 K and 26 K respectively. Thus, the optimum salt mole ratio of the H_2O/(LiBr+$LiNO_3$) mixture has been set to 0.143 (to allow margin of error in the sample preparation) because the minimum ratio that obtains a minimum solubility temperature of one composition determines the optimum mole ratio of lithium salts.

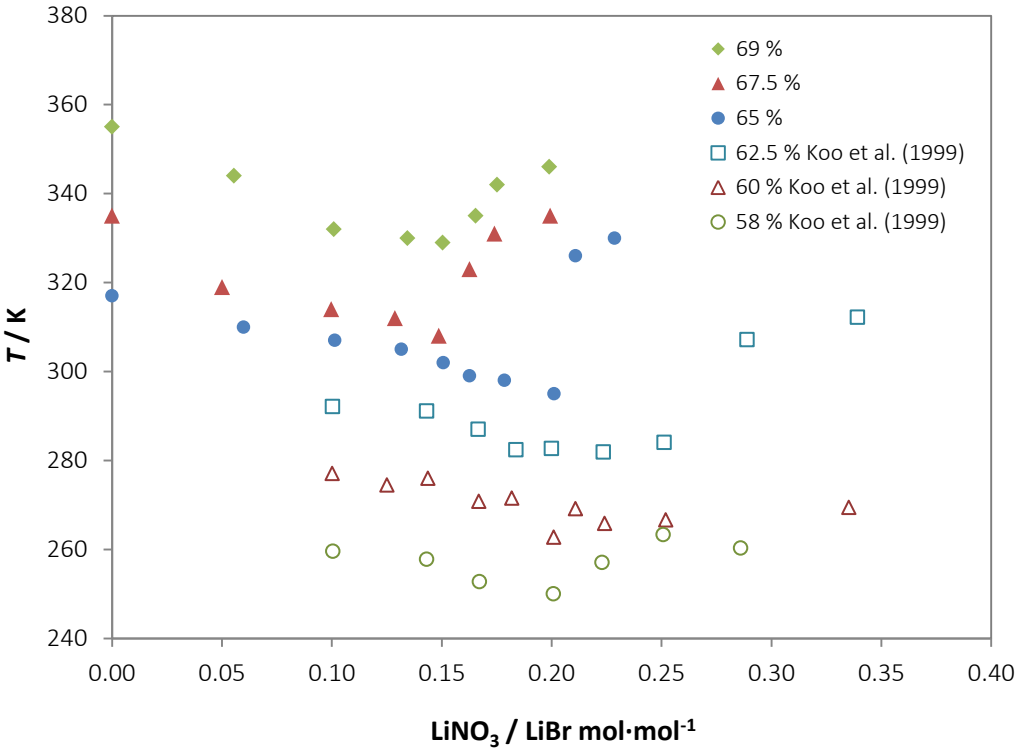

Figure 4.6. Solubility temperature of H_2O/(LiBr+$LiNO_3$) mixture at different $LiNO_3$/LiBr mole ratios and total salt mass compositions from 58 % to 62.5 % (lit.) and 65 % to 69 % (experimental)

In the *second stage*, it is analysed how the addition of LiI affects to the solubility of the H_2O/(LiBr+$LiNO_3$) mixture. Fixed the optimum mole ratio $LiNO_3$/LiBr obtained in the previous

mixture to 0.143, the solubility temperature of the H_2O/(LiBr+$LiNO_3$+LiI) system at LiI/$LiNO_3$ mole ratios from 0 to 2 has been measured.

As it can be observed in figure 4.7, there is no pronounced turning point from which the temperature increases as the previous case. Instead, the solubility temperature decreases up to the last ratio Li/$LiNO_3$ measured. For the total salt mass fraction of 0.69, the solubility temperature drops rapidly 18 K and then continues decreasing slowly. The same pattern happens with total salt mass fraction of 0.65, with a temperature drop of 11 K, but in this case there is a smooth turning point corresponding to the salt mole ratio of 0.5. For the mass fraction of 0.675 it is not observed a temperature drop as the other salt composition, but there is also a smooth turning point associated to salt the mole ratio of 0.5. Hence, the optimum Li/$LiNO_3$ salt mole ratio has been established to 0.5 because it provides a good decease in the solubility temperature with low amount lithium iodide.

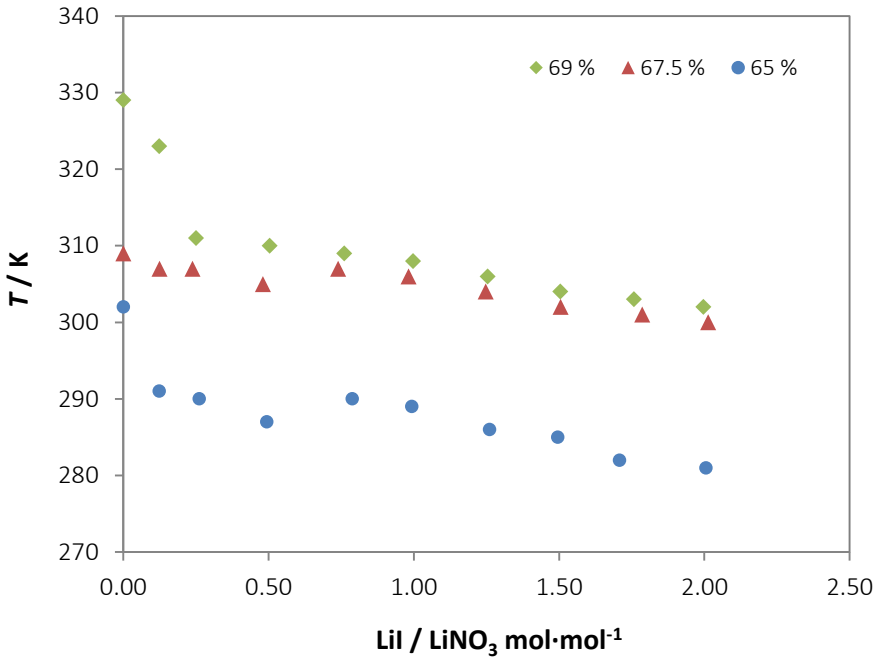

Figure 4.7. Experimental solubility temperature of H_2O/(LiBr+$LiNO_3$+LiI) mixture at different Li/$LiNO_3$ mole ratios and salt mass composition from 65 % to 69 %

In the *third stage* it is analysed how the addition of LiCl affects to the solubility of the H_2O/(LiBr+$LiNO_3$+LiI) mixture. For these experiments, the $LiNO_3$/LiBr and LiI/$LiNO_3$ mole ratios have been fixed to the optimum value obtained from the previous experiments, that is, 0.143 and 0.5 respectively. The solubility temperature of H_2O/(LiBr+$LiNO_3$+LiI+LiCl mixture has been measured at LiCl/LiI mole ratios from 0.125 to 2.000.

As expected according to the literature, there is no appreciable solubility improvement with the addition of lithium chloride. For the three absorbent compositions analysed, between 0 – 0.250 LiCl/LiI salt mole ratios, it is produced an increase in the solubility temperature and then slightly decreases again maintaining the solubility temperature constant up to LiCl/LiI mole ratio of 1 (figure 4.8). From this point, the solubility varies depending on the salt mass composition of the mixture. For salt mass fraction of 0.675 the solubility remains constant, obtaining the same solubility than the lower mole ratios measured. However, for mixtures with salt mass fractions of 0.65 and 0.69 it is produced a high worsening in the solubility. In the case of salt mass fraction of 0.65, a change of the mole ratio from 1 to 1.5 leads to an increase in the solubility temperature of 30 K and still increases 3 K when a mole ratio of 2 is achieved. The mixture with salt mass fraction of 0.69 shows a similar behaviour, when the mole ratio is increased from 1 to 1.5 the solubility temperature increases 16 K but remains constant when the mole ratio is increased to 2.

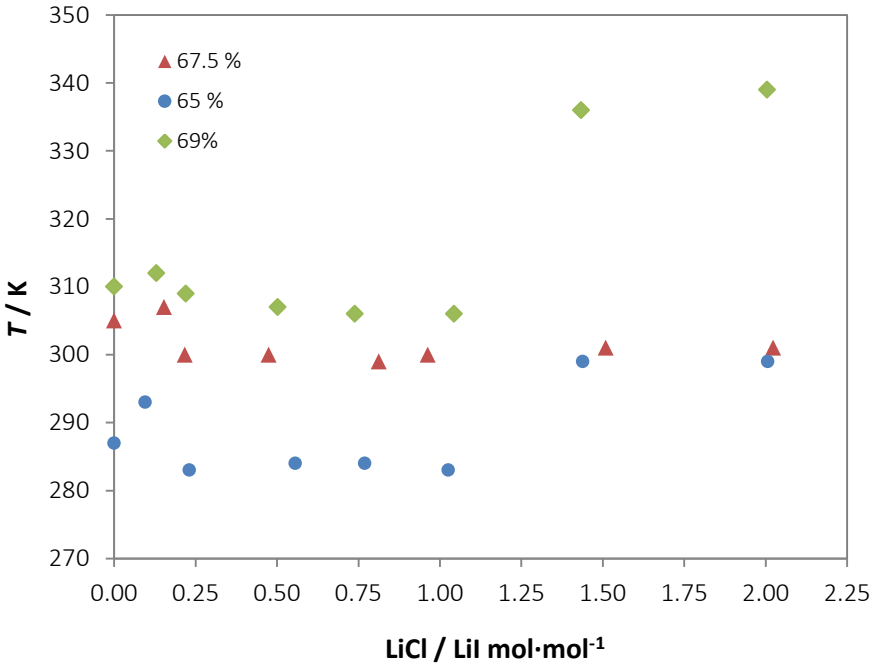

Figure 4.8. Experimental solubility temperature of H_2O/(LiBr+$LiNO_3$+LiI+LiCl) mixture at different LiCl/LiI mole ratios and salt mass compositions from 65 % to 69 %

Considering the obtained results, from the point of view of the improvement in solubility, the addition of LiCl to the mixture can be discarded. Also, from the point of view of vapour pressure (see section 4.7), it is shown that it doesn't provide a decrease of vapour pressure of the mixture, obtaining even worse results of vapour pressures for the higher salt compositions analysed.

Thus, from each one of the experiments carried out at total salt fraction range from 0.65 to 0.69 and salt mole ratios LiBr/$LiNO_3$, LiBr/LiI and LiCl/Li, the optimum mole ratio of lithium salts has been determined to be 7:1:0.5 (LiBr:$LiNO_3$:LiI) in the H_2O/(LiBr+LiNO3+LiI) system.

4.5.2. Solubility of the optimum mixture

Once the optimum mole ratio of lithium salts is obtained, the solubility temperature of the optimum mixture H_2O/(LiBr+$LiNO_3$+LiI) is precisely measured in a range of total salt mass fraction from 0.6245 to 0.6907, covering a solubility temperature range from 275.1 K to 309.8 K (figure 4.9).

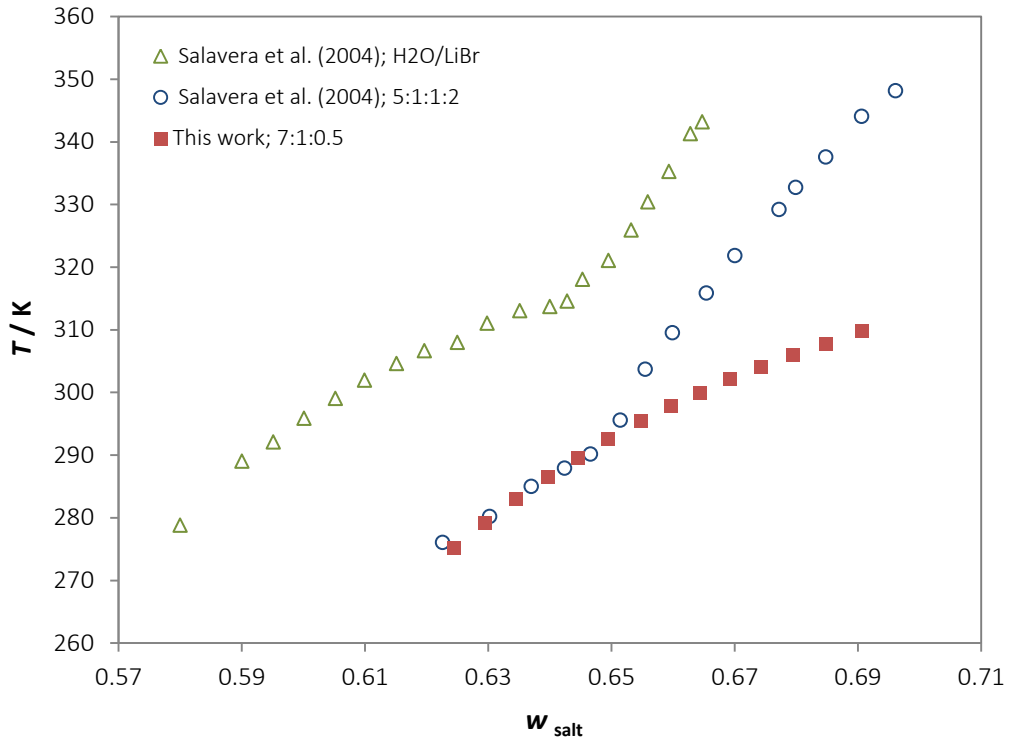

Figure 4.9. Experimental solubility temperature of H_2O/(LiBr+$LiNO_3$+LiI) mixture (molar salt ratio 7:1:0.5) and comparison with solubilities of H_2O(/LiBr+$LiNO_3$+LiI+LiCl) mixture (mole ratio 5:1:1:2) reported in literature

Figure 4.9 shows a comparison of the experimental solubility results obtained in this work (table 4.1) with the results obtained by Salavera et al. (2004) using the mixture proposed by Koo et al. (1999) (H_2O/(LiBr+$LiNO_3$+LiI+LiCl), mole salt ratio of 5:1:1:2), and the solubility of the H_2O/LiBr mixture. Both measured with the same experimental device and methodology than the used in this work.

As it can be observed, the solubility temperature increases as the lithium salt composition increases. The behaviour of the curves obtained by Salavera et al. (2004) present a turning point that corresponds to a change of the solid phase in equilibrium with the solvent (solid phase associated to n solvent molecules). However, the solubility of the optimum mixture obtained in this work doesn't present any turning point.

Table 4.1. Experimental solubility temperature of H_2O/(LiBr+$LiNO_3$+LiI) mixture (7:1:0.5)

w salt	*T* / K
0.6907	309.8
0.6848	307.8
0.6794	306.0
0.6743	304.1
0.6693	302.2
0.6644	300.0
0.6597	297.8
0.6548	295.4
0.6495	292.6
0.6446	289.6
0.6396	286.5
0.6346	283.0
0.6295	279.2
0.6245	275.1

The results obtained in this work present similar solubilities regarding the results presented by Salavera et al. (2004) for salt mass fractions up to 0.65. From this point, a significant improvement of the solubility is obtained as the salt composition increases, reaching a decrease of solubility temperature of 35 K for salt mass fraction of 0.69.

The solubility of the new composition mixture proposed in this work has been quantitatively compared with the solubility of the quaternary solution reported by Salavera et al. (2004) (table 4.3) by means of the correlation of the experimental results of this work using the following polynomial equation:

$$T = \sum_{i=0}^{2} A_i \, w^i \tag{4.1}$$

where w is the salt mass fraction and A_i are the coefficients listed in table 4.2. The maximum and average solubility temperature deviation obtained is 0.3 K and 0.1 K respectively.

Table 4.2. Coefficients of equation 4.1

A_0	$-1.77075 \cdot 10^3$
A_1	$5.77359 \cdot 10^3$
A_2	$-3.99868 \cdot 10^3$

Table 4.3. Comparison between solubility temperature of H_2O/(LiBr+$LiNO_3$+LiI+LiCl) (5:1:1:2) (Salavera et al., 2004) and H_2O/(LiBr+$LiNO_3$+LiI) (7:1:0.5) calculated with equation 4.1

w salt	*T* / K Salavera et al.	*T* / K This work	Δ*T*
0.6906	344.0	309.4	-34.6
0.6848	337.6	307.8	-29.7
0.6799	332.7	306.3	-26.4
0.6772	329.2	305.3	-23.8
0.6700	321.8	302.5	-19.3
0.6654	315.9	300.6	-15.3
0.6599	309.5	297.9	-11.6
0.6555	303.7	295.7	-8.0
0.6514	295.6	293.4	-2.1
0.6466	290.2	290.6	+0.5
0.6424	287.9	288.0	+0.1
0.6370	285.0	284.5	-0.5
0.6302	280.2	279.7	-0.5
0.6226	276.0	273.9	-2.2

To sum up, regarding the mixture proposed by Koo et al. (1999) the mixture proposed in this work provides not only a significant improvement in the solubility for salt mass fractions from 0.65, but also is constituted by lower amount of lithium nitrate, lithium iodide, and the lithium chloride is eliminated from the mixture.

4.6. Measurement uncertainty

4.6.1. Mass fraction uncertainty

The uncertainties associated to the salt mass fraction of the different aqueous mixtures of lithium salts are directly related to the balances Mettler AE260 and Mettler Toledo PR 2003, used to determine the mass of all compounds of the mixtures. The uncertainty sources of the mass balances given by the manufacturer include resolution, calibration, linearity, accuracy and reproducibility.

Since the first sample prepared is the most concentrated solution and the subsequent solutions are obtained by dilutions, the uncertainty of the mass of water propagates and increases as the number of dilutions increases. Hence, the minimum uncertainty corresponds to the initial prepared solution, and the maximum uncertainty corresponds to the most diluted solution. This results to an expanded uncertainty (k = 2) of the total salt mass fraction of 0.0003 and 0.0009 respectively.

4.6.2. Temperature uncertainty

The uncertainty of the temperature corresponds to the uncertainties associated to the resolution and calibration of the thermometer ASL F100 connected to a probe Pt100, as well as the homogeneity, stability and repeatability of the temperature measurements along the experiments. The expanded uncertainty (k = 2) obtained is 0.2 K. A detailed explanation of the uncertainties calculation is presented in *Annex B.*

4.7. Vapour pressure modelling

Vapour liquid equilibrium of water/salts mixtures are expressed with equation 4.2, in which due to the non-volatility of the lithium salts, only water is exchanged in vapour-liquid phases (detailed previously in section 3.5.1):

$$\emptyset_{\mathrm{w}}\, y_{\mathrm{w}}\, P = x_{\mathrm{w}}\, \gamma_{\mathrm{w}}\, \emptyset_{\mathrm{w}}^{\mathrm{s}}\, P_{\mathrm{w}}^{\mathrm{s}} \exp\left[\frac{v_{\mathrm{w}}(P - P_{\mathrm{w}}^{\mathrm{s}})}{RT}\right] \qquad (4.2)$$

The modelling of vapour pressure of the aqueous lithium salts mixtures has been performed with Aspen Properties software by means of asymmetric Electrolyte-NRTL activity coefficient model in order to analyse if lithium chloride decreases the vapour pressure of the optimum mixture experimentally obtained.

The explanation of the model is omitted because Aspen Properties uses the symmetric E-NRTL model explained in (section 3.4.1) but modified to work as asymmetric model (infinite dilution). Electrolyte-NRTL model, based on the representation of the excess Gibbs energy of aqueous electrolyte systems, allows obtaining good data correlation results over a wide range of salt composition and temperature.

4.7.1. Validation of vapour pressure modelling

In a first step, the vapour pressure modelling of LiBr, $LiNO_3$, LiI and LiCl aqueous solutions has been compared to reported literature data in a wide range of salt mass fractions and temperatures from 273.15 K to 483.7 5 K to validate and evaluate the reliability of the model for single electrolyte aqueous solutions (figures 4.10 – 4.13). In all cases, the relative deviation increases with salt mass fraction. In order to mitigate these deviations the interaction parameters have been fitted (eq. 3.75 and 3.76, Chapter 3) from reported literature values of vapour pressure (table 4.3).

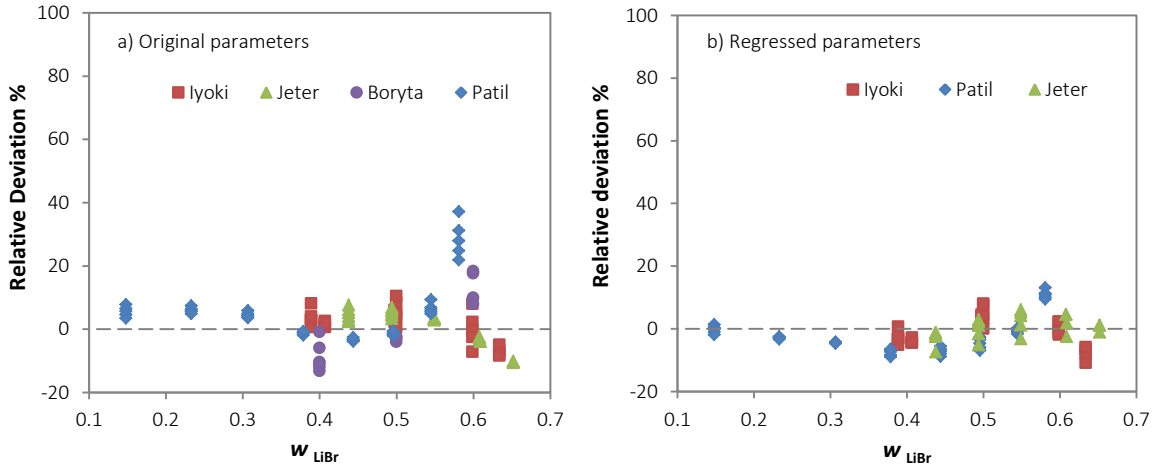

Figure 4.10. Deviation between calculated and experimental vapour pressure of H_2O/LiBr system (Iyoki and Uemura, 1989; Jeter et al., 1992; Boryta et al., 1975; Patil et al., 1990) and comparison between original and regressed electrolyte pair parameters

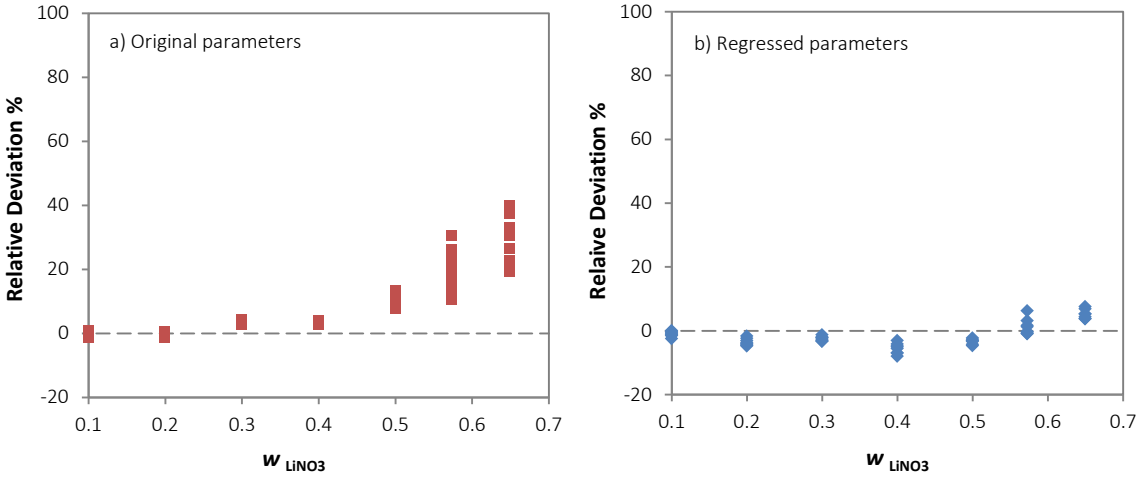

Figure 4.11. Deviation between calculated and experimental vapour pressure (Campbell et al., 1956) of $H_2O/LiNO_3$ and comparison between original and regressed electrolyte pair parameters

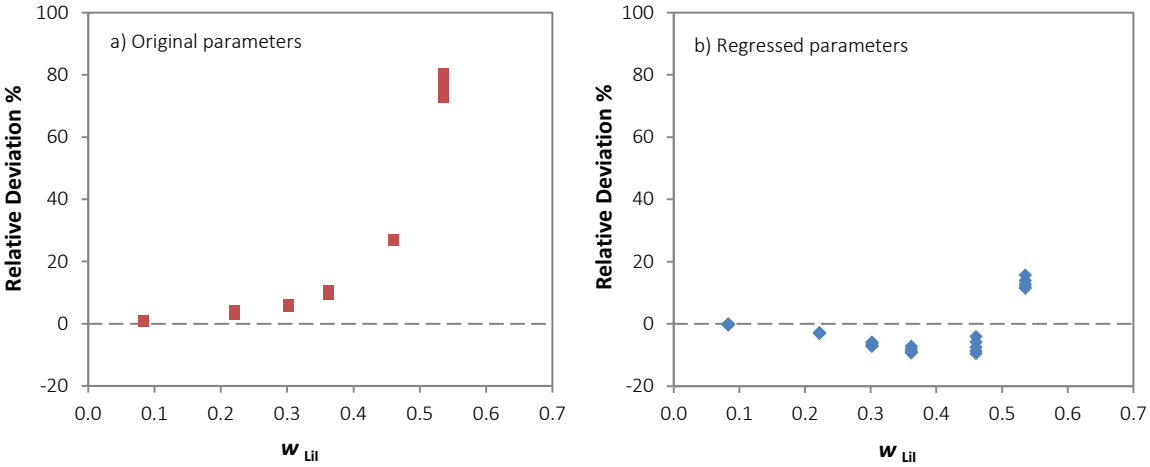

Figure 4.12. Deviation between calculated and experimental vapour pressure (Patil et al., 1990) of H_2O/LiI and comparison between original and regressed electrolyte pair parameters

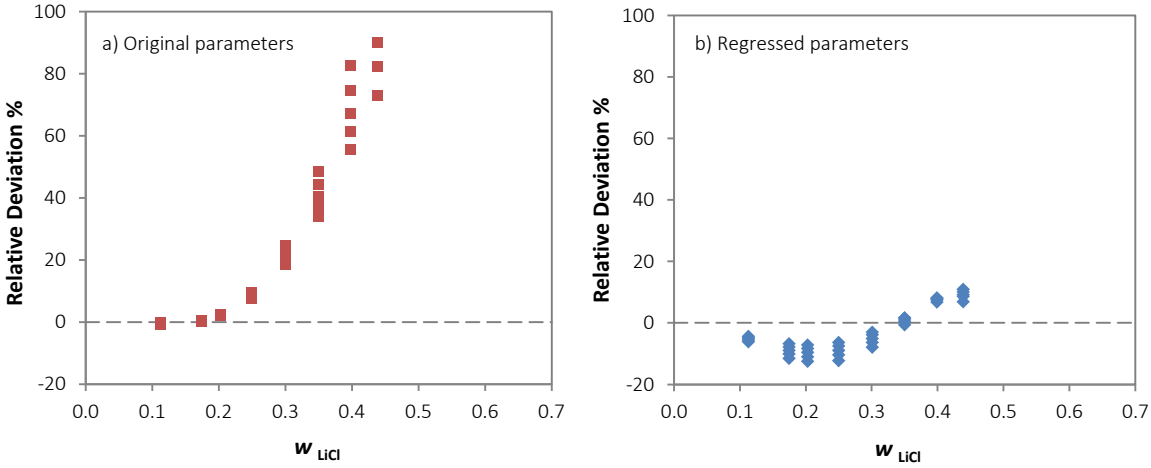

Figure 4.13. Deviation between calculated and experimental vapour pressure (Patil et al., 1990) of H_2O/LiCl and comparison between original and regressed electrolyte pair parameters

In the case of LiBr aqueous solutions, vapour pressure data of different authors have been used to analyse the relative deviation obtained by the vapour pressure modelling with the original parameters of Aspen Properties (figure 4.10a). In accordance with the results, up to salt mass fraction of 0.55 of LiBr the deviations obtained are lower than 10 % excepting with Boryta et al. (1975). For this reason, reported vapour pressure data by Boryta et al. (1975) has been discarded to perform the regression of experimental data for obtaining the electrolyte pair parameters. Once obtained the new parameters, the deviations are mainly lower 10 %. Regarding reported data of Iyoky and Uemura (1989), the root mean square deviation (RMSD) decreased from 5.1 % to 4.6 %, maintaining the maximum relative deviation in 11 %. Regarding Jeter et al. (1992), RMSD decreased from 5.5 % to 3.3 % and the maximum relative deviation from 10.7 % to 7.4 %. Finally, regarding Patil et al. (1990) RSMD decreased from 11.0 % to 6.0 % and maximum relative deviation from 37.1 % to 13.2 %. In the rest of $LiNO_3$, LiI and LiCl aqueous solutions, the regression of the binary parameters show a remarkable improvement in the maximum relative deviation, with all the points under 16 % and RSMD under 8 % (table 4.4).

Table 4.4. Maximum relative deviation and root mean square deviation before and after regression of electrolyte pair parameters of $H_2O/LiNO_3$, H_2O/LiI and H_2O/LiCl systems

	$H_2O/LiNO_3$		H_2O/LiI		H_2O/LiCl	
	Original parameter	Regressed parameter	Original parameter	Regressed parameter	Original parameter	Regressed parameter
Max. Rel. Deviation %	40	8	80	16	40	13
RMSD %	14	4	33	8	14	7

Table 4.5. Electrolyte pair parameters C, D, E for $LiNO_3$, LiI and LiCl aqueous solutions (eq. 3.75 and 3.76)

Species				Electrolyte pair parameters		
Molecule ***i*** or electrolyte ***i***		Molecule ***j*** or electrolyte ***j***		C	D	E
H_2O		Li^+	Br^-	75.6225	-33130.976	-54.1754
Li^+	Br^-	H_2O		14.2194	-5574.6973	-88.4163
H_2O		Li^+	NO_3^-	86.2138	54959.1331	82612.9897
Li^+	NO_3^-	H_2O		-2.1932	-98.0105	9.07161
H_2O		Li^+	I^-	-1074.8168	-487737.47	434076.891
Li^+	I^-	H_2O		-5.7405	437.2852	20.2003
H_2O		Li^+	Cl^-	-37.8535	9592.3604	412.34383
Li^+	Cl^-	H_2O		0.5487	-1208.2119	3.1180

* Nonranddom factor α = 0.0416 for H_2O/LiBr

** Nonranddom factor α fixed 0.2 for the rest of solutions (Chen et al. 1982)

As a summary, the calculated vapour pressures of each one of the lithium salts (LiBr, $LiNO_3$, LiI and LiCl) aqueous binary solutions of have been compared to see the behaviour they present at 303.15 K and a wide range of salt mass fraction (figure 4.14).

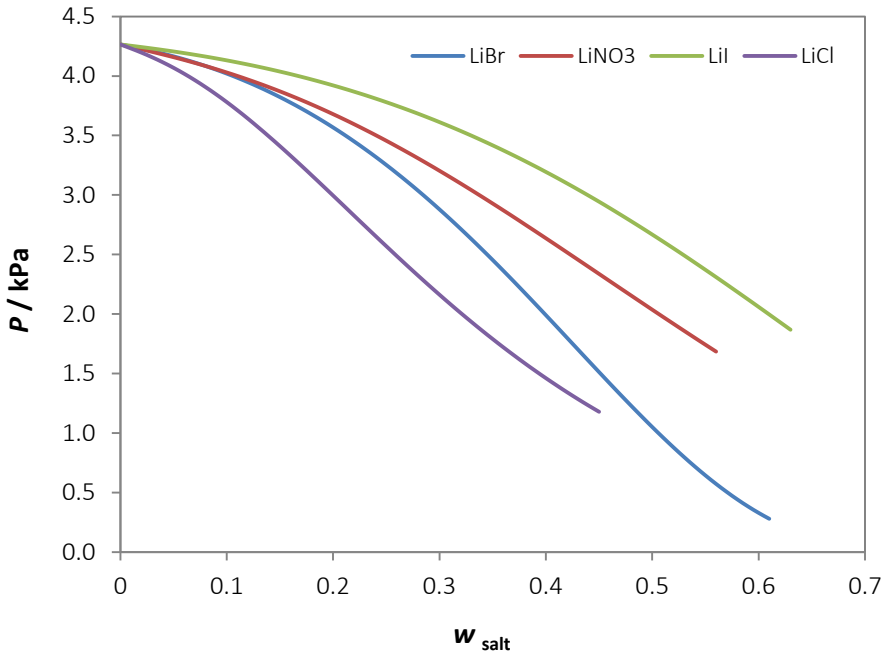

Figure 4.14. Vapour pressures of LiBr, $LiNO_3$, LiI and LiCl aqueous solutions at 303.15 K calculated using Electrolyte-NRTL model

The upper limit of salt mass fraction is determined by the solubility limit of the salt at the temperature of study, 303.15 K. As it can be observed, H_2O/LiI and H_2O/$LiNO_3$ presents higher vapour pressures than H_2O/LiBr solutions. However, H_2O/LiCl solutions present lower vapour pressure than the rest of solutions.

In order to validate the vapour pressure modelling for a multi-component electrolyte solution of lithium salts, figure 4.15 shows a comparison between calculated and reported literature values (Epelde et al., 2013) of vapour pressure of the mixture proposed by Koo et al. (1999) (H_2O/(LiBr+LiNO3+LiI+LiCl), mole salt ratio 5:1:1:2) in a range of total salt mass fraction from 0.40 to 0.65 and temperature range from 273 K to 393 K.

Although the results obtained show an appreciable deviation, especially in the temperature range from 288 K to 308 K, with a maximum relative deviation of 49.4 % and root mean square deviation of 22.2 %, the calculated vapour pressure presents the same behaviour and tendency

than experimental values, what means that the vapour pressure modelling is suitable for calculating vapour pressure of the lithium salts solutions.

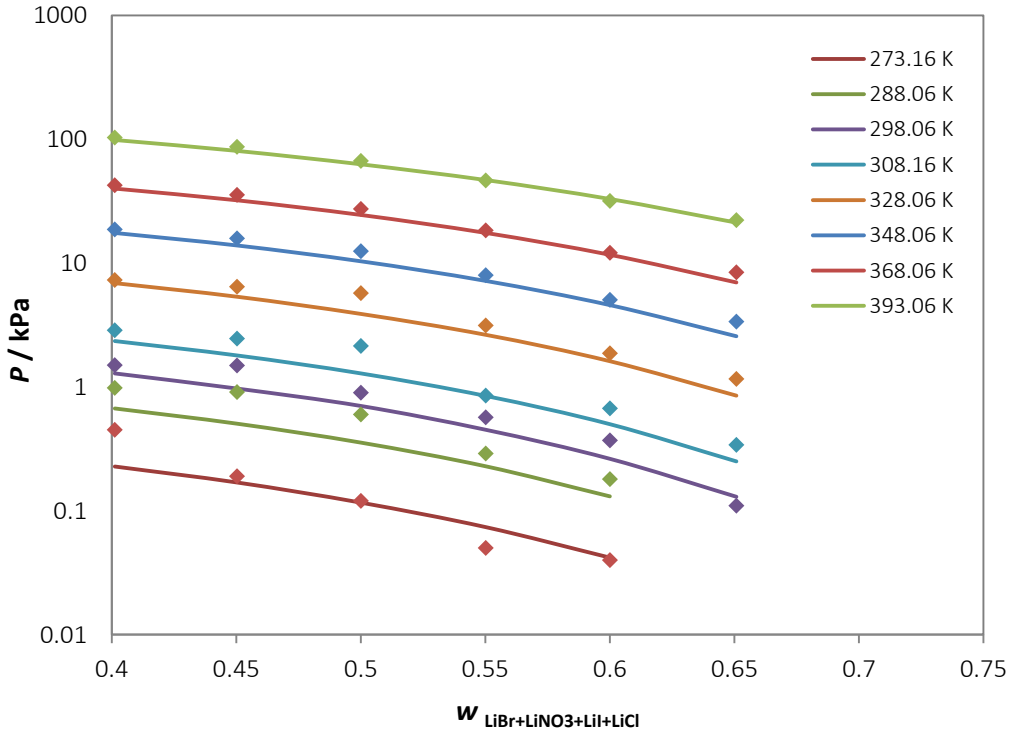

Figure 4.15. Vapour pressure of H_2O/(LiBr+LiNO3+LiI+LiCl) mixture (5:1:1:2).
◊, exp. data (Epelde et al., 2013). –, this work, calculated with Electrolyte-NRTL model

4.7.2. Vapour pressure modelling of the optimum mixture

Once obtained the scope and limitations of the vapour pressure modelling from the validation with single lithium salts solutions and the quaternary mixture proposed by Koo et al. (1999), in this section it has been modelled the vapour pressure of the optimum mixture of lithium salts obtained experimentally in this work (mole salt ratio 7:1:0.5, LiBr:$LiNO_3$:LiI) and the effect of the addition of LiCl on the vapour pressure of the mixture.

For this purpose, firstly the behaviour of the vapour pressure has been analysed when lithium nitrate is added over aqueous solutions of lithium bromide (H_2O/(LiBr+$LiNO_3$)). The modelling has been carried out at $LiNO_3$/LiBr mole ratios from 0 to 2 and total salt mass fractions from 0.58 to 0.69 at 363.15 K (figure 4.16). The high temperature chosen for the modelling is because at high temperatures the model provides better results and also it is assured no crystallization of the

solution. The results show that the vapour pressure increases as the $LiNO_3$/LiBr mole ratio increases. The difference of vapour pressure of all points analysed (optimum mole ratio from solubility analysis indicated with a circle) regarding H_2O/LiBr solution decreases with salt mass fraction (figure 4.16). In the case of addition of LiI (H_2O/(LiBr+$LiNO_3$+LiI)) maintaining fixed the obtained optimum mole ratio $LiNO_3$/LiBr, the same behaviour is obtained (figure 4.17).

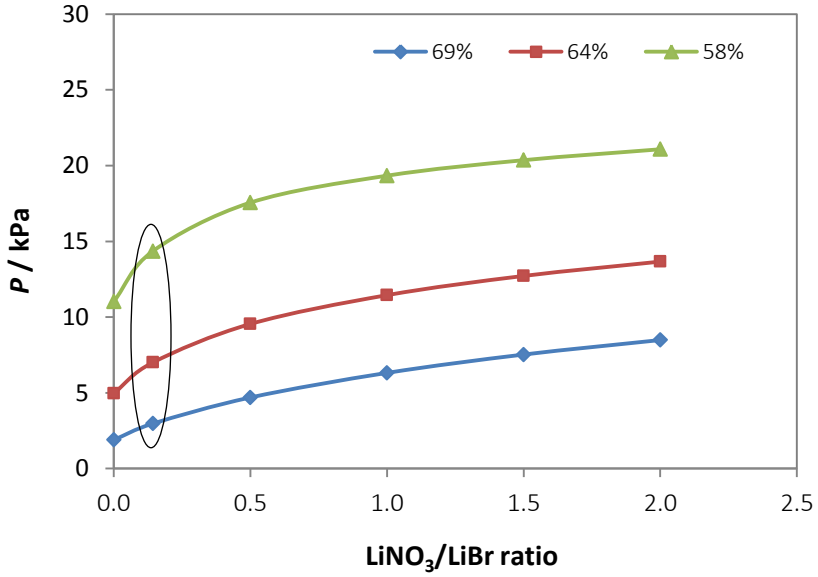

Figure 4.16. Effect of addition of $LiNO_3$ in the vapour pressure of H_2O/(LiBr+$LiNO_3$) mixture at 363.15 K

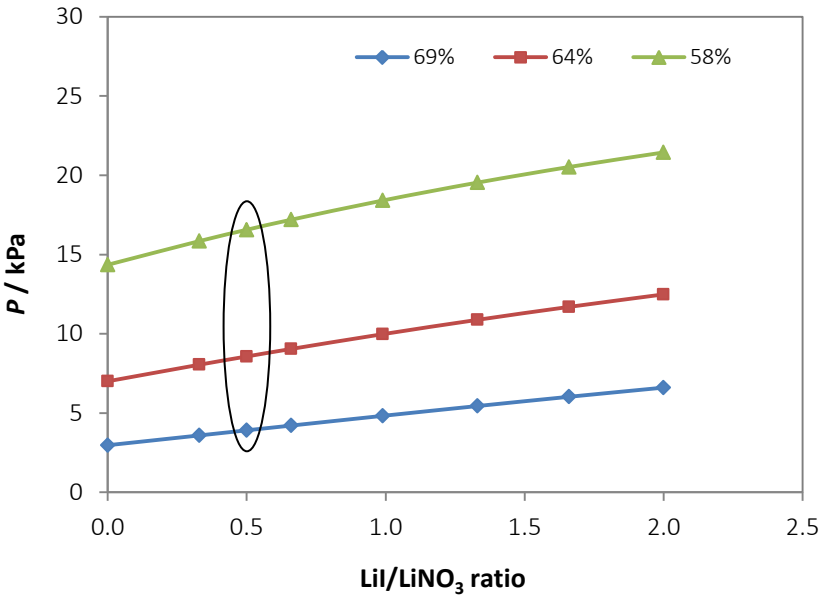

Figure 4.17. Effect of addition of LiI in the vapour pressure of H_2O/(LiBr+$LiNO_3$+LiI) mixture at 363.15 K

However, the addition of LiCl (H_2O/(LiBr+$LiNO_3$+LiI+LiCl)), maintaining fixed the obtained optimum $LiNO_3$/LiBr and LiI/$LiNO_3$mole ratios, doesn't obtain an appreciable decrease of the vapour pressure of the mixture, showing a steady plateau as the amount of lithium chloride increases (figure 4.18). At 363.15 K, the maximum decrease of vapour pressure obtained is 0.2 kPa, at total salt mass fraction of 0.58.

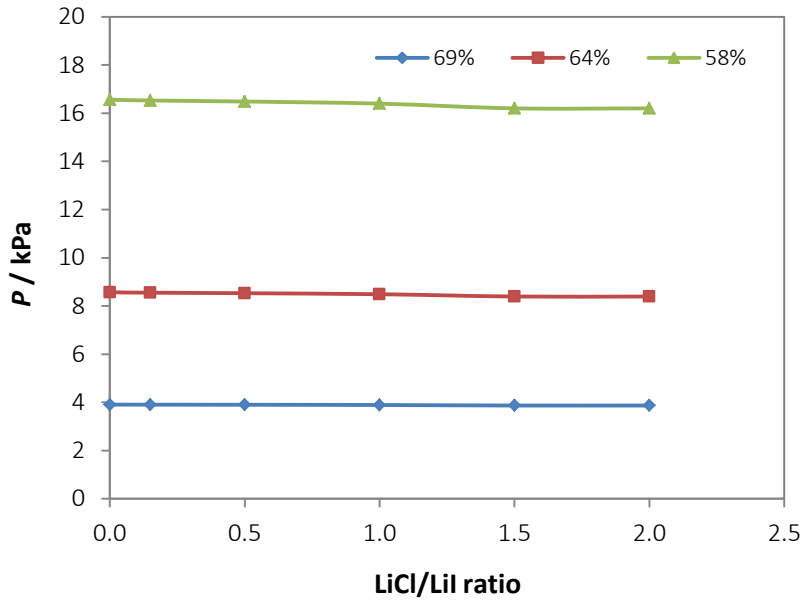

Figure 4.18. Effect of addition of LiCl in the vapour pressure of H_2O/(LiBr+$LiNO_3$+LiI+LiCl) mixture at 363.15 K

In order to understand the results obtained before with LiCl aqueous solutions, it has been modelled and analysed the variation of vapour pressure when is added LiCl at different mole ratios in the optimum mixture proposed in this work (7:1:0.5, LiBr:$LiNO_3$:LiI) for a total salt mass fraction range from 0.35 to 0.6 at 363.15 K (figure 4.19).

The results show a slight decrease of vapour pressure when the salt mole ratio is increased from 0 to 2. However, this improvement in the vapour pressure decreases as the salt composition increases, obtaining from 0.65 salt mass fractions a decrease of vapour pressure lower than 0.5 kPa. For this reason, the addition of LiCl is discarded from the point of view of the improvement of vapour pressure.

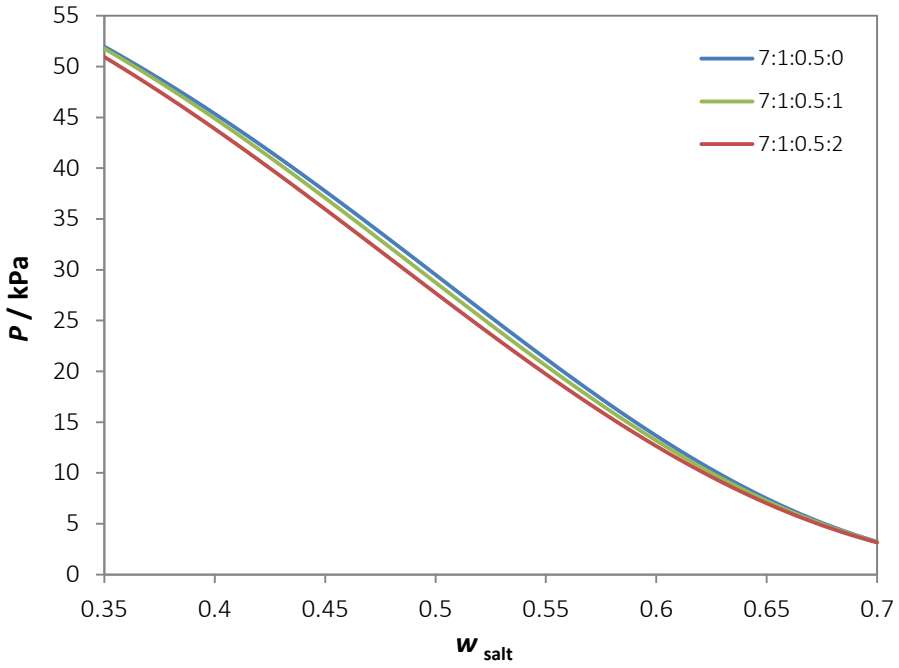

Figure 4.19. Effect of addition of LiCl in vapour pressure of optimum mixture (7:1:0.5, LiBr:$LiNO_3$:LiI) at 363 K

Finally, the calculated vapour pressures of LiBr aqueous solutions, calculated vapour pressures of the solution proposed by Koo et al. (1999), and the calculated vapour pressures of the optimum solution obtained in this work, have been compared in the figure 4.25 at 303.15 K (curves cut in the solubility limit) and at 363.15 K in figure 4.26.

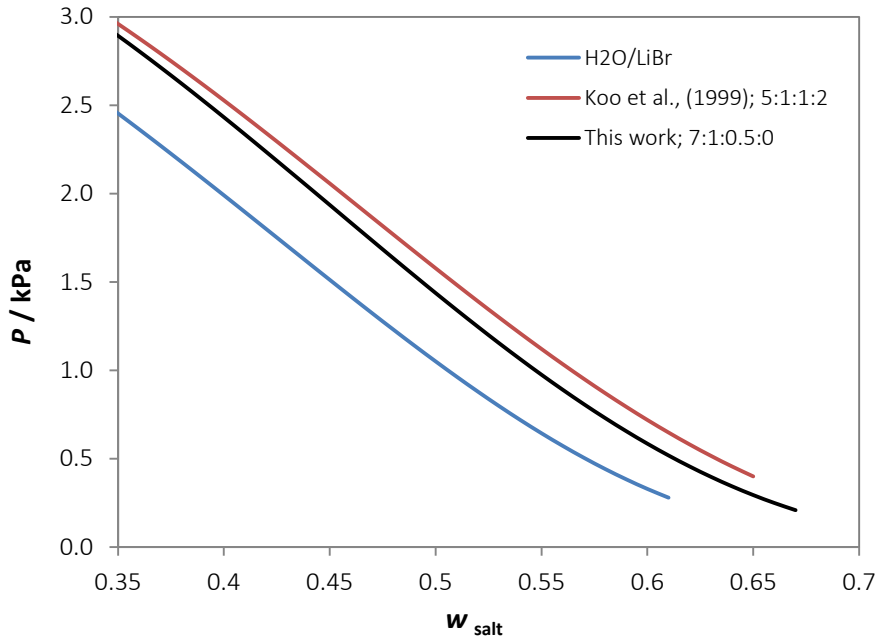

Figure 4.20. Calculated vapour pressure comparison between mixture proposed by Koo et al and the optimum mixture obtained in this work at 303.15 K

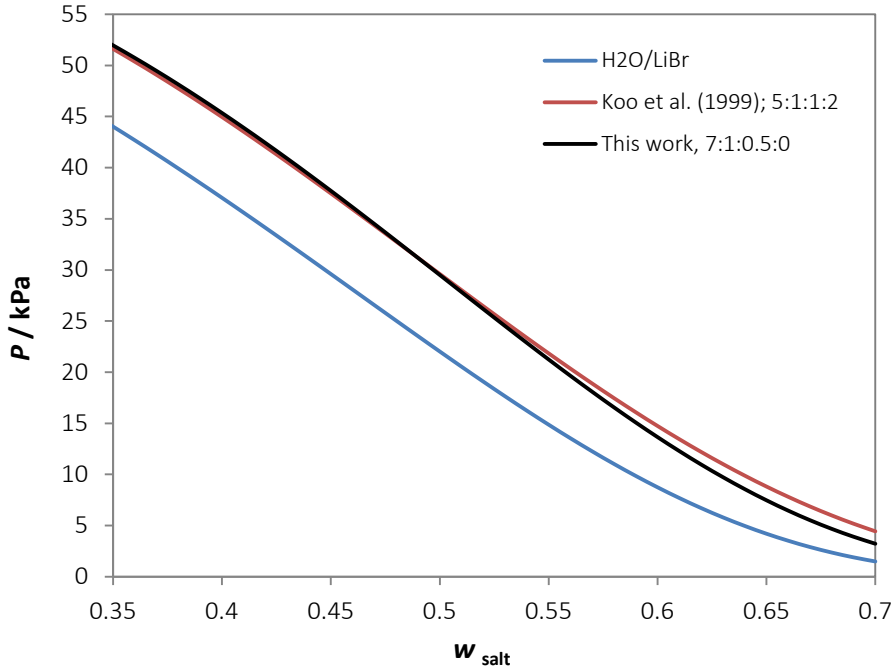

Figure 4.21. Calculated vapour pressure comparison between mixture proposed by Koo et al and the optimum mixture obtained in this work at 363.15 K

As it can be observed in figures 4.25 and 4.26, the modelling obtains different behaviours depending on the temperature. Regarding the solution proposed by Koo et al. (1999), at 303.15 K a decrease of vapour pressure is obtained from the initial total salt mass fraction analysed, achieving for salt mass fraction range between 0.60 and 0.65 a decrease of vapour pressure from 0.13 kPa to 0.05 kPa respectively. At 363.15 K the improvement is only obtained from total salt mass fraction of 0.5, obtaining a decrease of vapour pressure from 1.09 kPa to 1.22 kPa for salt mass fraction range between 0.60 and 0.70. It is important to mention that the results obtained at 363 K are more reliable due to the lower deviations obtained in the validation of the modelling (figure 4.15).

Therefore, it can be concluded that not only the mixture proposed in this work obtains better solubility than the mixture proposed by Koo et al. (1999) it has even a slight decrease of vapour pressure at high salt compositions.

4.8. Conclusions

In this study, a new aqueous solution based on the addition of lithium salts to the conventional H_2O/LiBr mixture has been optimised for improving the solubility (and corrosivity) without an excessive increase of the vapour pressure, as well as for allowing its use in absorption systems with air-cooled absorbers, which involves higher salt composition and consequently the crystallization risk becomes critical.

Different alternatives proposed in literature have been considered but only H_2O/(LiBr+$LiNO_3$+LiI+LiCl) (mole salt ratio 5:1:1:2) proposed by Koo et al. (1999) has been taken as reference because it is the mixture that achieves better solubility. In this context, as this mixture was optimized for salt mass fraction from 0.58 to 0.625, this study has performed an extension of the original solubility study of Koo et al. (1999) by measuring the ratio of salts that reaches the lowest solubility temperature in a salt fraction range from 0.65 to 0.69 (operation range of air-cooled absorbers).

The experimental solubility measurements of the different mole salt ratios have been roughly analysed by visual-polythermal method using in sample tubes. From each one of the experiments carried out at salt mass fractions between 0.65 and 0.69 and different LiBr/$LiNO_3$, LiBr/LiI and LiCl/Li mole ratios, the optimum mole ratio of lithium salts has been determined to be 7:1:0.5 in the H_2O/(LiBr+LiNO3+LiI) system. The addition of $LiNO_3$, H_2O/(LiBr+$LiNO_3$), supposes a remarkable solubility temperature decreasing of 15 K- 27 K depending of total salt mass fraction. The addition of LiI, H_2O/(LiBr+$LiNO_3$+LiI), leads an additional decreasing of 18 K and 11 K for salt mass fractions 0.69 and 0.65 respectively. Nevertheless, the addition of LiCl, H_2O/(LiBr+$LiNO_3$+LiI+LiCl), doesn't lead to improvements in solubility, so its addition is discarded.

The solubility of the obtained optimum mixture has been precisely measured in a solubility glass cell based on the visual-polythermal method. The measurements have been performed in a range of salt mass fractions from 0.6245 to 0.6907, covering a solubility temperature range from 275.1 K to 309.8 K. The comparison of the solubility of the mixture proposed in this work with the results obtained by Salavera et al. (2004) using the mixture proposed by Koo et al. (1999) shows similar results up to 0.65 salt mass fraction. From this point, a significant improvement of the solubility is obtained as the salt mass fraction increases. For a range of salt mass fractions from 0.655 to 0.69 decrease of solubility temperature from 8 K to 35 K is reached.

The study of the effect of the addition of lithium chloride on the vapour pressure of the optimum mixture obtained experimentally has been carried out by modelling the vapour pressure with asymmetric Electrolyte-NRTL activity coefficient model using Aspen Properties software.

The vapour pressure modelling has been validated first in LiBr, $LiNO_3$, LiI and LiCl single electrolyte solutions, which required the calculation of new electrolyte energy parameters from regression of experimental data to obtain root mean square deviations lower than 10 %. The validation in multi component electrolyte solutions has been made by comparing calculated and reported literature values of vapour pressure of the mixture proposed by Koo et al. (1999). Although the modelling presents a maximum relative deviation of 49.4 % and root mean square deviation of 22 %, since it presents the same trend than experimental values it can be concluded that the model is suitable for calculating vapour pressure of lithium salts mixtures solutions.

The results of the calculated vapour pressure of the proposed mixture have shown that the addition of LiCl doesn't significantly decrease the vapour pressure of the solution. Thus, from the point of view of vapour pressure is discarded the addition of LiCl. Finally, the calculated vapour pressure of the optimum mixture of this work has been compared with the calculated vapour pressure the solution proposed by Koo et al. (1999). At 303.15 a decrease of vapour pressure from 0.13 kPa to 0.05 kPa has been obtained in a range of salt mass fraction from 0.60 to 0.65. At 363 K the decrease of vapour pressure for a range of salt mass fraction from 0.60 to 0.70 has been between 1.09 kPa to 1.22 kPa.

As a final conclusion, the mixture proposed in this work is considered a better option than the mixture proposed by Koo et al. (1999) due to the improvement in solubility, the reduction in the number of salts, the reduction of required amount of $LiNO_3$ and LiI, and the reduction of the vapour pressure that it presents.

4.9. Nomenclature

P	pressure (kPa)
R	general gas constant ($J \cdot mol^{-1} \cdot K^{-1}$)
T	temperature (K)
w	mass fraction
x	liquid mole fraction
y	vapour mole fraction

Greek Letters

γ	activity coefficient
τ	asymmetric binary interaction energy parameters
α	NRTL symmetric non-randomness factor parameter
$\emptyset$	fugacity coefficient
ϑ	molar volume

Subscripts

w	water

Superscripts:

s	saturated state

4.10. References

Boryta, D.A.; Maas, A. J.; Grant, C.B. *Vapour Pressure-Temperature-Concentration Relationship for System Lithium Bromide and Water (40-70% Lithium Bromide)*. J. Chem. Eng. Data 20 (1975) 316-319.

Campbell, A.N.; Fishman, J.B.; Rutherford, G.; Schaefer, T.P.; Ross, L. *Vapor pressures of aqueous solutions of silver nitrate, of ammonium nitrate, and of lithium nitrate.* Canadian J. Chem. 34 (1956) 151-159.

Epelde, M.; Steiu, S.; Mesones, J.; Salavera, D.; Coronas, A. *Thermophysical Properties of H_2O + (LiBr + $LiNO_3$ + LiI + LiCl) Mixture For Absorption Refrigeration*. 4th IIR Conference on Thermophysical Properties and Transfer Processes of Refrigerants, Delft, The Netherlands, June 17-18, 2013.

Iyoki, S.; Iwasaki, S.; Kuriyama, Y.; Uemura, T. *Solubilities for the Two Ternary Systems Water + Lithium Bromide + Lithium Iodide and Water + Lithium Chloride + Lithium Nitrate at Various Temperatures.* J. Chem. Eng. Data 38 (1993) 396-398.

Iyoki, S.; Yamanaka, R.; Uemura, T. *Physical and thermal properties of the water-lithium bromide-lithium nitrate system*. J. Chem. Eng. Data 16 (1993) 191-200.

Iyoki, S.; Ohmori, S.; Uemura, T. *Heat Capacities of the Water-Lithium Bromide-Lithium Iodide System*. J. Chem. Eng. Data 35 (1990) 317-320.

Iyoki, S.; Iwasaki, S.; Uemura, T. *Vapor Pressures of the Water-Lithium Bromide-Lithium Iodide System.* J. Chem. Eng. Data 35 (1990) 429-433.

Iyoki, S.; Uemura, O. *Vapour pressure of the water-lithium bromide system and water-lithium bromide-zinc bromide-lithium chloride system at high temperatures*. Int. J. Refrigeration 12 (1989) 278-282.

Jeter, S.M.; Lenard, J.L.Y.; Teja, A.S. *Properties of lithium-bromide-water solutions at high temperatures and concentrations – part IV: vapour pressure*. ASHRAE Transactions 98 (1992) 167-172.

Koo, K.-K.; Lee, H.-R. *Solubilities, Vapor Pressures, Densities, and Viscosities of the(Water + Lithium Bromide + Lithium Iodide + Lithium Chloride) System.* J. Chem. Eng. Data 43 (1998) 722-725.

Koo, K.-K.; Lee, H.-R.; Jeong, S.; Oh, Y.-S.; Park, D.-R.; Back, Y.-S. *Solubilities, Vapor Pressures, and Heat Capacities of the Water + Lithium Bromide + Lithium Nitrate + Lithium Iodide + Lithium Chloride System.* Int. J. of Thermodynamics 20 (1999) 589-600.

Mock, B.; Evans, L.B.; Chen, C.-C. *Thermodynamic representation of phase equilibia of mixed-solvent electrolyte systems*. AIChE Journal 32 (1986) 1655-1664.

Patil, K.R.; Tripathi, A.D.; Pathak, G.; Katti, S.S. *Thermodynamic Properties of Aqueous Electrolyte Solutions. 1. Vapor Pressure of Aqueous Solutions of LiCl, LiBr, and LiI.* J. Chem. Eng. Data 35 (1990) 166-168.

Salavera, D.; Esteve, X.; Patil, K.R.; Mainar, A.M.; Coronas, A. *Solubility, Heat Capacity, and Density of Lithium Bromide +Lithium Iodide + Lithium Nitrate + Lithium Chloride Aqueous Solutions at Several Compositions and Temperatures.* J. Chem. Eng. Data 49 (2004) 613-619.

Salavera, D. *Propiedades Termofísicas de Nuevos Fluidos de Trabajo (H_2O+LiBr+$LiNO_3$+LiCl+LiI, NH_3+H_2O+NaOH y NH_3+H_2O+KOH) para Sistemas de Refrigeración por Absorción.* Doctoral Thesis Universitat Rovira i Virgili, Tarragona 2005.

Yoon, J.-I.; Kwon, O.-K.; Moon, C.-G.; Lee, H.-S.; Bansal, P. *Heat and mass transfer characteristics of a helical absorber using LiBr and LiBr + LiI + LiNO3 + LiCl solutions*. Int. J. of Heat and Mass Transfer 48 (2005) 2102–2109.

Chapter 5

Solubility Limit of CO_2 in Aqueous Methylpiperidine Solutions

5.1. Introduction

Vapour-compression refrigeration systems with CO_2 as refrigerant are used in industry to achieve lower refrigerating temperatures (evaporation temperatures up to -50 °C) than systems operated with ammonia. Though the main disadvantage is that requires higher working pressures, the friendly properties such as its natural origin, non-corrosivity, non-flammability or non-toxicity has promoted the study of its use in absorption refrigeration systems.

Although CO_2 is a promising refrigerant, nowadays there are only theoretical proposals for its integration in absorption refrigeration systems with suitable absorbents. These proposals have been based in the use of ionic liquids, alcohols or amines as absorbents in conventional absorption systems (Sen and Paolucci, 2006; Jones, 2002) or absorption/desorption cycles where the absorber and generator are the only components of the system (Jones, NASA, 2004).

Within this scope, in this chapter it has been studied the use of flow-calorimetric methodology to measure solubility of CO_2 in absorbents. This technique allows the simultaneous determination

of the enthalpies of solution and solubility limit of CO_2. Specifically, in this work it has been used 2-Methylpiperydine and 4-Methylpiperydine aqueous solutions, proposed for CO_2 capture processes.

Alkanolamines such as monoethanolamine (MEA) or diethanolamine (DEA) have been the most common CO_2 absorbents used over the years (Jung et al., 2012; Arcis et al., 2011, 2012), however, they have some drawbacks such as high degradation, foam formation, high corrosivity and the most important, they require much energy to desorb the CO_2, causing a significant reduction in the efficiency of the installation.

For this reason, the purpose of current researches lies in the reduction of the energy cost of CO_2 removal from the amine solution (Raynal et al., 2011). In this way, some investigations are focused in the use of aqueous methylpiperidine solutions (cyclic secondary amine) as absorbents because they exhibit liquid–liquid phase separation (amine/CO_2+water) when the system reaches a certain temperature and CO_2 composition, what reduces the energy requirements for the desorption process (Stephenson, 1993; Coulier et al., 2010).

Following with the studies of solubility carried out in the previous chapters, it has been studied the solubility limit of CO_2 in aqueous 2-methylpiperidine and 4-methylpiperidine solutions at absorbent mass fractions of 0.20 and 0.40, temperature of 338.5 K and working pressures of 5 bar, 10 bar and 15 bar because there is no data of enthalpy of solution and solubility available in literature. The solubility limit has been studied by measuring the enthalpy of solution of the systems CO_2/(2MP+H_2O) and CO_2/(4MP+H_2O) in a custom-made flow-mixing cell adapted to a calorimeter Calvet Setaram BT2.15.

This study has been carried out in the group of Thermodynamics and Molecular Interactions of the Institute of Chemistry of Clermont-Ferrand (France).

5.2. Experimental setup

The experimental device used for measuring the heat of absorption of CO_2 in aqueous amine solutions consists in a Calvet Setaram BT2.15 heat conduction differential calorimeter, which is a variation of the classical Setaram C-80 with the capability to work at low temperatures (from 77 K to 473 K).

Both CO_2 and aqueous amine solution are introduced into the calorimeter by two syringe pumps and its corresponding flow lines. Before entering the fluids into the calorimeter, they pass through three preheaters to adjust its temperature to the temperature of the calorimeter. Then, both fluids enter separately into the calorimetric block, where are mixed in the mixing unit of a custom-made flow-mixing cell, in which the heat effect during the absorption of the gas into the aqueous amine solution of amine is detected by the thermopiles of the calorimeter. The resultant solution leaves the calorimeter and the system through a buffer volume which helps to control the pressure of the system. Figure 5.1 shows a schematic diagram of the entire measurement equipment.

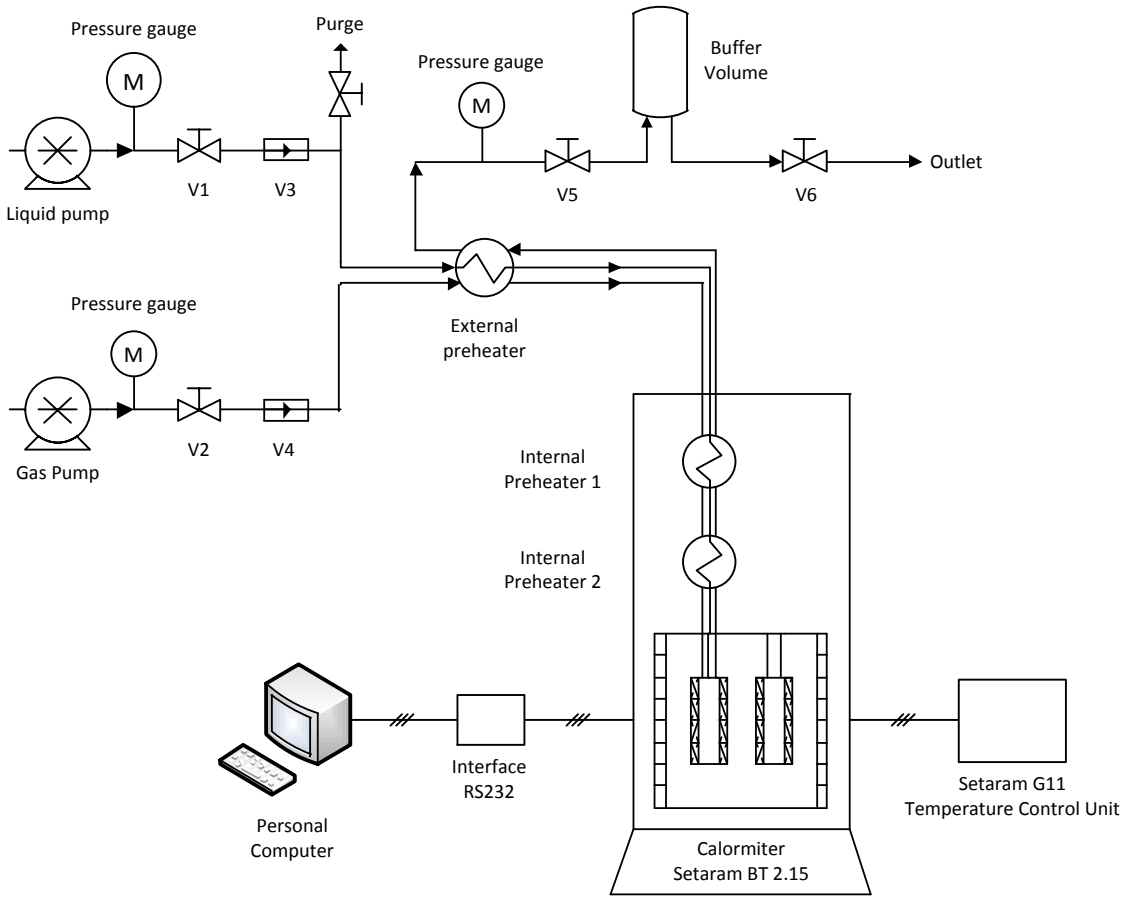

Figure 5.1. Schematic diagram of the entire experimental device

In the following sections is explained in detail the features of the calorimetric block, mixing cell, pumps used to introduce the fluids into the calorimeter, the characteristics and accessories of the flow lines, and the temperature and control system.

5.2.1. Calorimeter block

The measurement zone of calorimetric block is constituted by two holes in which are placed two cells, one is the measurement cell and the other is the reference cell. Both sample and reference cell are totally surrounded by an array of thermocouple detectors (also called thermopiles) allowing the measurement of all heat exchanged between the cells and the calorimetric block (exothermic or endothermic), including radiation, convection or conduction. The reference cell allows compensating the non-desired effects produced as well as the influence of external perturbations. The heat exchanged between the thermopile and the calorimetric bock is proportional to an electromotive force, which is amplified and sent to a personal computer by means of an interface RS232.

5.2.2. Mixing cell

The mixing cell is the most important part of the calorimeter because its correct design determines the obtainment of good enthalpy of solution results. The mixing cell (figure 5.2) is made of Hastelloy C22 to avoid corrosion. Two parallel tubes of 1.6 mm outside diameter, through which are driven the CO_2 and aqueous amine solution, are placed in the middle of the mixing cell and are silver-soldered to the mixing point M located at the bottom of the cell, where both fluids get in contact and are mixed. The correct design of this mixing point is critical because has to be able to provide a perfect mixing of both working fluids.

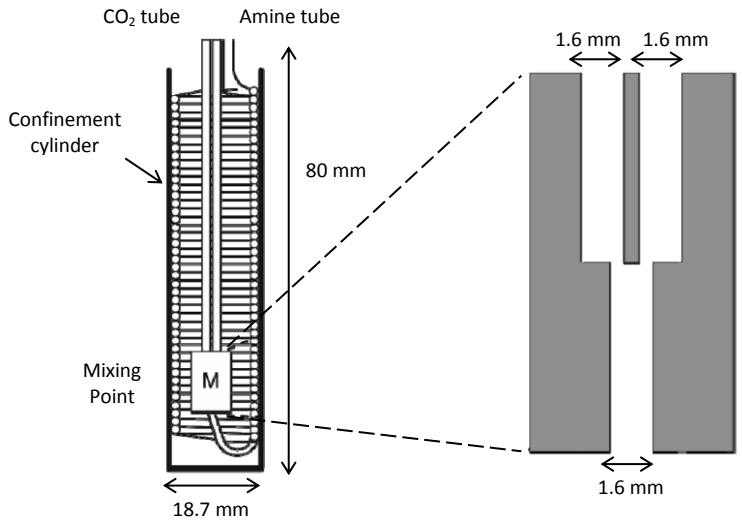

Figure 5.2. Diagram of mixing cell and detail of mixing point

At the outside of the mixing point it is silver-soldered a tube of 1.6 mm o.d. and 2.8 m long where takes place the quantitative mixing of the fluids. This tube is coiled in good thermal contact with the inner wall of the confinement cylinder (80 mm height and 18.7 mm i.d.) in order to transmit all heat produced in the absorption to the thermopiles of the calorimeter.

5.2.3. Impulsion pumps and flow lines system

Both fluids, aqueous amine solution and CO_2, are injected into the calorimeter by means of two high-pressure and low-flow precision syringe pumps provided by ISCO, model 100DM, which have a capacity of 103 mL, flow range from 0.00001 to 30 mL/min and flow accuracy of 0.5 % of the full scale.

The syringe pumps have two flow lines connected to the outlet, located at the top side, with one high pressure valve installed in each of them. One of the lines allows the suction of the fluid into the syringe pump and the other impulses the fluid into the calorimeter. The syringes are maintained at a constant temperature of 298.15 K by using a thermostatic bath, with water as refrigerant fluid, to maintain the mass flow rate of the pumps constant.

The flow lines are made by stainless steel, with an internal and external diameter of 1.0 mm and 1.6 mm respectively. To isolate the flow lines from the syringe pumps there are installed one valve in each flow line (V1 – V2, figure 5.1) and also they incorporate non-return valves (V3-V4, figure 5.1) to avoid possible contamination of the pumps.

Due to the corrosivity of the pure amines analysed (methylpiperidine), its insertion in the syringe pumps is not recommended. To overcome this problem, in the liquid flow line is connected a loop with a total volume of 30 mL, where the corrosive fluid can be directly inserted in it and be pushed into the calorimeter by the pump filled with water. In the loop is installed a six-way valve which allow its connection or disconnection from the flow line, which means that allows the loading and emptying of the loop and its bypass when the loop is not required.

5.2.4. Temperature control system

The temperature of the calorimeter is measured by a platinum temperature probe Pt200 and controlled with a precision of ± 0.01 K by Setaram G11 system controller, which also amplifies and digitalises the thermopile sign. Additionally, the fluids injected in the calorimeters need to be preheated to avoid temperature drops inside the mixing cell and thus allow a better control of temperature. For this reason, three preheaters are installed in the system: one outside and two inside the calorimeter, being all thermoregulated by heating cartridges and a platinum resistance thermometer connected to a PID controller.

The external preheater is located just above the calorimetric block and consists of a copper cylinder with tubing coiled on its outer surface. The internal preheaters are located inside the calorimeter block housing the mixing cell and consist on a cooper cylinder with tightly fitted tubing placed in grooves inside the cylinder. The temperatures of the external and first internal preheaters are controlled by two Eroelectronic LFS controllers, with a precision ± 0.1 K. The second internal preheater is thermoregulated by a Fluke Hart Scientific 2200 controller with a precision of ± 0.01 K.

5.2.5. Pressure control system

The pressure of the system is measured at the outlet of the calorimeter by means of a Keller pressure transducer connected to a pressure indicator Druck DPI260 with an accuracy of ± 0.3 % full scale. The valve V6 (figure 5.1), which connects the flow line to the outlet of the system, allows the increase of the pressure by its connection to a nitrogen pressurized line, as well as the decrease of the pressure by the discharge of amine and gas from the system. A buffer volume is located at the end of the flow line, before valve V6, to provide a better control and stability of the pressure when it is adjusted to the desired value.

5.3. Experimental procedure

5.3.1. Chemicals

2-methylpiperidine (purity ≥ 0.98) and 4-methylpiperidine (purity ≥ 0.96) are supplied by Aldrich. Water is distilled and degassed under vacuum before use (resistivity 18.2 MΩcm). Carbon dioxide (purity 99.998 %) is obtained from Saga. All chemicals are used without further purification.

5.3.2. Sample preparation and insertion into the calorimeter

The aqueous solutions of 2-methylpiperidine and 4-methylpiperidine are prepared by mass with distilled and degassed water with an uncertainty of the mass fraction lower than 0.001. Before introducing the samples into the syringe pumps they are cleaned with ethanol and dried with pressurized nitrogen in order to avoid contamination of the samples.

The CO_2 is introduced into the syringe pump directly from the carbon dioxide pressurized line. Maintaining the impulsion valve of the pump closed, the suction valve attached to the CO_2 line is opened and the syringe pump is directly filled by the automatic filling function of the pump. Since the entering gas is pressurized, the desired pressure is then adjusted by means of the suction valve.

The filling procedure of the aqueous amine syringe pump is practically the same. The only difference is that in this case the aqueous amine is introduced from a tube connected to the suction line and not from a pressurized line as explained for carbon dioxide. For this reason, once the syringe pump is filled, both suction and impulsion valves are closed and the pressure is set by adjusting the desired pressure in the pump with the automatic function incorporated. In both cases, the pressure of the pumps must be higher than the pressure of the system in order to transport of the fluids into the calorimeter.

Once both fluids are introduced in their respective pumps, they are driven into the calorimeter by the adjustment of the desired flow rate in the control unit of the pumps. Typical flow rates used in the experiments cover a range of 0.05 to 0.3 $mL \cdot min^{-1}$ for aqueous amine solutions and from 0.17 to 1.06 $mL \cdot min^{-1}$ for CO_2.

5.3.3. Pressure and temperature adjustment

Since the pumps are pressurized, when both fluids are driven into the calorimeter the pressure of the system changes and increases. The pressure can be adjusted to the desired value by opening valve V6 (figure 5.1), which involves the extraction of both fluids from the system into a container. The pressure of the system can also be increased by introducing pressurized nitrogen into the flow line (and consequently into the buffer volume) through valve V6, which at the same time permits the adjustment of the desired pressure. The temperature of the calorimeter is adjusted in the temperature control unit Setaram G11. The temperature of the preheaters is adjusted in the equipment calibration procedure.

5.3.4. Heat flow data acquisition

The heat flow produced when the carbon dioxide is absorbed by the aqueous amine is registered by the thermopiles of the calorimeter, which transmits the obtained signal *S* (mV) to a personal computer. The heat flow signal is represented in front of the time (figure 5.3). Negative signals represents that energy is delivered to the calorimetric block (exothermic reaction) and positive signals represents that energy has been absorbed from the calorimetric block (endothermic reaction).

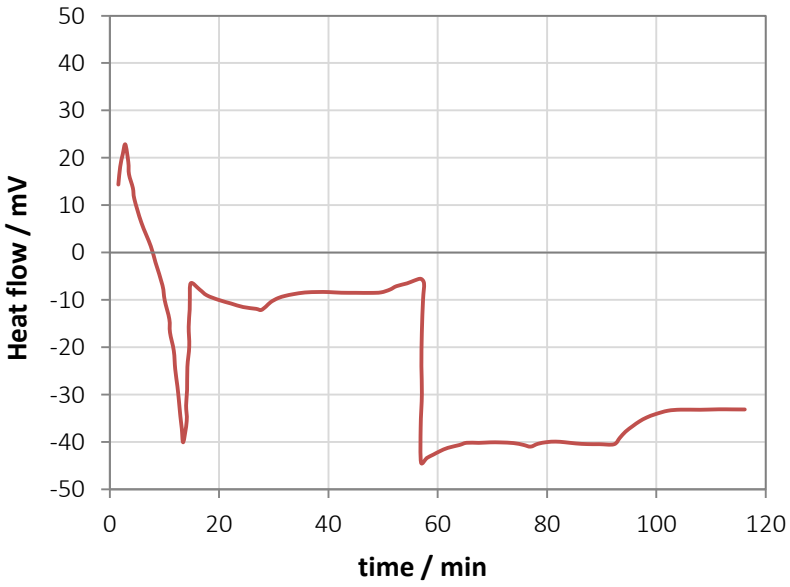

Figure 5.3. Typical heat flow behaviour along the experiments

In figure 5.3 it can be observed an example of the behaviour of the signal obtained when is produced the absorption. At the beginning the signal presents sharp changes until the mixture of both fluids becomes correct and the signal achieves a stable behaviour. The signal is considered stable when it achieves a sinusoidal tendency, with a maximum difference between the higher and lower value of ± 2-4 mV. The time necessary to get the stable signal value is not constant, depends of the conditions of the experiment, but usually takes between 1.5 – 2 hours at the beginning of the experiment and later, when small flow rate changes are made, takes usually between 0.5 – 1 hour.

5.3.5. Density measurements of aqueous amine solutions

The densities of the aqueous 4-Methylpiperydine solutions (densities of aqueous 2-methylpiperidine solutions obtained previously by Coulier et al., 2010), required for the calculation of the molar flow-rate, have been measured at the temperature of the syringe pumps (298 K) and the working pressure of the experiments (5 bar – 15bar).

The experimental device is a vibrating tube flow densimeter Anton Paar DMA HP connected to a controller DMA 5000 to read the measurements. The densimeter works at pressures up to 700 bar and temperatures up to 473 K. The pressure of the densimeter is measured by a Druck PMP 4010 pressure transducer connected to a pressure indicator Druck DPI 280 with accuracy of ± 0.1 % full scale.

The vibrating tube densimetry (figure 5.4) is based on the mechanical oscillation principle, which consists on the variation of the oscillation period of a fluid with unknown density regarding another fluid of known density when are contained in a U-shape mechanical oscillator.

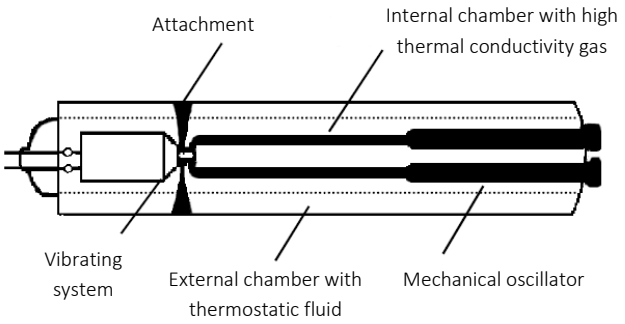

Figure 5.4. Internal diagram of a U-tube mechanical oscillator (Salavera, 2005)

The oscillating period can be expressed as follows:

$$\tau = 2\pi \sqrt{\frac{m - \rho V_0}{C}} \tag{5.1}$$

where m is the mass of the oscillator, V_0 is the inner volume, ρ is the density of the fluid and C is the oscillating constant. Equation 5.1 can be expressed in terms of density as:

$$\rho = \frac{C\,\tau^2}{2\,\pi^2\,V_0} - \frac{m}{V_0} \tag{5.2}$$

This expression can be rewritten as function of two calibration parameters A and B:

$$\rho = \mathrm{A}\,(\tau^2 - \mathrm{B}) \tag{5.3}$$

where A and B correspond to the following equations:

$$\mathrm{A} = \frac{\rho_1 - \rho_2}{\tau_1^2 - \tau_2^2} \tag{5.4}$$

$$\mathrm{B} = \frac{\tau_2^2\,\rho_1 - \tau_1^2\rho_2}{\tau_1^2 - \tau_2^2} \tag{5.5}$$

The parameters A and B depend on the temperature as well as the pressure, and are obtained from the calibration of the densimeter by measuring the oscillating period of two fluids (subindex 1 and 2 of equations 5.4 and 5.5) with known density at the working temperature and pressure conditions.

The calibration has been carried out by the average of two pair of fluids: water-hexane and water-octane at 303.15 K (temperature of pump) at 5 and 10 bar (calorimeter working pressures). The densities of the fluids have been obtained from National Institute of Standards and Technology (NIST) webpage. These fluids have been chosen because their densities are situated above (water) and bellow (hexane and octane) regarding the aqueous amine solutions under study. Table 5.1 shows the results of 4-methylpiperidine solutions with amine mass composition of 20 % and 40 %, 303.15 K and pressures of 5 bar and 10 bar. As expected, no appreciable changes in density of liquids are obtained when the pressure is increased.

Table 5.1. Densities of aqueous 4-methylpiperidine solutions at 303.15 K

Pressure	4-MP 20 %	4-MP 40 %
5 bar	0.97164	0.94402
10 bar	0.97182	0.94420

5.3.6. Calculation of solution enthalpy and CO_2 solubility limit.

The experiments to obtain the enthalpy of solution have been carried out as function of CO_2 loadings at constant temperature and pressure. The carbon dioxide loading α is defined as the total molar flow rate of CO_2 divided by the total molar flow rate of amine (eq. 5.6).

$$\alpha = \frac{\dot{n}_{CO_2}}{\dot{n}_{\text{amine}}} \tag{5.6}$$

Molar flow rates have been calculated from the volumetric flow rates of syringe pumps (mL/min), mass composition of the aqueous amine solution and the molar mass and densities of both fluids (densities of CO_2 obtained from NIST).

The enthalpy of solution is calculated directly from the thermopile signal S_{M} (mV) and the molar flow rate $\dot{n}$ (mol·s^{-1}) of the solution as follows:

$$\Delta_{\text{sol}}H = \frac{S_{\text{M}} - S_{\text{LB}}}{K \cdot \dot{n}} \tag{5.7}$$

As it can be seen, in equation 5.7 also appears the terms S_{LB} and K. S_{LB} is called the base line signal and corresponds to the thermopile signal when only water is measured in the calorimeter. This base line is determined by establishing a signal close to zero with the temperature adjustment of the preheaters. The term K corresponds to the thermopile sensitivity (mV·mW^{-1}), which is used to convert the thermopile signal to heat power and is given by the calorimeter manufacturer (Setaram). This sensitivity however has been recalibrated by measuring the heat of mixing of a well-known binary system such as ethanol-water, using the enthalpy data of Ott et al. (1986). The results obtained in the calibration of the preheaters to establish the baseline and the recalibration of the thermopile signal are shown in the *Equipment calibration* section.

The solubility limit of the carbon dioxide into the absorbent is determined graphically from the results of solution enthalpy expressed in terms of kJ per mole of amine when are plotted in front of the CO_2 loading.

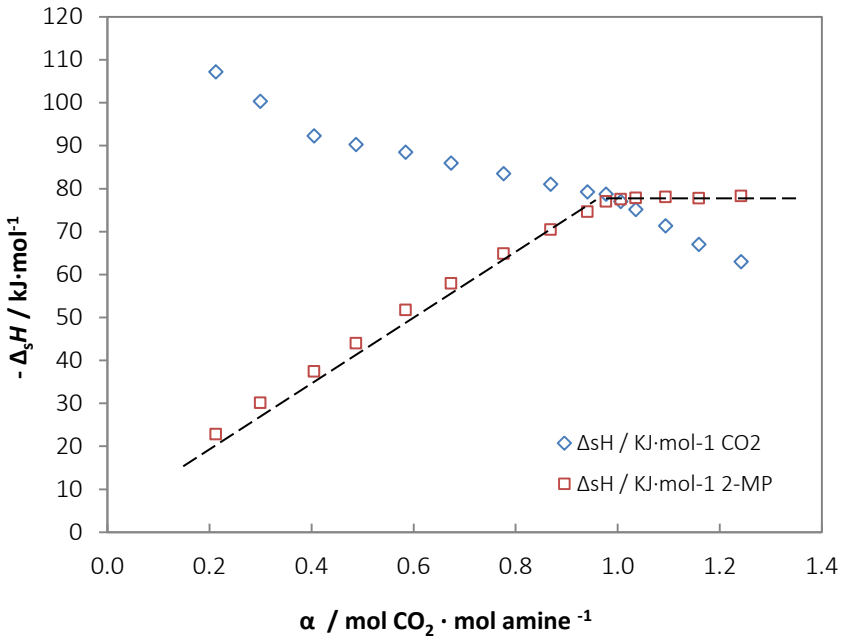

Figure 5.5. Example of graphical determination of solubility limit of CO_2 in aqueous amine solution

Figure 5.5 shows an example of enthalpy of solution expressed in kJ per mole of CO_2 (diamonds) and in terms of kJ per mole of 2-methylpiperidine amine (squares). The $-\Delta_{sol}H/(kJ \cdot mol^{-1}$ of amine) presents two well differenced behaviours, in the first one, the enthalpy of solution shows a linear increase as the loading α increases. This behaviour corresponds to the unsaturated solution. The second behaviour of the enthalpy presents a plateau and corresponds to the saturated solution. Therefore, the intersection between the unsaturated and saturated domain corresponds to the solubility limit of the CO_2 in the amine solution.

5.4. Equipment calibration

5.4.1. Base line S_{LB}

The obtainment of the base line has been carried out by means of experiments with only water flowing through the calorimeter. The objective of these experiments is to obtain a signal value close to zero by adjusting the temperature of the preheaters (table 5.2) when the flow rate is

changed. The base line calibration has been made at the temperature of the enthalpy of solution experiments, which is 338.15 K.

Table 5.2. Preheaters calibration for calorimeter temperature of 338.15 K

Calorimeter Temperature	External Preheater / K	Internal Preheater 1	Internal Preheater 2
338.15 K	338.65 K	338.65 K	335.35 K

As it can be seen in figure 5.6 and table 5.3, with the temperature of the preheaters adjusted it was possible to achieve a signal close to 0 for flow rates up to 0.4 mL/min, but for higher values (up to 0.8 mL/min) as the flow rate increases the signal obtained increases exponentially. This behaviour is typical in the calibration of the baseline, for this reason it has been accepted for its use in the enthalpy of solution experiments.

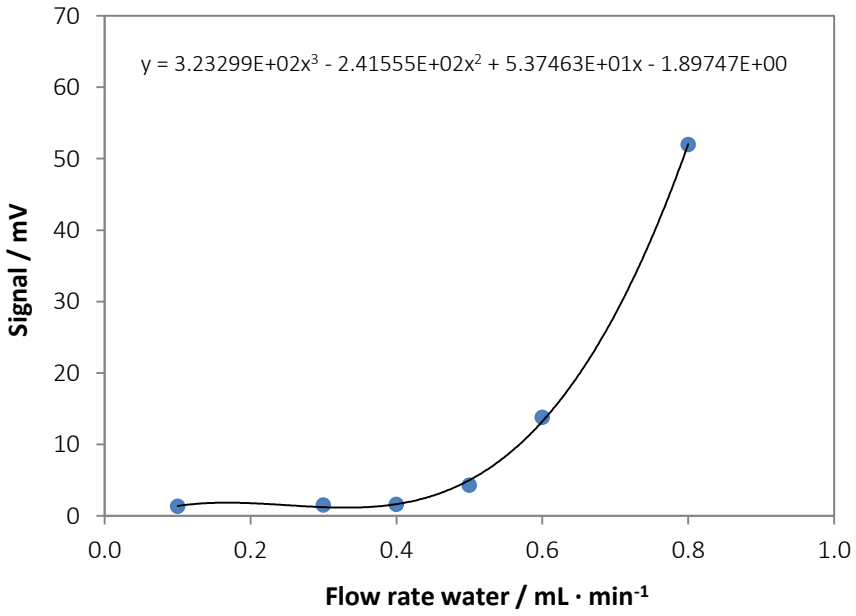

Figure 5.6. Flow-heat signal obtained for different flow rates of water

Table 5.3. Tabulated values of calorimeter signal for different flow rates of water

Flow rate / mL·min^{-1}	Signal / mV
0.1000	1.32
0.3000	1.53
0.4000	1.6
0.5000	4.3
0.6000	13.8
0.8000	51.95

The signal values obtained have been fitted to a cubic polynomial equation, shown in figure 5.6, in order to adapt the base line made with water to the flow rates of the experiments with CO_2 and aqueous amine solutions, allowing the calculation of the base line for each one of the experiments carried out.

5.4.2. Calorimeter sensitivity adjustment

The thermopile sensitivity K used to convert the thermopile signal to heat power has been chemically recalibrated from the value given by Setaram by measuring the heat of mixing of the system ethanol + water in a range of ethanol mole fraction from 0.0276 to 0.3769 at 338.15 K (temperature of solution enthalpy experiments).

The enthalpy of mixing of the mixture ethanol + water was first calculated with equation 5.7 using the original sensitivity provided by the manufacturer (K = 3.700), and the values obtained were compared with those values provided by Ott et al. (1986). Then, the sensibility was adjusted in order to minimize the difference between the experimental results and the reported literature values with the following objective function, where n represents the number of experiments:

$$\text{F. O.} = \sum_{i=1}^{n} \left(\Delta_{\text{m}} H^{E}_{\text{exp}} - \Delta_{\text{m}} H^{E}_{\text{calc}} \right) \tag{5.8}$$

The minimum of the function objective corresponded to a value K= 3.689. Figure 5.7 and table 5.4 show experimental results of enthalpy of mixing and its comparison with calculated values of reported literature data.

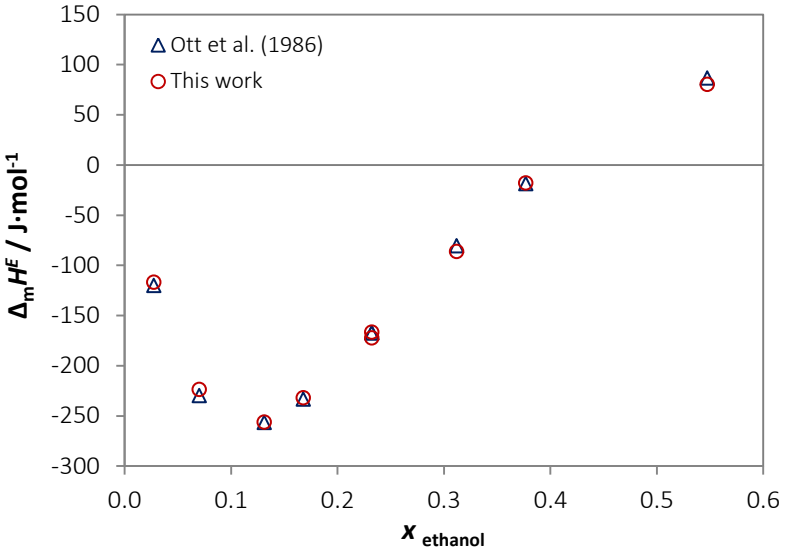

Figure 5.7. Experimental and literature reported values of enthalpy of mixing of ethanol+water at 338.15 K

As can be appreciated in the results obtained, there is good agreement between the experimental results and literature data, obtaining a maximum relative deviation of 7.7 % and root mean square deviation of 4.0 %.

Table 5.4. Experimental and literature reported values of enthalpy of mixing of ethanol+water at 338.15

x ethanol	$\Delta_m H^E_{exp}$ / J·mol^{-1}	$\Delta_m H^E_{lit}$ / J·mol^{-1}
0.0276	-116.8	-120.1
0.0703	-223.8	-229.7
0.1314	-256.4	-256.5
0.1678	-232.2	-233.4
0.2322	-166.7	-167.4
0.2322	-86.2	-80.5
0.3121	-18.0	-18.6
0.3769	80.3	86.5

5.5. Uncertainty estimation

The uncertainties associated to the molar flow rates of the high-pressure pumps depend on the uncertainty of the fluids density and the uncertainty of the volumetric flow rate of the pump (equation 5.9).

$$\delta \dot{n}_i = \dot{n}_i \sqrt{\left(\frac{\delta \rho_i}{\rho_i}\right)^2 + \left(\frac{\delta n_{i,V}}{n_{i,V}}\right)^2} \tag{5.9}$$

The relative error of the volumetric flow rate of the pump ($\delta\, n_{i,V}/n_{i,V}$) is established by the manufacturer to ± 0.3 % for both gas and liquid fluids. The uncertainty of the density of the amine aqueous solutions corresponds to 0.0001 g·cm^3. The uncertainty of molar flow rate of the amine has been estimated to 0.3 %. For CO_2, the uncertainty of the molar flow rate has been estimated to be 1 % at 5 bar, 0.6 % at 10 bar and 0.45 % at 15 bar.

The uncertainty of the CO_2 loading depends on the uncertainties of the molar flow rate of carbon dioxide and the amine (eq. 5.10). For working pressures of 5 bar, 10 bar and 15 bar the uncertainties obtained were 1.1 %, 0.7 % and 0.5 % respectively.

$$\delta \alpha = \alpha \sqrt{\left(\frac{\delta \dot{n}_{amine}}{\dot{n}_{amine}}\right)^2 + \left(\frac{\delta \dot{n}_{CO_2}}{\dot{n}_{CO_2}}\right)^2} \tag{5.10}$$

The uncertainties associated to the enthalpy of solution are determined by the uncertainties of the thermopile sensitivity (estimated to 2 %), the calorimetric signals and the molar flow rate of gas or amine depending on the enthalpy of solution that is analysed (eq. 5.11).

$$\delta \Delta_{\mathrm{sol}} H = \Delta_{\mathrm{sol}} H \sqrt{\left(\frac{\delta K}{K}\right)^2 + \left(\frac{\delta \Delta S}{\Delta S}\right)^2 + \left(\frac{\delta \dot{n}_i}{\dot{n}_i}\right)^2} \tag{5.11}$$

where ΔS is the difference of thermopile signal S_{M} and baseline S_{LB}. The uncertainty of the signal is associated to the detection limit (0.02 mV) as well as the fluctuation of the signal obtained, which has been observed to be between 1 % and 5 %.

5.6. Experimental results

5.6.1. Solubility limit of CO_2 in aqueous amine solutions

The enthalpy of solution of CO_2 in aqueous 2-methylpiperidine and 4-methylpiperidine solutions (amine mass fraction of 0.4 for 2-methylpiperidine and 0.2 – 0.4 for 4-methylpiperidine) have been measured as function of CO_2 loadings at 338.15 K and working pressures from 5 to 15 bar (figures 5.8 – 5.10). The values obtained of enthalpy of solution are tabulated in *Annex C*.

In all cases the absorption process produces exothermic heat flows. The representation of the enthalpy of solution in terms of $kJ \cdot mol^{-1}$ of CO_2 or amine shows two well differenced behaviours. When the enthalpy of solution is represented in $kJ \cdot mol^{-1}$ of CO_2 the most exothermic effect is obtained for the lowest loadings and then decreases as the loading increases. On the other hand, the enthalpy of solution represented in $kJ \cdot mol^{-1}$ of amine shows a linear increase of the exothermic effect as the loading increases (unsaturated solution) until reaching the solubility limit of CO_2 in amine solution, from which the enthalpy presents a plateau that indicates that the solution is saturated and no more carbon dioxide can be dissolved. The experimental results of the solubility limit ($mol_{CO_2} \cdot mol_{amine}^{-1}$) are directly determined from the results represented in the graphs. For the methylpiperidine solutions analysed, the solubility limit also corresponds to the intersection of both curves of enthalpy of solution ($kJ \cdot mol^{-1}$ of CO_2 / $kJ \cdot mol^{-1}$ of amine)

Previous studies (Arcis et al., 2011, 2012) determined that this methodology allows obtaining solubility limit with lower deviation than 5 % when is compared to the values obtained by specific experimental methodologies such as phase equilibrium measurements.

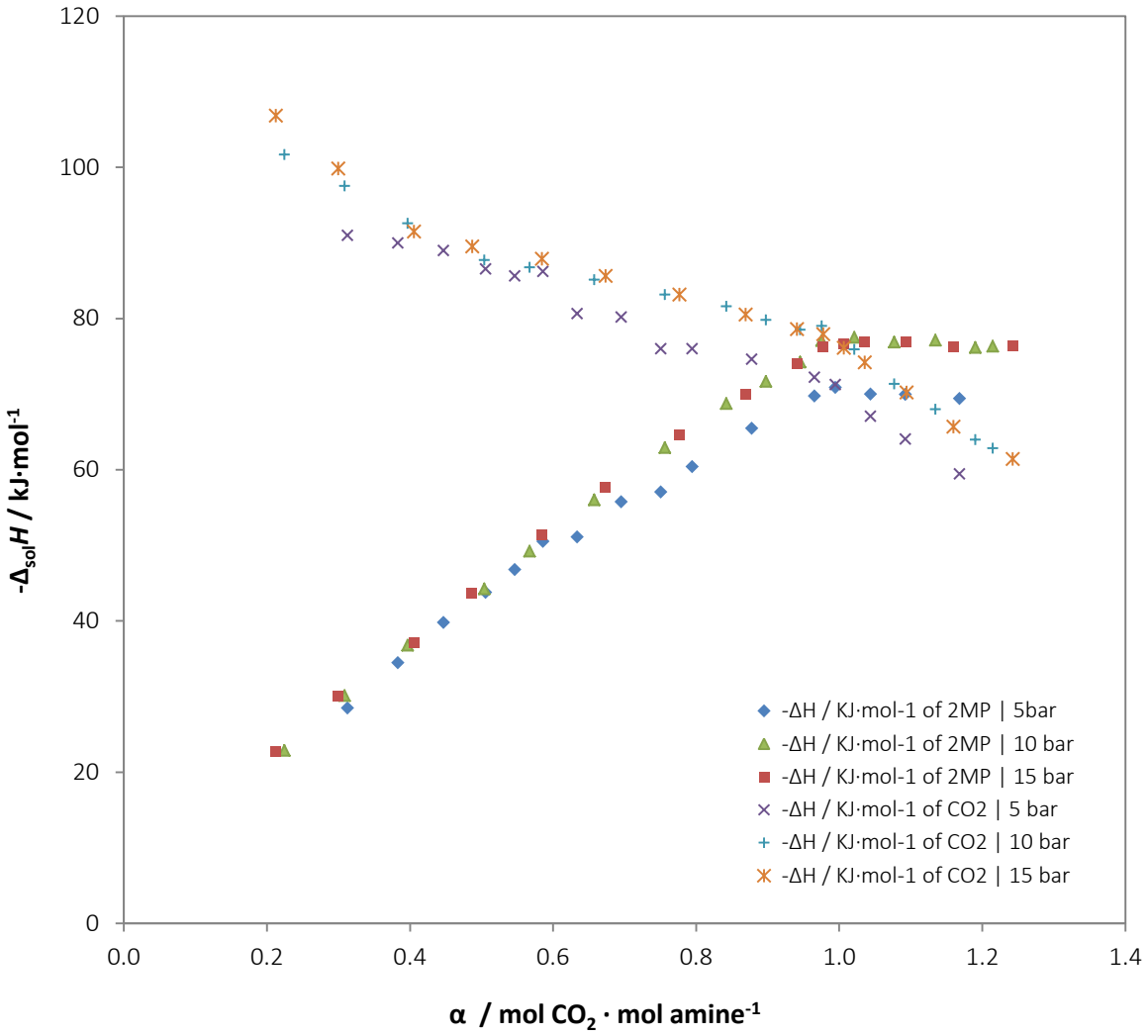

Figure 5.8. $-\Delta_{sol}H$ / kJ·mol^{-1} of 2-methylpiperidine (40 % amine mass composition) at 338.15 K and working pressures from 5 bar to 15 bar

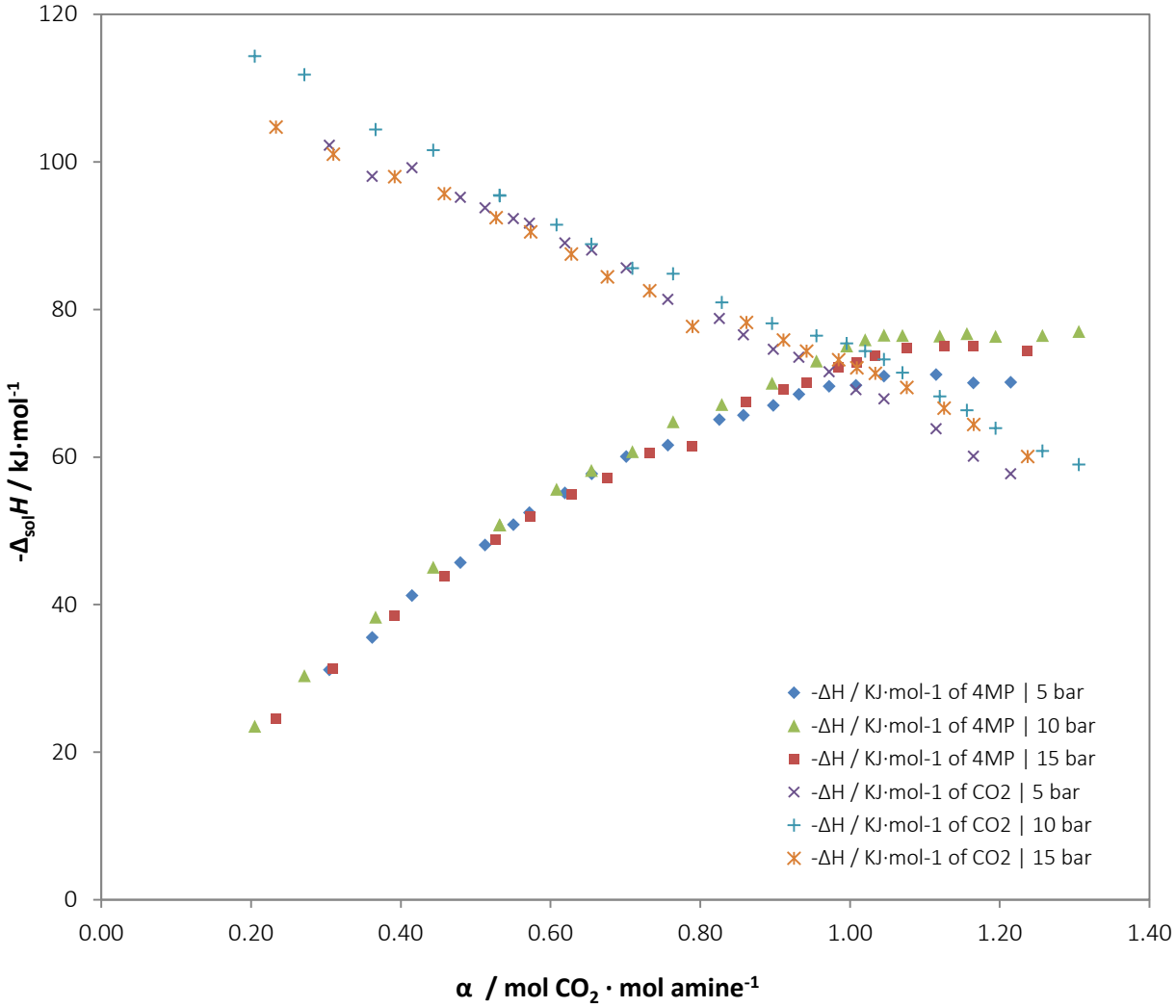

Figure 5.9. $-\Delta_{sol}H$ / kJ·mol^{-1} of 4-methylpiperidine (20 % amine mass composition) at 338.15 K and working pressures from 5 bar to 15 bar

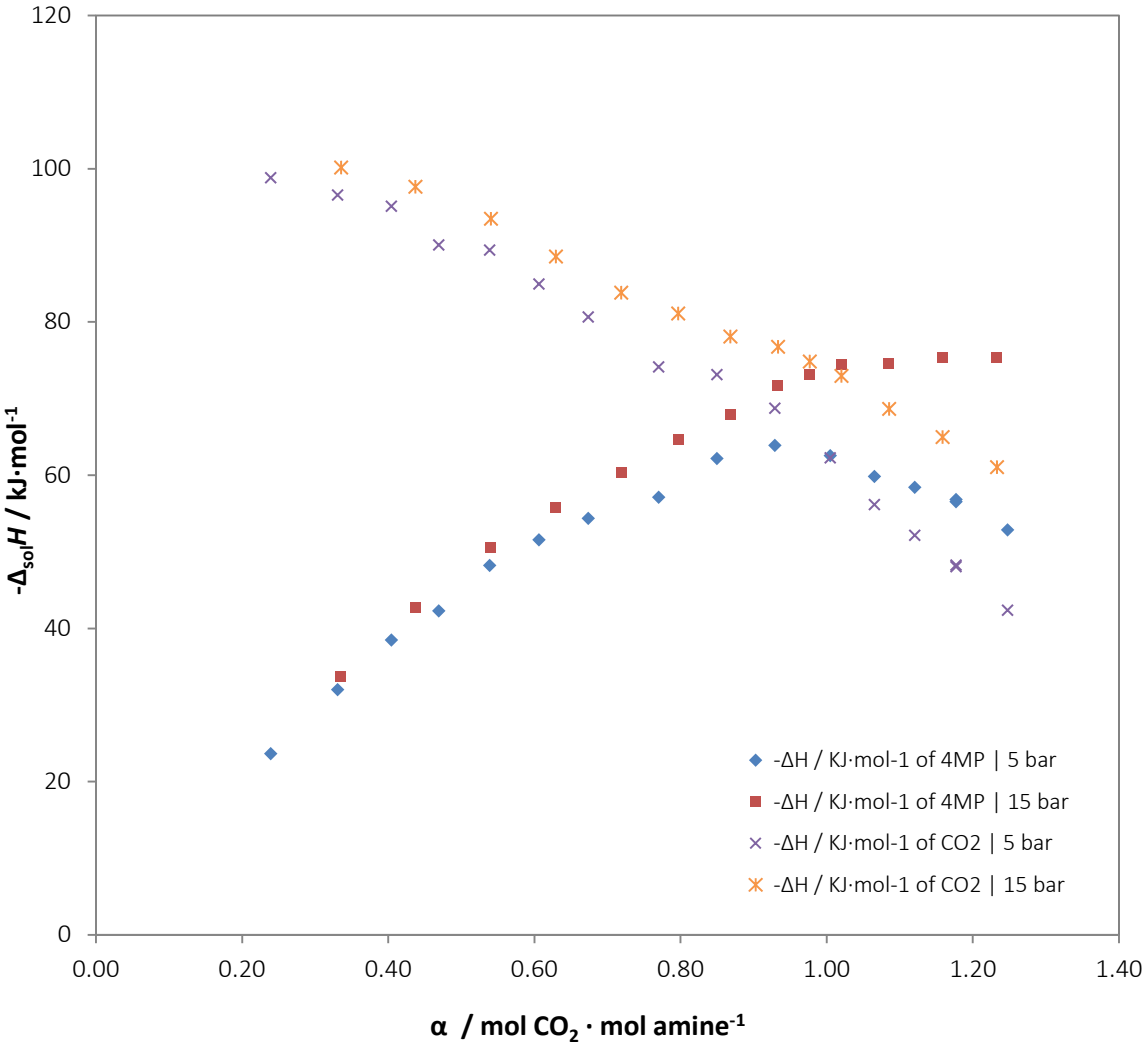

Figure 5.10. $-\Delta_{sol}H$ / kJ·mol^{-1} of 4-methylpiperidine (40 % amine mass composition) at 338.15 K and working pressures from 5 bar to 15 bar

Figure 5.8 shows the enthalpy of solution of CO_2 in an aqueous solution of 2-methylpiperidine (amine mass fraction of 0.40). The exothermic effect of the absorption expressed as kJ·mol^{-1} of amine follows the same linear increase for the three pressures measured until reaching a loading of 0.6, from which for 5 bar it is produced a lower heat flow. The differences are evaluated from the loading corresponding to the solubility limit, which shows a stable plateau, obtaining an average difference of 5 kJ·mol^{-1}.

In the case of the absorption of CO_2 in an aqueous solution of 4-methylpiperidine (amine mass fraction of 0.20), the behaviour obtained is similar to 2-methylpiperidine (figure 5.9). The lower exothermic effect corresponds to the lower pressure measured; however, in this case it is obtained

a higher heat flow for 10 bar than 15 bar, which can be attributed to a lack of accuracy in the experiments carried out.

The experiments for 4-methylpiperidine solutions with amine mass fraction of 0.40 show that, as the previous analysis, up to a loading of 0.6 the enthalpy of solution expressed as $kJ \cdot mol^{-1}$ of amine is the same for both pressures measured and then, from this point the differences increases. However, for this amine composition at 5 bar it is not obtained a plateau when the solubility point is reached, the enthalpy of solution decreases as loading increases.

In tables 5.5 – 5.7 are presented the experimental values of the solubility limit of carbon dioxide in aqueous amine solutions.

Table 5.5. Solubility limit of CO_2 in aqueous solution of 2-methylpiperidine ($w_{2MP} = 0.400$) at 338.15 K

P / bar	s / $mol_{CO_2} \cdot mol_{amine}^{-1}$
5.6	0.966
10.4	0.976
15.5	0.978

Table 5.6. Solubility limit of CO_2 in aqueous solution of 4-methylpiperidine ($w_{4MP} = 0.200$) at 338.15 K

P / bar	s / $mol_{CO_2} \cdot mol_{amine}^{-1}$
5.5	1.008
10.5	1.021
15.7	1.034

Table 5.7. Solubility limit of CO_2 in aqueous solution of 4-methylpiperidine ($w_{4MP} = 0.400$) at 338.15 K

P / bar	s / $mol_{CO_2} \cdot mol_{amine}^{-1}$
5.3	0.929
15.4	1.021

The solubility limit presents low differences in the two amines studied as well as when it is increased the working pressure or the amine composition, being in all cases the solubility around 1 $mol_{CO_2} \cdot mol_{amine}^{-1}$. Regarding the working pressure, as expected, it can be appreciated how the

solubility slightly increases as system pressure increases. This is caused by the Le Châtelier principle, which states that if the pressure of the system is increased more gas molecules collide with the surface of the liquid to enter the solution, shifting the reaction in the direction in which gas moles disappear to minimize the pressure. The comparison of solubility limit of CO_2 in 4-methylpiperidine solutions shows that solubility decreases with amine composition. This behaviour is due to the decrease of the number of water molecules available to solvate carbon dioxide when is increased the amine composition. The uncertainties associated to the solubility limit, which depends on the accuracy of the determination of the first point of the plateau, have been estimated to be between 5 % and 10 %.

5.7. Conclusions

In this chapter it has been measured the solubility limit of CO_2 in aqueous solutions of 2-Methylpiperydine and 4-methylpiperidine (amine mass fraction of 0.20 and 0.40) at 338.15 K and 5 bar, 10 bar and 15 bar working pressures. The aim of studying these amines, used in CO_2 capture processes, lies in the fact that they present a liquid-liquid phase separation at a certain temperature and CO_2 composition, decreasing thus the energy necessary to separate the CO_2 from the amine in the desorption process of the cycle (amine regeneration).

The solubility of carbon dioxide in the amine has been obtained by means of the measurement of the enthalpy of solution in a custom-made flow-mixing cell adapted to a calorimeter Calvet Setaram BT2.15. The base line signal is obtained by the adjustment of the temperature of the calorimeter preheaters when only water flows through it. The sensibility factor is recalibrated by minimizing the differences between the measured and the literature reported values of the enthalpies of mixing of the system ethanol + water.

The enthalpy of solution expressed as $kJ \cdot mol^{-1}$ of amine presents a linear increase until reaching the solubility limit. From this point the solution is saturated of CO_2 and no more exothermic effect is produced, obtaining a plateau as the CO_2 loading increases. The comparison of the heat flow obtained at the three pressures analysed shows that the lower enthalpies of solutions are obtained at the lower pressure.

The solubility limit of carbon dioxide in the amines studied scarcely changes for both 2-methylpiperidine and 4-methylpiperidine solutions as well as with changes in amine composition or

system pressure, obtaining results of around 1 $mol_{CO_2} \cdot mol_{amine}^{-1}$. However, the results show that solubility is slightly increased with pressure and slightly decreased when is increased the amine composition.

This study has permitted to learn and understand the flow-calorimetric methodology to measure solubility limit of gases into amines. Previous studies have confirmed the obtainment of good agreement regarding specific experimental methodologies, with deviations lower than 5 % in the experimental solubility limit measurements, which confirms that this method is suitable for measuring the solubility limit of gases in absorbents.

5.8. Nomenclature

C	oscillating constant
$\Delta_{\mathrm{m}}H$	enthalpy of mixing (J·mol^{-1})
$\Delta_{\mathrm{sol}}H$	enthalpy of solution (kJ·mol^{-1})
K	thermopile sensitivity (mV·mW^{-1})
m	mass (kg)
$\dot{n}$	molar flow rate (mol·s^{-1})
P	pressure (bar)
S	thermopile signal
s	limit of solubility
T	temperature (K)
V_0	oscillator inner volume
x	mole fraction

Greek Letters

ρ	density (kg·m^{-3})
τ	oscillating period
δ	uncertainty
α	loading

Subscripts

i	component i

Superscripts:

E	excess property

5.9. References

Arcis, H.; Ballerat-Busserolles, K.; Rodier, L.; Coxam, J.-Y. *Enthalpy of Solution of Carbon Dioxide in Aqueous Solutions of Monoethanolamine at Temperatures of 322.5 K and 372.9 K and Pressures up to 5 MPa.* J. Chem. Eng. Data 56 (2011) 3351–3362.

Arcis, H.; Ballerat-Busserolles, K.; Rodier, L.; Coxam, J.-Y. *Measurement and Modeling of Enthalpy of Solution of Carbon Dioxide in Aqueous Solutions of Diethanolamine at Temperatures of (322.5 and 372.9) K and Pressures up to 3 MPa*. J. Chem. Eng. Data 57 (2012) 840−855.

Arcis, H.; Ballerat-Busserolles, K.; Rodier, L.; Coxam, J.-Y. *Enthalpy of Solution of Carbon Dioxide in Aqueous Solutions of Triethanolamine at Tempereatures of 322.5 K and 372.9 K and Pressures up to 5 MPa*. J. Chem. Eng. Data 57 (2012) 3587 − 3597.

Arcis, H.; Ballerat-Busserolles, K.; Rodier, L.; Coxam, J.-Y. *Temperatures of liquid–liquid separation and excess molar volumes of {N-methylpiperidine–water} and {2-methylpiperidine–water} systems*. Fluid Phase Equilibria 296 (2010) 206–212.

Jones, J.A. United States Patent. No: US 6,374,630 B1 (2002).

Jones, J.A. Champagne Heat Pump, NASA Technical Support Package (2004), www.techbriefs.com/tsp.

Jung, J.; Jeong, Y.S.; Lee, U.; Lim, Y.; Yang, S.; Lee, C.S.; Kim, J.; Han, C. Post-Combustion CO_2 Capture Process with Aqueous MEA: An Advanced MEA Process using a Phase Separation Heat Exchanger. Computer Aided Chemical Engineering 31 (2012) 505–509.

Ott, J.B.; Cornett, G.V.; Stouffer, C.E.; Woodfield, B.F.; Guanquan, C.; Christensen, J.J. *Excess enthalpies of (ethanol+water) at 323.15, 333.15, 348.15, and 373.15 K and from 0.4 to 15 MPa.* J. Chem. Thermodynamics 18 (1986) 867-875.

Raynal, L.; Bouillon, P.-A.; Gomez, A.; Broutin, P. *From MEA to demixing solvents and future steps, a roadmap for lowering the cost of post-combustion carbon capture*. Chemical Engineering Journal 171 (2011) 742-752.

Salavera, D. *Propiedades Termofísicas de Nuevos Fluidos de Trabajo (H_2O+LiBr+$LiNO_3$+LiCl+LiI, NH_3+H_2O+NaOH y NH_3+H_2O+KOH) para Sistemas de Refrigeración por Absorción.* Doctoral Thesis Universitat Rovira i Virgili, Tarragona 2005.

Sen, M.; Paolucci, S. *Using Carbon Dioxide and Ionic Liquids for Absorption Refrigeration*. 7th IIR Gustav Lorentzen Conference on Natural Working Fluids, Norway (2006).

Stephenson, R.M. *Mutual Solubility of Water and Pyridine Derivatives*. J. Chem. Eng. Data 38 (1993) 428–431.

National Institute of Standards and Technology (NIST): http://webbook.nist.gov/chemistry/

Chapter 6

Conclusions and Future Work

6.1. Conclusions

Nowadays, the incessant growth of the population and the progressively evolution of the developing countries has entailed an important increasing of the global energy requirements. Within the scope of the refrigeration of buildings, absorption refrigeration systems have demonstrated to provide remarkable electricity savings regarding classical compression systems. However, though they present weaknesses such as cost and performance, its advantages has driven research in the improvement of their characteristics and new working fluids.

The study of the solubility of the new working fluids proposed in literature for improving the features of the conventional H_2O/LiBr and NH_3/H_2O mixtures becomes an important task because they present a partial solubility that impose restrictions in the operability and applications of the refrigeration systems. In this context, this thesis has presented an experimental and theoretical study of solubility new absorbents in natural refrigerants (NH_3, H_2O and CO_2) for absorption refrigeration cycles.

- *Regarding absorption systems with NH_3 as refrigerant:*

  - The solubility of $NH_3/LiNO_3$, NH_3/NaSCN and $NH_3/(H_2O+NaOH)$ mixtures was measured with a new experimental device designed and built for this work based on the visual-polythermal method and with the capacity to work at moderate-high pressures,.
  - The new device and the measurement procedure were validated at atmospheric pressure with $H_2O/LiNO_3$ mixture, and at 20 bar with $NH_3/LiNO_3$. The deviations obtained were lower than the estimated uncertainty of the measure (0.5 K), concluding that they are adequate for measuring the solubility temperature of salts in aqueous and non-aqueous solvents at pressure conditions.
  - A new image processing method based on the analysis of photographs taken from the inner of the cell was developed to provide a more objective criterion in the solubility measurements.
  - The comparison of the results obtained with the $H_2O/LiNO_3$ solution between visual and image processing methods showed a maximum difference in solubility temperature of 0.2 K, which means that the image processing method is suitable to perform proper solubility measurements.
  - The solubility temperature of $NH_3/LiNO_3$ mixture was measured in a range of salt mass fraction from 0.48 to 0.78.
  - The solubility temperature of NH_3/NaSCN was measured at 20 bar in a salt mass fraction range from 0.53 to 0.69.
  - Solubility of NaOH in NH_3/H_2O could not be performed as in the other experiments because at certain composition presents its solubility limit, what causes the impossibility to dissolve it by increasing temperature. The maximum quantity of ammonia which allows a saturated $NaOH/H_2O$ solution was experimentally determined. The results were performed for salt mass fractions from 0.02 to 0.15, obtaining a maximum quantity of ammonia mass fractions from 0.38 to 0.235.
  - The modelling of the solid-liquid equilibrium of $H_2O/LiNO_3$, $NH_3/LiNO_3$ and NH_3/NaSCN mixtures was carried out by means of the activity coefficient models LIQUAC (for the mixture with water as solvent) and Symmetric Electrolyte-NRTL (for the mixtures with ammonia as solvent).

- For mixtures with ammonia the model requires the use of experimental solubility data, what make it not as predictive method as in the case of the solubility modelling of systems with water as solvent.
- The solubility modelling results showed deviations lower than 7 % regarding experimental data, concluding that the modelling allows obtaining good and reliable results.

- *Regarding absorption systems with H_2O as refrigerant*

  - An extension of the solubility study carried out by Koo et al. (1999) with the solution H_2O/(LiBr+$LiNO_3$+LiI+LiCl) (salt mole ratio 5:1:1:2) was carried out with the aim of improving the solubility at higher salt mass compositions (65 % - 69 %) in order to make the solution feasible for air-cooled absorption systems.
  - The optimum salt mole ratio of the mixture was performed with a rough visual-polythermal method. The optimum ratio obtained was 7:1:0.5 (LiBr:$LiNO_3$:LiI). Lithium chloride was discarded because it did not show improvement in solubility.
  - The accurate solubility temperature of the optimum mixture obtained was measured by a visual-polythermal method, in a range of total salt mass fractions from 0.6245 to 0.6907.
  - Results obtained were compared with the reported data by Salavera et al. (2004) using the mixture proposed by Koo et al. (1999). Similar results were obtained up to salt mass fraction of 0.65. At higher salt compositions it was obtained a decrease of solubility temperature from 8 K to 35 K.
  - The effect of addition of LiCl in vapour pressure of optimum mixture was studied by modelling the vapour-liquid equilibrium with the asymmetric Electrolyte-NRTL activity coefficient model using Aspen Properties software.
  - A new set of parameters of the model were fitted from reported literature data of the single solutions in order to obtain deviations between experimental and calculated vapour pressure lower than 10 %. The validation with quaternary solution H_2O/(LiBr+$LiNO_3$+LiI+LiCl) (5:1:1:2) obtained a noticeable deviation (RMSD 22.2 %); however as it follows the same trend than experimental values, and it can be concluded that the model is suitable for calculating vapour pressure of lithium salts mixtures solutions.

- The results of the vapour pressure modelling of the optimum mixture proposed in this work showed that the LiCl doesn't decrease significantly the vapour pressure of the solution. Thus, the addition of LiCl was not justified and was discarded.
- The calculated vapour pressure of the mixture proposed in this work showed a slight decrease regarding the calculated vapour pressure of the mixture proposed by Koo et al. (1999). In the range of salt mass fractions from 0.60 to 0.70, a decrease of vapour pressure between 0.13 kPa to 1.2 Kpa was obtained respectively.
- The mixture proposed in this work provides improvement in solubility, eliminates the LiCl from the mixture, reduces the required quantity of $LiNO_3$ and LiI, and slightly reduces the vapour pressure of the mixture. Thus, the new mixture is considered a promising working fluid that could work with air-cooled absorption systems.

- *Regarding absorption systems with CO_2 as refrigerant*

  - A flow-calorimetric methodology was used to measure the solubility of CO_2 in amines.
  - This method allows obtaining at the same time the enthalpies of solution and the solubility limit of the CO_2 in the aqueous amine solutions.
  - The solubility limit of CO_2 in aqueous 2-Methylpiperydine and 4-Methylpiperydine solutions (amine mass fraction of 0.20 and 0.40) was measured at 338.15 K and 5 bar, 10 bar and 15 bar.
  - The study of these amines, used in CO_2 capture processes, lies in the fact that they present a liquid-liquid equilibrium from certain temperature and CO_2 composition, decreasing thus the energy necessary to separate the CO_2 from the amine in the desorption process.
  - The solubility limit of carbon dioxide presents scarce changes for both methylpiperidine solutions. Changes in amine composition or pressure presents no significant variations in the solubility limit, obtaining results of around 1 $mol_{CO_2} \cdot mol_{amine}^{-1}$. However, the results show that solubility slightly increases with pressure and slightly decreases when the amine composition increases.
  - The flow-calorimetric method is presented as an adequate technique to measure the solubility limit of gases into absorbents. Previous studies have confirmed good agreement

with specific experimental methodologies, with deviations lower than 5 % in the experimental solubility limit measurements.

6.2. Future Work

From the results obtained in this study, in the next future the following task can be considered:

- Improving the image processing method, validating with other reference systems, especially at moderate-high pressure.
- Experimental measurement of the thermophysical properties, especially the vapour pressure, of the new mixture proposed in this work, H_2O/(LiBr+$LiNO_3$+LiI) with salt mole ratio 7:1:0.5.
- Modelling of the performance of air-cooled absorption systems with the working fluid H_2O/(LiBr+$LiNO_3$+LiI) (salt mole ratio 7:1:0.5).
- Applying the flow-calorimetric technique to the measurement of the solubility limit of CO_2 with other absorbents like ionic liquids.

Appendix

Appendix A

Matlab Program for Image Processing

The measurement of the number of red colour pixels of the pictures has been carried out in two separate programs. First one provides the resultant red channel image from the comparison of the picture at each temperature and the blank image taken when all salt is dissolved. The second program takes the image obtained in the first program and measures the total number of red colour pixels.

Program 1

```
clc
clear all
addpath(genpath('C:\Matlab'))

ZoneY=(1330:1536);
ZoneX=(650:1550);

disp('Select blank file?')
blankFile=uigetfile('.jpg')
blank=imread(blankFile);
blank=double(blank);
blankLayer=blank(:,:,1);

disp(['Select image file/s?'])
sampleFile=uigetfile('.jpg','Multiselect','on')
sampleFile=char(sampleFile);
sampleFile=strvcat(sampleFile);
number=size(sampleFile);
for i=1:number(1)
sample=imread(sampleFile(i,:));
sample=double(sample);
sampleLayer=sample(:,:,1);
sampleMatrix(:,:,i)=sampleLayer;
```

```
blankMatrix(:,:,i)=blankLayer;
end

sampleMatrix=sampleMatrix(ZoneY,ZoneX,:);
blankMatrix=blankMatrix(ZoneY,ZoneX,:);

subRow=round(sqrt(number(1)))
subCol=round(number(1)/subRow)+1

for i=1:number(1)
    final(:,:,i)=blankMatrix(:,:,i)-sampleMatrix(:,:,i);
    subplot(subRow,subCol,i)
    image(final(:,:,i))
end
```

Program 2

```
clc;
close all;
imtool close all;
clear;

% Read the figure image.
rgbImage = imread('figure.png');
[rows columns numberOfColorBands] = size(rgbImage);
subplot(2, 2, 1);
imshow(rgbImage, []);
title('Original Color Image', 'Fontsize', fontSize);
set(gcf, 'Position', get(0,'Screensize'));

redPlane = rgbImage(:, :, 1);
greenPlane = rgbImage(:, :, 2);
bluePlane = rgbImage(:, :, 3);

[pixelCountR grayLevelsR] = imhist(redPlane);
subplot(2, 2, 2);
bar(pixelCountR, 'r');
title('Histogram of red plane', 'Fontsize', fontSize);
xlim([0 grayLevelsR(end)]); % Scale x axis manually.
```

Appendix B

Uncertainty Calculation

B.1. Introduction

The purpose of a measurement is to determine the value of a specific magnitude to be measured, called measurand. In any measurement always appear a series of errors from different sources: the measurand, the procedure of the measurement, the measurement instrument, the operator, etc., which are classified in systematics and accidental (random) errors.

Systematic errors are repeated constantly along the experiment and the final result is always affected in the same way. Calibration errors or non-appropriate experimental conditions are the causes which origin them. These errors can be corrected if the error sources are known. When it is not possible to apply a correction the systematic error is added to the expanded measurement uncertainty. Accidental or random errors are the errors due to unpredictably circumstances and vary oscillating around a mean value. It is not possible to control it, but it can be reduced by increasing the number of experiments. These kinds of errors are due to causes such as changes of the surrounding conditions along the experiment or appreciation errors (e.g. human limitations).

The measurement uncertainty is an estimation of the possible error in a measurement. It can be defined as the estimation of a range of values which contains the true value of the measurement.

The evaluation of the measurement uncertainties have been carried out in accordance with the rules of the guide of *Expression of the Uncertainty of Measurement in Calibration* from European co-operation for Accreditation EA 4/02.

B.2. Evaluation of uncertainties

The uncertainty of a measurement associated with an input is evaluated according to two different types of evaluation:

- *Type A evaluation of standard uncertainty*:
  In this method the uncertainty is estimated by the statistical analysis (standard deviation) of a series of measurements made under the same conditions. In this evaluation the uncertainty sources follow a normal distribution.

- *Type B evaluation of standard uncertainty*:
  In this case the uncertainty is evaluated with other than the statistical analysis of a series of observations. It is estimated by scientific knowledge based on all available information such as manufacturer specification, calibration certificates or experience of previous experiments. In this evaluation the uncertainty sources follow a rectangular distribution.

B.3. Calculation of the standard and expanded uncertainty

The calculus of the uncertainties has been carried out by means of the law of propagation of uncertainty, in which if an output Y_i is function of n inputs variables X_i, $Y_i = f(X_1, X_2 \ldots . X_n)$, the standard uncertainty of variable Y_i, $u(Y_i)$, is obtained as function of the standard uncertainties of the inputs X_i, $u(X_i)$ with the next equation:

$$u(Y_i) = \sqrt{\sum_{i=1}^{n} [u(X_i)^2 \, c_i^2]} \tag{B.1}$$

The standard uncertainties associated to each one of the input uncertainty sources, $u(X_i)$, are calculated by the relation of the estimated value of the input source and its probability of distribution (eq. B.2). Normal distributions correspond to divisor 1, however, rectangular distributions corresponds to divisor $\sqrt{3}$.

$$u(X_i) = \frac{\text{Estimated value}}{\text{Divisor}} \tag{B.2}$$

The sensibility factor c_i corresponds to the partial derivative of the function f regarding X_i (eq. B.3). It describes how the output Y_i is influenced by variations of the input X_i.

$$c_i = \frac{\partial f}{\partial X_i} \tag{B.3}$$

The uncertainties obtained by the equation B.1 are called standard uncertainties and they assure that the real value has 66.7 % of probability to be within the calculated uncertainty. To increase the level of confidence, the uncertainty is multiplied to a coverage factor *k,* obtaining thus the expanded uncertainty $U(Y_i)$.

$$U(Y_i) = k \cdot u(Y_i) \tag{B.4}$$

In this work, it has been selected a coverage factor k=2 in order to provide a confidence level of 95.45 %. As example, in the following two sections are shown in detail the uncertainty sources as well as the final uncertainties obtained of mass fraction and temperature in the solubility temperature determination of sodium thiocyanate in ammonia.

B.3.1. Mass fraction uncertainty

Table B.1. Uncertainty of mass balance Mettler AE260 DeltaRange (NaSCN mass measurement)

Source	Unit	Estimation	Divisor	Sensibility factor	$u^2(m)$
Resolution	g	0.0001	$2\sqrt{3}$	1	$8.33 \cdot 10^{-10}$
Calibration	g	0.0001	2	1	$2.50 \cdot 10^{-9}$
Linearity	g	0.0002	1	1	$4.00 \cdot 10^{-8}$
Precision	g	0.0001	1	1	$1.00 \cdot 10^{-8}$
Reproducibility	g	0.0001	1	1	$1.00 \cdot 10^{-8}$
u(m)					0.0003
U(m)				k=2	0.0006

Table B.2. Uncertainty of sodium thiocyanate mass

Source	Unit	Estimation	Divisor	Sensibility factor	$u^2(m_{NaSCN})$
Funnel NaSCN	g	0.0003	1	1	$6.33 \cdot 10^{-8}$
Funnel NaSCN rest	g	0.0003	1	1	$6.33 \cdot 10^{-8}$
u (m_{NaSCN})					0.0004
U (m_{NaSCN})				k=2	0.0008

Table B.3. Uncertainty of mass balance Mettler Toled PR2003 DeltaRange (NH_3 mass measurement)

Source	Unit	Estimation	Divisor	Sensibility factor	$u^2(m)$
Resolution	g	0.01	$2\sqrt{3}$	1	$8.33\cdot10^{-6}$
Calibration	g	0.01	2	1	$2.50\cdot10^{-5}$
Precision	g	0.01	1	1	$1.00\cdot10^{-4}$
Linearity	g	0.005	1	1	$2.50\cdot10^{-5}$
Reproducibility	g	0.003	1	1	$9.00\cdot10^{-6}$
u(m)					0.01
U(m)				k=2	0.02

Table B.4. Uncertainty of ammonia mass

Source	Unit	Estimation	Divisor	Sensibility factor	$u^2(m_{NH3})$
Cylinder NH_3	g	0.01	1	1	$1.67\cdot10^{-4}$
Cylinder NH_3 rest	g	0.01	1	1	$1.67\cdot10^{-4}$
u (m_{NH3})					0.02
U (m_{NH3})				k=2	0.04

Table B.5. Uncertainty of sodium thiocyanate mass fraction (w_{NaSCN}=0.5627)

Source	Unit	Estimation	Divisor	Sensibility factor	$u^2(w)$
Mass NaSCN	g	0.0004	1	0.0305	$1.49\cdot10^{-10}$
Mass NH_3	g	0.02	1	-0.0392	$6.16\cdot10^{-7}$
u (w)					0.0008
U (w)				k=2	0.0016

Since the salt mass fraction of the different solutions prepared depends on the mass of sodium thiocyanate and the mass of ammonia, it has a sensibility factor that takes into account the change of the salt mass fraction when the mass of salt or water is changed in each of the experiments. The sensibility factors associated to NaSCN mass fraction are calculated as follows:

$$\frac{\delta w_{\mathrm{NaSCN}}}{\delta m_{\mathrm{NaSCN}}} = \frac{m_{\mathrm{NH_3}}}{\left(m_{\mathrm{NaSCN}} + m_{\mathrm{NH_3}}\right)^2} \tag{B.5}$$

$$\frac{\delta w_{\mathrm{NaSCN}}}{\delta m_{\mathrm{NH_3}}} = \frac{-m_{\mathrm{NaSCN}}}{\left(m_{\mathrm{NaSCN}} + m_{\mathrm{NH_3}}\right)^2} \tag{B.6}$$

B.3.2. Temperature uncertainty

Table B.6. Uncertainty solubility temperature of NaSCN in NH_3

Source	Unit	Estimation	Divisor	Sensibility factor	$u^2(T)$
Calibration	K	0.2	2	1	$1.00 \cdot 10^{-2}$
Resolution	K	0.1	$2\sqrt{3}$	1	$8.33 \cdot 10^{-4}$
Homogeneity	K	0.4	$\sqrt{3}$	1	$5.33 \cdot 10^{-2}$
Stability	K	0.1	$\sqrt{3}$	1	$3.33 \cdot 10^{-3}$
Repeatability	K	0.05	1	1	$2.50 \cdot 10^{-3}$
$u(T)$					0.265
$U(T)$				k=2	0.5 K

The homogeneity is evaluated as the maximum temperature difference when the probe is placed at different positions inside the cell. The repeatability is the standard deviation of the measurements and the stability is difference between the maximum and the minimum temperature measured.

Appendix C

Enthalpy of Solution of Aqueous Methylpiperidine Solutions

C.1. CO_2/(H_2O+2-Methylpiperidine) System

Table C.1. Enthalpies of solution of CO_2 in aqueous 2-methylpiperidine solutions (40 % amine mass composition) at 338.15 K and 5 bar

α / mol CO_2 · mol 2MP^{-1}	-$\Delta_{sol}H$ / kJ·mol^{-1} of 2MP	-$\Delta_{sol}H$ / kJ·mol^{-1} of CO_2
0.695	55.7	80.2
0.546	46.8	85.6
0.795	60.4	76.0
0.878	65.5	74.6
0.995	70.9	71.2
0.634	51.1	80.6
0.751	57.0	76.0
0.506	43.8	86.5
0.447	39.8	89.0
0.383	34.5	90.0
0.313	28.5	91.0
0.586	50.5	86.2
1.093	70.0	64.0
0.966	69.7	72.2
1.044	70.0	67.0
1.168	69.4	59.4

Table C.2. Enthalpies of solution of CO_2 in aqueous 2-methylpiperidine solutions (40 % amine mass composition) at 338.15 K and 10 bar

α / mol CO_2 · mol $2MP^{-1}$	$-\Delta_{sol}H$ / kJ·mol^{-1} of 2MP	$-\Delta_{sol}H$ / kJ·mol^{-1} of CO_2
0.842	68.7	81.6
0.945	74.2	78.5
1.021	77.5	75.9
1.135	77.1	68.0
0.976	77.1	79.0
0.898	71.7	79.8
1.077	76.9	71.3
1.215	76.3	62.8
0.756	62.9	83.2
0.567	49.2	86.8
0.397	36.8	92.6
0.225	22.8	101.7
0.309	30.1	97.5
0.504	44.2	87.7
0.658	56.0	85.1
1.190	76.1	64.0

Table C.3. Enthalpies of solution of CO_2 in aqueous 2-methylpiperidine solutions (40 % amine mass composition) at 338.15 K and 15 bar

α / mol CO_2 · mol $2MP^{-1}$	$-\Delta_{sol}H$ / kJ·mol^{-1} of 2MP	$-\Delta_{sol}H$ / kJ·mol^{-1} of CO_2
0.869	69.99	80.50
0.978	76.18	77.90
1.094	76.80	70.19
0.941	73.94	78.57
1.036	76.84	74.19
1.160	76.16	65.66
1.007	76.64	76.13
1.243	76.29	61.39
0.777	64.59	83.16
0.585	51.40	87.89
0.487	43.63	89.53
0.406	37.12	91.50
0.674	57.69	85.63
0.300	29.95	99.85
0.213	22.73	106.81

C.2. CO_2/(H_2O+4-Methylpiperidine) System

Table C.4. Enthalpies of solution of CO_2 in aqueous 4-methylpiperidine solutions (20 % amine mass composition) at 338.15 K and 5 bar

α / mol CO_2 · mol 4MP^{-1}	$-\Delta_{sol}H$ / kJ·mol^{-1} of 4MP	$-\Delta_{sol}H$ / kJ·mol^{-1} of CO_2
0.702	60.1	85.6
0.826	65.0	78.8
0.551	50.8	92.3
0.898	67.0	74.6
0.757	61.6	81.3
0.619	55.1	89.0
0.480	45.7	95.2
0.415	41.2	99.2
1.215	70.1	57.7
1.165	70.0	60.1
1.115	71.1	63.8
1.046	70.9	67.8
0.655	57.7	88.0
0.572	52.4	91.7
0.362	35.5	98.0
0.305	31.1	102.2
0.513	48.1	93.7
0.932	68.5	73.5
0.972	69.6	71.6
1.008	69.7	69.1
0.858	65.6	76.5

Table C.5. Enthalpies of solution of CO_2 in aqueous 4-methylpiperidine solutions (20 % amine mass composition) at 338.15 K and 10 bar

α / mol CO_2 · mol 4MP^{-1}	$-\Delta_{sol}H$ / kJ·mol^{-1} of 4MP	$-\Delta_{sol}H$ / kJ·mol^{-1} of CO_2
1.306	77.0	59.0
0.956	73.0	76.4
0.829	67.1	80.9
0.709	60.7	85.6
1.070	76.5	71.4
1.195	76.4	63.9
1.120	76.4	68.2
1.257	76.5	60.8
0.896	70.0	78.1
0.996	75.1	75.4
1.046	76.5	73.2
1.021	75.9	74.3
1.157	76.7	66.3
0.764	64.8	84.8
0.655	58.2	88.8
0.532	50.8	95.4
0.532	50.8	95.5
0.444	45.0	101.6
0.367	38.3	104.4
0.608	55.6	91.4
0.271	30.3	111.8
0.205	23.5	114.3

Table C.6. Enthalpies of solution of CO_2 in aqueous 4-methylpiperidine solutions (20 % amine mass composition) at 338.15 K and 15 bar

α / mol CO_2 · mol 4MP^{-1}	$-\Delta_{sol}H$ / kJ·mol^{-1} of 4MP	$-\Delta_{sol}H$ / kJ·mol^{-1} of CO_2
0.790	61.4	77.7
0.862	67.4	78.2
0.985	72.1	73.2
1.010	72.8	72.1
0.942	70.0	74.3
0.911	69.1	75.8
0.733	60.5	82.5
0.628	55.0	87.5
0.574	51.9	90.5
1.166	75.0	64.4
1.076	74.7	69.4
1.034	73.8	71.3
0.528	48.8	92.4
0.458	43.8	95.7
1.238	74.3	60.0
0.392	38.4	98.0
1.126	75.0	66.6
0.310	31.3	101.0
0.234	24.5	104.7
0.676	57.1	84.4

Table C.7. Enthalpies of solution of CO_2 in aqueous 4-methylpiperidine solutions (40 % amine mass composition) at 338.15 K and 5 bar

α / mol CO_2 · mol $4MP^{-1}$	$-\Delta_{sol}H$ / kJ·mol^{-1} of 4MP	$-\Delta_{sol}H$ / kJ·mol^{-1} of CO_2
0.331	32.0	96.5
0.770	57.1	74.1
0.674	54.3	80.6
0.607	51.5	84.9
0.539	48.2	89.4
0.404	38.4	95.1
0.239	23.6	98.8
0.470	42.3	90.0
1.121	58.4	52.1
1.005	62.5	62.2
0.929	63.9	68.7
0.850	62.1	73.1
1.065	59.8	56.1
1.177	56.8	48.2
1.177	56.5	48.0
1.248	52.8	42.3

Table C.8. Enthalpies of solution of CO_2 in aqueous 4-methylpiperidine solutions (40 % amine mass composition) at 338.15 K and 15 bar

α / mol CO_2 · mol $4MP^{-1}$	$-\Delta_{sol}H$ / kJ·mol^{-1} of 4MP	$-\Delta_{sol}H$ / kJ·mol^{-1} of CO_2
0.869	67.8	78.1
0.977	73.1	74.8
1.086	74.5	68.6
1.021	74.4	72.9
0.934	71.7	76.7
0.797	64.6	81.1
0.719	60.3	83.8
0.630	55.7	88.5
0.541	50.5	93.4
0.437	42.7	97.6
0.336	33.6	100.1
1.159	75.3	64.9
1.233	75.3	61.0